

COMPETING ORDERS IN S-WAVE AND P-WAVE SUPERCONDUCTORS

by

QI LI

A DISSERTATION

Presented to the Department of Physics
and the Graduate School of the University of Oregon
in partial fulfillment of the requirements
for the degree of
Doctor of Philosophy

June 2008

University of Oregon Graduate School

Confirmation of Approval and Acceptance of Dissertation prepared by:

Qi Li

Title:

"Competing Orders in s-wave and p-wave Superconductors"

This dissertation has been accepted and approved in partial fulfillment of the requirements for the degree in the Department of Physics by:

John Toner, Chairperson, Physics
Nilendra Deshpande, Member, Physics
Stephen Gregory, Member, Physics
Dietrich Belitz, Member, Physics
Andrew Marcus, Outside Member, Chemistry

and Richard Linton, Vice President for Research and Graduate Studies/Dean of the Graduate School for the University of Oregon.

June 14, 2008

Original approval signatures are on file with the Graduate School and the University of Oregon Libraries.

experiments to distinguish vortex lattices from skyrmion lattices by means of their melting curves and their μ SR signatures.

CURRICULUM VITAE

NAME OF AUTHOR: Qi Li

PLACE OF BIRTH: Lanzhou, China

DATE OF BIRTH: March 27, 1976

GRADUATE AND UNDERGRADUATE SCHOOLS ATTENDED:

University of Oregon

Lanzhou University, Lanzhou, China

DEGREES

Doctor of Philosophy in Physics, 2008, University of Oregon

Master of Science in Physics, 2002, Lanzhou University

Bachelor of Science in Physics, 1999, Lanzhou University

ACADEMIC INTERESTS

Critical Phenomena and Phase Transition, Field Theory

Strongly Correlated Systems

PROFESSIONAL EXPERIENCE

Research Assistant, Department of Physics, University of Oregon, Eugene,
2005-2008

Teaching Assistant, Department of Physics, University of Oregon, Eugene,
2002-2005

Teaching Assistant, Lanzhou University, Lanzhou, Gansu, China, 2000-2001

PUBLICATIONS

Qi Li, D. Belitz , and T. R. Kirkpatrick “Nearly ferromagnetic superconductors,”
Phys. Rev. B **74**, 134505 (2006)

Qi Li, J. Toner , and D. Belitz , “Elasticity and Melting of Skyrmion Flux
Lattices in p-Wave Superconductors,” Phys. Rev. Lett **98**, 187002 (2007)

Qi Li, J. Toner , and D. Belitz , ”Skyrmion versus vortex flux lattices in p
-wave superconductors” arXiv:0711.4154. (submitted to Phys. Rev. B)

ACKNOWLEDGMENTS

First of all, I would like to acknowledge the continuous support and guidance of my adviser, Dietrich Belitz. He taught me a lot of physics and mathematics. More importantly, as a foreign student, I learned the importance of communicating efficiently and clearly from him. I will never forget his patient editing of my conference talks and papers. His attitude toward physics research is so respectful that I am always stimulated to catch up with him.

I appreciate the help of John Toner, whose insightful ideas have had a great impact on my understanding of physics. I am constantly amazed by his ability to quickly come up with smart solutions for complicated problems. From him, I learned not only physics but also American jokes.

I would like to thank my teachers in the physics department. This includes Nilendra Deshpande, Paul Csonka and too many others to be listed here. Particularly, I appreciate the discussions after class with Nilendra. These really helped me understand the physics better.

I would also like to thank a few postdocs of Dietrich: Jörg Rollbühler, who discussed a lot of physics problems with me; Sumanta Tewari who gave me some good suggestion on the research project; Ronojoy Saha' who would always open his door to me and talk with me for hours.

And finally I would like to thank my family. I could never have made this far without my parents' continuous encouragements. Thanks also to my wife, Zheng Xu, my Ph.D life was never lonely.

TABLE OF CONTENTS

Chapter	Page
I. INTRODUCTION	1
1.1 Phase Transitions and Critical Phenomena	4
1.1.1 Mean Field Treatment	4
1.1.2 Fluctuations and the Renormalization Group	6
1.2 Magnetic Order	10
1.2.1 Heisenberg Model and O(n) Model	10
1.2.2 X-Y Model and Topological Phase Transition	12
1.3 Superconducting Order	14
1.4 Organization	19
II. NEARLY FERROMAGNETIC SUPERCONDUCTORS	21
2.1 Introduction	21
2.2 Phenomenological Arguments	23
2.2.1 Paramagnetic Systems	23
2.2.1.1 Thermodynamic Critical Field	24
2.2.1.2 London Penetration Depth	25
2.2.1.3 Critical Current	29
2.2.2 Systems at a Ferromagnetic Instability	30
2.3 Generalized Ginzburg-Landau Theory	32
2.3.1 LGW Theory for Superconducting and Magnetic Fluctuations	33
2.3.2 Effective Theory for Paramagnetic Superconductors	34
2.3.3 Superconductors at Magnetic Criticality	38
2.3.3.1 Thermodynamic Critical Field	38
2.3.3.2 Generalized London Equation	39
2.3.3.3 Penetration Depth, and Critical Current	42
2.3.3.4 Critical Field H_{c2}	43
2.4 Discussion and Conclusion	44

Chapter	Page
III. NATURE OF PHASE TRANSITION IN P-WAVE SUPERCONDUCTORS	50
3.1 Introduction	50
3.2 Model	51
3.3 Nature of The Phase Transition	53
3.3.1 Mean Field Approximation	53
3.3.2 Renormalized Mean-field Theory	55
3.3.3 ϵ -expansion about $d = 4$	56
3.3.4 $1/n$ -expansion in $d = 3$	60
3.4 Discussion and Conclusion	66
IV. SKYRMION IN P-WAVE SUPERCONDUCTORS	68
4.1 Introduction	68
4.2 Formulation of the Skyrmion Problem	71
4.2.1 The Action in The London Approximation	71
4.2.2 Saddle-point Solutions of the Effective Action	74
4.2.2.1 Meissner Solution	75
4.2.2.2 Vortex Solution	76
4.2.2.3 Skyrmion Solution	78
4.3 Analytic Solution of the Single-skyrmion Problem	80
4.3.1 Zeroth Order Solution	81
4.3.2 Perturbation Theory for $R \gg 1$	82
4.3.3 Energy of a Single Skyrmion	85
4.3.4 Spectral Methods	87
4.4 Observable Consequences of the Skyrmion Energy	90
4.4.1 $B(H)$ for a Skyrmion Lattice	91
4.4.2 Elastic Properties of the Skyrmion Lattice	92
4.4.3 μ SR Signature of a Skyrmion Flux Lattice	98
4.5 Conclusion	101
APPENDICES	
A. INTEGRAL FORMULAS USED IN CHAPTER III	102

Chapter	Page
B. MISCELLANEOUS TECHNIQUES IN CHAPTER IV	103
B.1 Properties of Orthogonal Unit Vectors	103
B.2 Solutions of the ODEs for g and h	103
B.3 Contributions to E_s	105
BIBLIOGRAPHY	107

LIST OF FIGURES

Figure	Page
1.1 Phase diagram of water and two paths for two different kinds of phase transitions.[1] See the text for additional information.	2
1.2 Mean field phase diagram of type I and type II superconductors. See the text for additional information.	19
2.1 Magnetic induction schematically as a function of position at a vacuum (V) - normal metal (N) - superconductor interface (S) (a), and at a vacuum - superconductor interface (b).	26
2.2 Schematic phase diagram showing a normal metal (NM), a ferromagnet (FM), a superconductor (SC), and a ferromagnetic superconductor (FMSC) in a temperature (T) - control parameter (x) plane. The solid line denotes the superconducting transition, the dashed line, the magnetic one. Along $x = 0$ there is only one phase transition at the superconducting T_c . See the text for additional explanation.	46
2.3 Same as Fig. 2.2, but with a magnetic transition for $x = 0$ at a temperature $T_m < T_c$. On the $x = 0$ axis it is shown that T_m splits into the bare magnetic transition temperature T_m^0 and the physical transition temperature T_s to a state with spiral magnetic order, Ref.[2]. See the text for additional explanation.	47
3.1 Mean-field phase diagram of a p -wave superconductor as described by Eq. (3.1). See the text for additional information.	54
3.2 Vertices from Eq. (3.3). Solid lines denote the ψ field and dashed lines its complex conjugate. Wavy lines denote the vector potential. Dotted lines separate the localized interaction between paired electrons.	57
3.3 Diagrams renormalize the coupling parameters	57
3.4 Diagrams renormalize the coupling parameter u	58

Figure	Page
3.5 Renormalization group flows for $n=500$. The top right fixed point is stable in the u - v plane, so it is the critical fixed point	59
3.6 All the self energy graphs contribute to the critical exponent. The first row is from the ungauged part and the second row is from gauged part.	61
3.7 Dressed coupling parameter and renormalized photon propagator.	63
4.1 External field (H) vs. temperature (T) phase diagram for vortex flux lattices. Shown are the Meissner phase, the vortex lattice phase, the vortex liquid, and the normal state. Notice that the vortex lattice is never stable sufficiently close to H_{c1}	69
4.2 Order parameter configurations showing a vortex (a), and a skyrmion (b). The local order parameters are represented by arrows on loci of equal distance from the center of the defect. If the order parameter space is two-dimensional, only vortices are possible, and there is a singularity at the center of each vortex, (a). If the order-parameter space is three-dimensional, a skyrmion can form instead, where the spin direction changes smoothly from “down” at the center to “up” at infinity, (b).	70
4.3 Configurations of the vectors $\hat{\ell}$, \hat{m} , and \hat{n} in a Meissner phase. All three vectors point in the same direction everywhere.	76
4.4 Configurations of the vectors $\hat{\ell}$, \hat{m} , and \hat{n} for a vortex. $\hat{\ell}$ is constant, whereas \hat{m} and \hat{n} rotate about the vortex core. Notice that the vector shown in Fig. 4.2(a) is \hat{n}	77
4.5 Configurations of the vectors $\hat{\ell}$, \hat{m} , and \hat{n} for a skyrmion. Notice that the vector shown in Fig. 4.2(b) is $\hat{\ell}$	82
4.6 Numerical data for the energy per skyrmion per unit length (circles) together with the best fit to a pure $1/R$ behavior (dashed line) from Ref. [3], and the perturbative analytic solution given by Eq. (4.34) (solid line). A numerical solution using spectral methods is indistinguishable from the perturbative one.	88
4.7 Shearing of the skyrmion lattice results in a change in the distance between skyrmion centers, and hence in their effective interaction. See the text for additional information.	94

Figure	Page
4.8 External field (H) vs. temperature (T) phase diagram for skyrmion flux lattices. In contrast to the vortex case, see Fig. 4.1, there is a direct transition from the skyrmion flux lattice to the Meissner phase. The theory predicts the shape of the melting curve only close to T_c , see Eq. (4.61); the rest of the curve is an educated guess.	98

CHAPTER I

INTRODUCTION

A material can exhibit various phases under different physical conditions. An obvious example is that water can be in the solid, liquid, or gas phase in different temperature regions. Different phases can be characterized by different symmetries which reflects different orders. In the solid phase of water, it has crystal symmetry which defines discrete periodic lattice order. In the liquid or gas phase, water has continuous rotational and translational symmetry. As we can see from this simple example, phase transitions exist in nature. There are two kinds of phase transitions in this example, a discontinuous phase transition, and a continuous phase transition. Everyday experience tells us that, during the process of ice melting or water evaporation, heat has to be transferred to let the processes continue. This heat is called latent heat and is always associated with a discontinuous phase transition which is also referred to as a first order phase transition. As shown in the Fig. 1.1, an arbitrary path *A* which crosses the liquid-gas coexistence curve will lead to an abrupt density change. However, at the critical point with a pressure of about $2.2 \times 10^8 Pa$ and a temperature of about 647K, there is no way to distinguish the liquid phase from the gas phase because they are at the same density. Any path in the phase diagram, which goes right through the critical point, for instance, path *B* will have no latent heat. This kind of phase transition is usually called continuous phase transition or second order phase transition. In this example, the density difference between liquid and gas characterizes the phase transition and is called order parameter. Water has some critical phenomena which are very fascinating. One of them is called critical opalescence. Close to the phase transition point, there are regions of larger or lesser

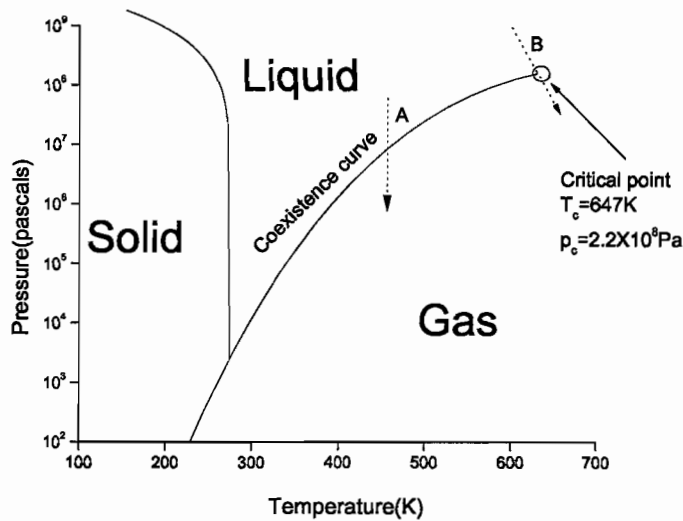


FIGURE 1.1: Phase diagram of water and two paths for two different kinds of phase transitions.[1] See the text for additional information.

densities. We can define the coherence length ξ to be the mean distance between two nearest higher density regions. If we follow the path *B* in the Fig. 1.1, the liquid phase coherence length will increase from a few interatomic distance to a few hundred nanometers when the water gets closer to the critical point. This length scale is comparable to the visible light wavelength, so light scattering increases dramatically. Then the system looks “milky”. Finally, exact at the critical point, the coherence length diverges and water looks homogeneous. In short, when the order parameter changes continuously from zero to non-zero by changing a control parameter, it is called a continuous phase transition. Otherwise, it is called discontinuous phase transition. Here, we will present a few more examples of continuous phase transitions.

Besides order defined in real space mentioned above, order can also occur in spin space, leading to magnetic order. Such order comes from the electrons’ spin interaction effect. In the ferromagnetic exchange interaction case, spins tend to align parallel to each other to minimize the free energy at a sufficiently low temperature.

This leads to a ferromagnetic ground state. This ground state breaks the spin rotational symmetry and is reflected by the well known fact that magnetic materials will have a non-zero magnetization below the critical Curie temperature. So the magnetization is the natural order parameter for the ferromagnet to paramagnet transition.

In addition to the spin-spin interaction between electrons, there is an electron-phonon interaction which can lead to a ground state of electron pairs which have antiparallel spins (singlet pairing) and are called Cooper pairs. These bounded pairs account for the mechanism of superconductivity, and the pairing wave function for Cooper pairs can be used as the order parameter for the normal metal to superconductor phase transition.

An interesting question is whether superconducting order and magnetic order can coexist? Naively speaking, ferromagnetic order tries to align the spins of electrons, whereas superconducting order wants the spins of the Cooper pair antiparallel. These two effects seem irreconcilable. However, experiments do show possible coexistence of ferromagnetism and superconductivity[4]. Furthermore, mean field phase boundaries have been proposed for the s-wave ferromagnetic superconductors. It was suggested that coexisting superconducting and magnetic order might simultaneously appear via a continuous phase transition, but nobody has seriously looked into the magnetic critical region. This situation is proposed to be relevant to explaining a recent experiment on the material MgCNi_3 . We will discuss this issue in Chapter II by a mean field treatment and scaling analysis of the continuous phase transition.

Another candidate for the coexistence of the two competing orders is p-wave superconductors. In this case, electrons show triplet pairing instead of conventional singlet pairing. Triplet pairing leads to Cooper pairs with parallel spins. An example is the ABM state in superfluid ^3He . One would expect that a similar situation can also occur for the charged superfluid case, that is, for electrons in metals.

1.1 Phase Transitions and Critical Phenomena

Continuous phase transitions and critical phenomena have been an interesting topic for the last few decades. A continuous phase transition occurs when a symmetry of the system is spontaneously broken at some value of a control parameter, for instance, temperature. We will start with a well known example, the Ising model with Z_2 symmetry, then we will discuss more general magnetic systems like the $O(3)$ Heisenberg model and the X-Y model. Finally, critical phenomena in s-wave superconductors and p-wave superconductors will be briefly discussed.

1.1.1 Mean Field Treatment

The Hamiltonian for a spin system can be written in the following form

$$H = - \sum_{\langle i,j,\alpha \rangle} J^\alpha S_i^\alpha S_j^\alpha \quad (1.1)$$

Here, the indexes i and j denote the lattice points where spins are situated, and α denotes the spin component. $\langle \dots \rangle$ means only the nearest spin neighbors will be summed over and J^α is the coupling strength between nearest neighbors. Here, we will discuss classical spins only, so spins take the values of real vector variables.

For the Ising model, the spin variable can only take the values of ± 1 which means spin up or down. Correspondingly, only one component J^α in Eq. (1.1) is nonzero. Such a simplified model has Z_2 symmetry and is often realized by the crystal-field effects. If the coupling constant J is positive, the minimum energy configuration is obvious: spins point in the same direction. This leads to a non-zero magnetization M which is called the ordered phase. Landau introduced the concept of the order parameter (O.P) to describe continuous phase transitions. A zero O.P corresponds to the disordered phase and a non-zero one to the ordered phase. The Landau free energy concept is based on this idea. Because the order parameter changes value continuously from zero to non-zero at the phase transition, it must be very small

near the transition point. Then the Landau free energy can be expanded as a scalar function of the order parameter and must have invariance properties corresponding to the symmetry of the disordered system. For the Ising model, the O.P is the magnetization and the Landau free energy takes the form

$$f = \frac{1}{2}tM^2 + uM^4 - h \cdot M \quad (1.2)$$

Here, h denotes an external magnetic field, and for $h = 0$, the Landau free energy indeed is invariant under spin inversion. $t = (T - T_c)/T_c$ is the distance from the phase transition point, where its value changes from positive to negative. u is another parameter that must be positive in order to have a continuous phase transition. In field theory language, the tM^2 term is also referred to as the mass term, and the u term as the potential energy term which accounts for the interaction between particles. From this Landau energy, the behavior of some physical observables can be predicted. In the absence of an external field h , if t is positive, to minimize the Eq.(1.2), $M = 0$ has to be satisfied. This is the disordered phase where spins point in random directions. If t is negative, the optimal M to minimize f is

$$M = \sqrt{\frac{-t}{4u}} \quad (1.3)$$

which describes a magnetically ordered phase. Throughout the following discussion, t is assumed to be negative if not explicitly defined otherwise.

From the Landau energy, some critical exponents can be extracted. For instance, β describes the temperature dependence of the order parameter via $M \propto (-t)^\beta$. From Eq.(1.3), $\beta = 1/2$ is predicted for Ising systems. There are several other critical exponents, for instance, γ and δ , which are defined as the temperature dependence of the magnetic susceptibility and the field dependence of the magnetization via $\chi \propto |t|^{-\gamma}$ and $M(t = 0) \propto h^{1/\delta}$, respectively. These two can be deduced from

the equation of state

$$tM + 4uM^3 = h \quad (1.4)$$

which is obtained from minimizing f in Eq.(1.2). The magnetic susceptibility χ is defined as

$$\chi = \frac{\partial M}{\partial h} \quad (1.5)$$

From Eq. (1.4), we get $\chi = 1/|t|$, which implies $\gamma = 1$. Finally, the dependence of M on the external field h at the phase transition point ($t = 0$) is,

$$M = \left(\frac{h}{4u}\right)^{1/3} \quad (1.6)$$

So the critical exponent δ is 3. In the real 3d Ising systems, $\beta \sim 0.33$, $\gamma \sim 1.2$, $\delta \sim 4.3$. This discrepancy between the prediction of mean field theory and the observed values of the critical exponent will be further discussed in the following sections.

1.1.2 Fluctuations and the Renormalization Group

Mean-field theory correctly describes the qualitative features of continuous phase transitions, but it may not be sufficient to describe the system more accurately. For instance, thermal fluctuations can drive the system away from its mean field configuration and may even destroy the phase transition. This can be seen from the following arguments. To take into consideration fluctuations, the order parameter must be a spatially dependent field. To account for how the O.P field can fluctuate from point to point, a spatial derivative has also to be included in the free energy density. So the fluctuating Landau energy density is

$$f(\mathbf{x}) = \frac{1}{2}tM(\mathbf{x})^2 + uM(\mathbf{x})^4 + \frac{c}{2}\nabla M(\mathbf{x})^2 \quad (1.7)$$

It should be noted that there is a characteristic length scale in Eq.(1.7). By comparing the dimension of the first term and the third term, a coherence length

is defined as $\xi = \sqrt{c/|t|}$. This length characterizes the distance over which O.P can not change too much. At the phase transition, ξ diverges, meaning a spatially homogeneous state.

Now the question is: when are the fluctuations large enough to lead to a breakdown of the mean field results? This question can be answered simply by comparing the fluctuation effects to the mean field results. [5] The fluctuation is defined as $\delta M(\mathbf{x}) = M(\mathbf{x}) - M$. Here M is the mean field value as stated in Eq. (1.3) and $M(x)$ is the fluctuating field which can vary from its mean value by an amount of $\delta M(x)$. Now the spatially averaged fluctuation is

$$V_\xi^{-2} \int_{V_\xi} d^d x d^d x' \langle \delta M(x) \delta M(x') \rangle \sim T \xi^{-(d-2)} / c \quad (1.8)$$

Here, $V_\xi \propto \xi^d$ is the characteristic volume of the system. The $\langle \dots \rangle$ means a thermal average of the function in the brackets. By doing the average with the Gaussian approximation of Eq. (1.7), we get the approximate relation in Eq. (1.8). It can be seen the dimensionality plays an important role in the phase transition. This is because for a continuous phase transition, the coherence length must diverge at phase transition point. So if the spatial dimension is less than 2, fluctuations according to Eq. (1.8) are too large to allow for a finite temperature continuous phase transition. Thus $d_{lc} = 2$ is usually called lower critical dimension. Comparing Eq. (1.8) to the mean field result $M^2 = |t|/4u$, we immediately get the criteria for the mean field theory to be valid: it is a spatial dimension $d > d_{uc} = 4$. This means that for physical systems in 3d, we have to take the fluctuations into account.

Before we look into the treatment of these fluctuations in detail, we first discuss the scaling hypothesis which can successfully relate the critical exponents with a few assumptions.[6]The static scaling hypothesis states that the free energy density is a generalized homogeneous function of the experimental control parameters, for instance, reduced temperature t and magnetic field H ,

$$f(s^{a_t}t, s^{a_H}H) = sf(t, H) \quad (1.9)$$

Here, s is an arbitrary number which is called factor of scale transformation. a_t and a_H are exponents which can be related to the critical exponents introduced in the previous section. For instance,

$$\beta = \frac{1 - a_H}{a_t} \quad (1.10)$$

Though the scaling hypothesis can interpret all the critical exponents in terms of a_t and a_H , it can not tell anything about their values. However, it does exploit the properties of the system under scale transformations. This is crucial for understanding the phase transition and is the base for the renormalization group concept.

Now we can have a close look at how the free energy Eq. (1.7) changes under scale transformations. From statistical physics, the probability for a system to have a particular configuration is proportional to its Boltzmann factor

$$P[f(\mathbf{x})] \propto e^{-\int f(\mathbf{x})d\mathbf{x}/T} \quad (1.11)$$

Here, the free energy is $F = \int f(\mathbf{x})d\mathbf{x}$. Now such a probability can be transformed under a scale transformation of $f(x)$. This can be seen by introducing a parameter space which is spanned by all the parameters in Eq. (1.7),

$$\mu = (t, u, c) \quad (1.12)$$

Firstly, we perform a coarse graining procedure of the original $f(\mathbf{x})$ which is generally referred to as a Kadanoff transformation. In Fourier space, this transformation can simply be expressed as the following equation.

$$e^{-F^r[M(k)]/T} = \int e^{-F[M(k)]/T} \prod_{\Lambda > k > \Lambda/s} DM_k \quad (1.13)$$

Here, Λ is an ultraviolet cutoff, and s is a scale factor which is taken to be larger than 1, with DM_k the functional integral measure. This functional integral is treated as a perturbed Gaussian integral. The integral over the momentum shell $\Lambda > k > \Lambda/s$ corresponds to a scale transformation for the lattice constant $a \rightarrow sa$. This means that F^r is a free energy for a larger spin block system than the original system. To recover the size of the original system, a second scale transformation has to be applied. It is defined as,

$$\begin{aligned} a &\rightarrow a/s \\ M &\rightarrow M\zeta \end{aligned} \tag{1.14}$$

Here, ζ is a parameter which is called the rescaling parameter of field and can be chosen to let some parameter remain fixed under the scale transformation, for instance c . After those two steps of transformation, a new set of parameters can be written as

$$\mu' = (t', u', c') \tag{1.15}$$

This set of new parameters is called renormalized parameters. “Unimportant” information has been eliminated (integrated out) in the renormalization process. It is natural to ask what the result is when the above two processes have been repeated over and over? A simple answer is that it will reach a fixed point in the parameter space. Let R be the renormalization processes defined as above, then a point in the parameter space evolves under the renormalization process,

$$\mu' = R\mu \tag{1.16}$$

As can be seen from Eq.(1.13) and Eq.(1.16), the operator R must be some complicated functions whose arguments are the parameters defined in Eq.(1.15)

together with the scale factor s . If the scale factor s is taken to be infinitesimally close to 1 and the renormalization process is repeated infinitely many times, it can be shown that Eq.(1.16) reduces to a set of ordinary differential equations(ODEs). This set of ODEs will be referred to as flow equations.

These flow equations have a natural ending point, which is a fixed point that satisfies $\mu^* = R\mu^*$. In another word, it is invariant under renormalization. It is not hard to see that fixed point $(u^*, r^*) = (0, 0)$ will always appear. This is due to the fact that a Gaussian action remains Gaussian under renormalization. Such a fixed point is sometimes called a trivial fixed point. All of the critical exponents are related to properties of the flow equations in the vicinity of a fixed point. This will be shown explicitly in the following section and in Chapter III.

1.2 Magnetic Order

1.2.1 Heisenberg Model and O(n) Model

An extension of the Ising models for magnets is the Heisenberg model. Since spins have three components, the order parameter for a Heisenberg magnet is naturally a vector in spin space denoted by \mathbf{M} . Now the free energy must be invariant under the group $O(3)$, so it reads as,

$$f(\mathbf{x}) = \frac{1}{2}t\mathbf{M}_\alpha(\mathbf{x})\mathbf{M}_\alpha(\mathbf{x}) + u\mathbf{M}_\alpha(\mathbf{x})\mathbf{M}_\alpha(\mathbf{x})\mathbf{M}_\beta(\mathbf{x})\mathbf{M}_\beta(\mathbf{x}) + \frac{c}{2}\partial_i\mathbf{M}_\alpha(\mathbf{x})\partial_i\mathbf{M}_\alpha(\mathbf{x}) \quad (1.17)$$

Here, α and β are the spin indexes and range from 1 to n , with $n = 3$. i is the spatial index and takes values from 1 to the spatial dimension d . More generally, we will consider models when n can be any integer and d can be any positive real number.

The mean field result of Eq.(1.17) is, $\mathbf{M}(\mathbf{x}) = 0$ for positive t . This corresponds to the disordered state. For negative t , $\mathbf{M}(\mathbf{x}) = \sqrt{\frac{-t}{4u}}\hat{n}$. Here, \hat{n} is an arbitrarily

chosen unit vector in spin space. This mean-field result is almost the same as for the Ising model we discussed in the last section, and thus will not change the critical exponents. So within the mean field approximation, it seems that magnetic systems have universal critical exponents that are independent of n and d . However, if we do the renormalization process described in last section for the $O(n)$ model, we get different results. The flow equations for the parameters of the Eq. (1.17) are[1]

$$\begin{aligned}\frac{dt(l)}{dl} &= 2t(l) + 4k_d(n+2)\frac{u(l)}{1+t(l)} \\ \frac{du(l)}{dl} &= \epsilon u(l) - 4k_d(n+8)\frac{u^2(l)}{(1+t(l))^2},\end{aligned}\quad (1.18)$$

Here, $s = 1 + dl$ is the factor of scale transformation through every renormalization process and $\epsilon = 4 - d$ is the parameter that controls the perturbation expansion of Eq.(1.13), with k_d a positive constant for any fixed spatial dimension. For convenience, we have chosen the rescaling parameter $\zeta^2 = s^{(d+2)}$ to keep the parameter c fixed. Besides the trivial Gaussian fixed point $((u^*, r^*) = (0, 0))$, there is an order of ϵ fixed point which reads

$$\begin{aligned}u^* &= \frac{\epsilon}{4(n+8)k_d}, \\ t^* &= \frac{-(n+2)}{2(n+8)}\epsilon.\end{aligned}\quad (1.19)$$

The following arguments can be derived from the above relation. Firstly, the negative value of t^* and positive value of u^* are in the expected region of mean field result, thus make perfect sense for the continuous phase transition. Secondly, fixed point values are very close to the Gaussian fixed point which is consistent with the spirit of perturbation expansion. Thirdly, the remarkable feature of those fixed points is that they depend only on the spatial dimension and the field dimension.

Whereas mean-field theory predicts that the critical behavior is independent of these parameters, this result clearly states that fluctuations violate the mean field prediction and cause a diverse world of magnetic orders.

It should also be noted that if ϵ is negative, as a result of spatial dimension is larger than 4, from Eq.(1.19), u^* is negative! This observation doesn't necessarily mean there must be a first order phase transition. Actually, the trivial Gaussian fixed point is stable and all the critical exponents recover the mean field values. Here, stability of a fixed point is defined whether the flow near it will be attracted in or expelled out. In the vicinity of a stable fixed point, there is unique direction (qualitatively about t direction) which will guide the flow to either a positive t region (higher temperature, disorder phase) or a negative t region (lower temperature, ordered phase), whereas from all the directions, flows will be attracted to the fixed point.

We focus on the $d < 4$ case. So critical exponents can be extracted from those non-trivial fixed points by the method introduced by [7]. We only list some of them for future reference,

$$\beta = 1/2 - \frac{3\epsilon}{2(n+8)},$$

$$\gamma = 1 + \frac{(n+2)\epsilon}{2(n+8)} \tag{1.20}$$

$$\delta = 3 + \epsilon \tag{1.21}$$

For $d = 3$ ($\epsilon = 1$), these predicted critical exponents fit the experimental values much better than the mean field values. As ϵ goes to zero, the system behaves more mean field like.

1.2.2 X-Y Model and Topological Phase Transition

The X-Y model is the model from the above discussion with $n = 2$. For a long time it was thought to be nothing more than an anisotropic Heisenberg model. Namely,

the exchange coupling constant J^α has only two non-zero components. This can be realized by a crystal field in a plane. So the results for the $O(n)$ model in the last section are still valid. However, a novel topological phase in this model was discovered in 1973[8]. Here, we will briefly introduce the concept of topological phase transitions. This will be revisited in Chapter III.

The $O(2)$ model has two independent real valued components of the O.P and is equivalent to a $U(1)$ field description. So we can write the $O(2)$ order parameter as $\psi(x)e^{i\phi(x)}$, where $\psi(x) \in R$ is the amplitude of the complex field and $\phi(x)$ is the phase which takes values in the range $[0, 2\pi]$. It should be noted that $\phi(x)$ can also be interpreted as the angle between nearest neighbor spins. If we keep the amplitude of the field fixed equal to the optimal mean field value and only consider the fluctuations of the phase, we get a free energy density

$$f(\mathbf{x}) = \frac{c}{2} \nabla \phi(\mathbf{x})^2 \quad (1.22)$$

Minimization of this free energy requires

$$\nabla^2 \phi(\mathbf{x}) = 0 \quad (1.23)$$

A trivial solution is $\phi(\mathbf{x}) = const$, which corresponds to a configuration where spins align everywhere. This is the ground state. However, there are other possibilities. For instance, in dimension 2, we can add a source term on the right hand side of Eq. (1.23) to describe a non-differentiable angle ϕ at $x = 0$ which can also be interpreted as a topological point defect.

$$\nabla^2 \phi(\mathbf{x}) = 2\pi Q \delta(\mathbf{x}) \quad (1.24)$$

Here δ is the Dirac delta function in 2d. If we interpret $\phi(\mathbf{x})$ as the electrostatic potential, this equation is exactly the 2d Poisson equation which describes a Coulomb problem with Q as the charge. Q must be an integer because $\phi(x)$ is periodic. Due

to this reason, Q is usually called the topological charge number or winding number or fluxoid number in the superconductor context.

A solution to Eq. (1.24) can be easily obtained and the corresponding free energy is proportional to $\log[R]$, where R is the size of the defect. This is larger than the ground state energy. However, the energy cost to align all the spins in the same direction (i.e, to destroy the defect) is of order R which is much larger than the defect energy $\log[R]$ if R is large. This leads to the conclusion that the defects are stable. Correlation functions of such topological excitations can also be calculated which show an algebraically decay. To distinguish this from long range order, when correlation functions do not decay at all, such order is often referred to as quasi-long-range order. In other words, at some finite temperature, topological defects will appear and cause a weakly correlated system. This kind of phase transition is called Kosterlitz-Thouless transition and it is a particular example of a topological phase transition.

1.3 Superconducting Order

The microscopic mechanism for conventional superconductivity was explained by the famous BCS theory. The wave function $\psi(\mathbf{x})$ for the Cooper pairs can be considered the order parameter, with $|\psi(\mathbf{x})|^2$ the density of Cooper pairs. In the simplest case, $\psi(\mathbf{x})$ is a complex scalar, which means that the electrons forming pairs have opposite spins (spin singlet case), so the total spin of a pair is zero. Besides spin, Cooper pairs also carry charge and therefore couple to photons. This can be described as follows. The gradient of the wave function is usually interpreted as a velocity in quantum mechanics. For the charged Cooper pairs, it is a charge current and naturally will couple to the photon field. So the free energy for the s-wave

superconductors is,

$$F = \int d\mathbf{x} \left[\frac{1}{2m} |(\nabla - iq\mathbf{A}(\mathbf{x}))\psi(\mathbf{x})|^2 + \frac{t_1}{2} |\psi(\mathbf{x})|^2 + \frac{u_1}{4} |\psi(\mathbf{x})|^4 + \frac{1}{8\pi} \mathbf{B}^2(\mathbf{x}) - \frac{1}{4\pi} \mathbf{H}(\mathbf{x}) \cdot \mathbf{B}(\mathbf{x}) \right]. \quad (1.25)$$

Here, \mathbf{A} is the vector potential and \mathbf{H} is the external field, with q the charge of the Cooper pair, and $\mathbf{B} = \nabla \times \mathbf{A}$ is the magnetic induction. The first term in the above equation is usually called the supercurrent energy, the second and third terms are called the condensation energy. The fourth term is the magnetic energy of a superconductor in the absence of an external field, and the fifth term is a magnetic energy in an external field. The difference between those two kinds of magnetic energy is that the first one denotes the self property of a superconductor, namely the U(1) gauge symmetry requires this term to be present, whereas the latter is due to the interaction energy between the superconductor and the external field. In the coefficient of the magnetic energy, we have included the vacuum magnetic permeability μ_0 and we choose cgs units to let it be 1. We will see in Chapter II that this coefficient can be renormalized by coupling the magnetization to the superconducting O.P. It is easy to check that the above free energy is invariant under local gauge (U(1)) transformations,

$$\begin{aligned} \mathbf{A} &\rightarrow \mathbf{A} + \nabla\Lambda(\mathbf{x}) \\ \phi(\mathbf{x}) &\rightarrow \phi(\mathbf{x}) + q\Lambda(\mathbf{x}) \end{aligned} \quad (1.26)$$

Here, $\phi(\mathbf{x})$ is the phase of the complex order parameter $\psi(\mathbf{x}) = |\psi(\mathbf{x})|e^{i\phi(\mathbf{x})}$, and $\Lambda(\mathbf{x})$ is an arbitrary scalar field. Since this kind of order parameter has been discussed in the context of X-Y model, it is natural to think that s-wave superconductors

have the same topological defects as we have seen in the last section, and that such topological defects may play a role in the phase transition of superconductors.

The ground state of Eq. (1.25) is $\psi_0 = \sqrt{\frac{-t_1}{u_1}}$ at zero external field. The corresponding magnetic induction $\mathbf{B}(\mathbf{x})$ decays exponentially with a characteristic penetration depth λ which sets the length scale for the magnetic induction to drop to zero

$$\lambda = \sqrt{m/(4\pi q^2 \psi_0^2)}. \quad (1.27)$$

Hence, the superconductor expels magnetic flux. This is called the Meissner phase. If the amplitude of the order parameter is kept fixed at ψ_0 , and only the fluctuations of phase $\phi(\mathbf{x})$ are allowed, then the saddle point equation for the magnetic induction can be fully decoupled from the one for the amplitude of order parameter. This approximation is usually called London approximation. The corresponding London equation reads

$$\nabla^2 \mathbf{B}(\mathbf{x}) - \mathbf{B}(\mathbf{x})/\lambda^2 = -\Phi_0/\lambda^2 \nabla \times \nabla \phi(\mathbf{x}) = -\Phi_0/\lambda^2 \delta(\mathbf{x}) \quad (1.28)$$

To get the second “=” in the Eq.(1.28), we assume there is an external field which is applied in the z direction. In this case, the system has a cylindrical symmetry, so phase $\phi(\mathbf{x})$ can be interpreted as the polar angle, where \mathbf{x} is confined to the $x - y$ plane, with $\Phi_0 = hc/2e$ the flux quantum in SCI units. This equation is similar to Eq. (1.24). However, the physical meaning of a defect at $\mathbf{x} = 0$ is a fully penetrated magnetic field. The solution of above equation is called a single vortex which is a zeroth-order Hankel function of imaginary argument. It decays exponentially for large $|\mathbf{x}|$, which means vortices have a short range interaction.

There is another length scale in the free energy which can be defined by comparing the terms quadratic in $\psi(\mathbf{x})$ in Eq.(1.25), $\xi = \sqrt{1/m|t_1|}$. This length scale sets the characteristic distance for superconducting order to drop to zero.

Besides these length scales, there are also two important energy scales. From experiment, it is known that too strong an external magnetic field can destroy the superconductivity even at very low temperature. This can be explained from Eq. (1.25) by comparing the condensation energy and the magnetic energy. If the magnetic energy dominates, the current induced by the magnetic induction can destroy Cooper pairs and is referred to as a depairing current. Then the system must be in the normal state. We will see this point more clearly in Chapter II.

These two energy scales compete with each other as a function of temperature and magnetic field. If the condensation energy is larger, the system is superconducting, when the magnetic energy is larger, the system will be in the normal state. The two energy scales being equal defines a field scale $H_c(T)$ which is known as the thermodynamic critical field. For field strength below H_c , the superconducting state will presumably be found. However this is not always the case, as will be seen in the next few paragraphs.

It is also helpful to compare the two length scales defined above and define a dimensionless parameter $\kappa = \lambda/\xi$. If κ is much less than 1, therefore the correlations of magnetic induction can be ignored and the system is dominated by the condensation energy, so the Meissner phase is realized. If κ is much greater than 1, the magnetic energy is dominant. In this case, to minimize the free energy, $\psi(\mathbf{x})$ can be treated in the London approximation. This is exactly the same situation as we have discussed for the topological phase in the X-Y model in connection with Eq. (1.24). The above two cases are usually categorized as type I and type II superconductors. More careful analysis shows that $\kappa = 1/\sqrt{2}$ separates these two cases[9]. Though fluctuations can induce these vortices, only an external field can stabilize them. The minimum external field required to induce a single vortex is called lower critical field H_{c1} . It can be found by comparing the free energy of a system with no flux at just below H_{c1} with the free energy just above H_{c1} from Eq. (1.25). By comparing energies in the two cases, in the large κ limit, H_{c1} is

$$H_{c1} = \frac{H_c}{\sqrt{2}\kappa} \log \kappa \sim (\Phi_0/\lambda^2) \log \kappa \quad (1.29)$$

This result can also be made plausible as follows. Because flux lines are far apart from each other, and each carries a fluxoid with an length scale λ , the natural guess from dimension analysis is $H_{c1} \sim \Phi_0/\lambda^2$. From this relation, it can be seen even at the field lower than the thermodynamic critical field H_c , flux lines can penetrate superconductors, so the superconductivity is not as strong as one would expect for type II superconductors.

Careful analysis of the magnetic induction by solving the Ginzburg-Landau(G-L) equations which minimize the free energy given by Eq.(1.25) shows that close to H_{c1} , the magnetic induction is $B \sim \log(H - H_{c1})^{-2}$. [9] This relation shows that B is continuous at H_{c1} . This indicates a continuous phase transition at H_{c1} . However, some experiments show a B-H curve that is not continuous as predicted by the G-L argument given here. The discussion of this point is beyond the scope of this thesis and can be found elsewhere [9]. The last relevant concept for this thesis in the context of type II superconductors is the upper critical field H_{c2} . A field strength stronger than H_{c2} will destroy superconductivity totally. However, for a field slightly below H_{c2} , the flux lines have a large density and overlap each other. Though H_{c2} can be calculated from G-L theory, a simpler estimate can be obtained as follows. Because ξ measures the core size of a single flux line which is also the minimum size of a flux defect, if neighboring flux lines are too close together and reach the minimum distance- ξ they can afford, then the superconductivity breaks down. This immediately leads to the conclusion $H_{c2} \sim \Phi_0/\xi^2$. A more careful calculation from G-L theory gives the result $H_{c2} = \Phi_0/2\pi\xi^2$. The upper critical field is the nucleation field for the Cooper pairs and type II superconductors will have a continuous phase transition at this point.

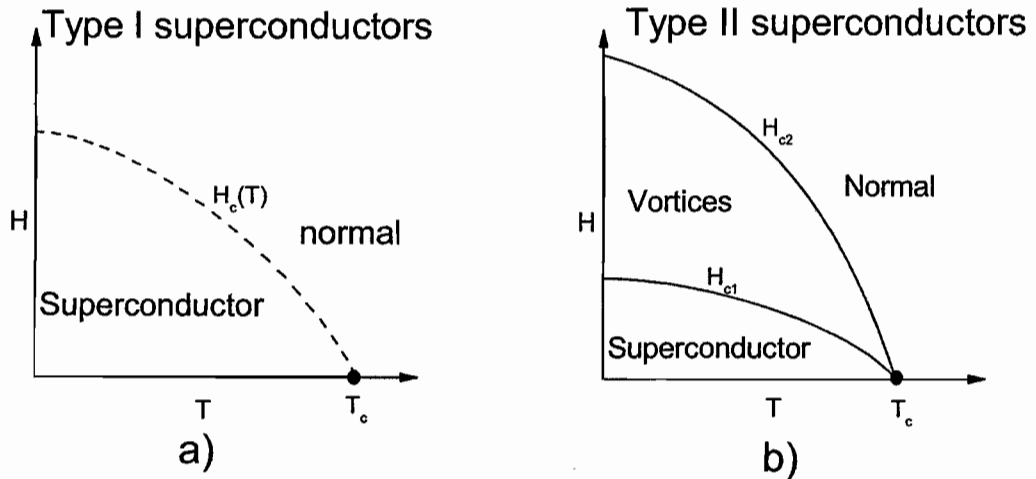


FIGURE 1.2: Mean field phase diagram of type I and type II superconductors. See the text for additional information.

Now we summarize the phase transitions in an external field in Fig. 1.2, For type I superconductors, H_c has the physically most important meaning, and a first order phase transition occurs at this field strength. For type II superconductors, only H_{c1} and H_{c2} make physical sense at which continuous phase transitions occur.

1.4 Organization

This dissertation is organized as follows. Chapter II will focus on the coexistence of ferromagnetic and magnetic order in the s-wave superconductors. By using the static scaling hypothesis and critical exponents for the magnetic system, we will discuss an unconventional behavior of the temperature dependence of the critical current. This is relevant to understanding an experiment on the material MgCNi_3 . This work has been published as Ref. [10] with Dietrich Belitz and Theodore R. Kirkpatrick. We independently derived all the equations almost at the same time.

Chapter III is a study of the nature of the phase transition in p-wave

superconductors. Renormalization group method and large n expansion techniques will be applied to attack the problem. These techniques strongly suggest that p-wave superconductors have a weakly first order phase transition. However, in a generalized model of p-wave superconductors, we find a new class of fixed points which suggests that p-wave superconductors have novel topological excitations.

Chapter IV investigates skyrmion lattices in p-wave superconductors. Firstly, we invent an unusual perturbation method to solve the skyrmion configuration in the London approximation for the p-wave case. Then magnetic properties, for instance, the magnetization curve and the melting curve are predicted to distinguish skyrmions from Abrikosov vortices. Finally, we point out that μSR experiments can be applied to distinguish these two topological excitations. A short version of this work has been published in Ref. [11] and a longer paper is available as Ref. [12]. This work is a result of a close collaboration with Dietrich Belitz and John Toner, who contribute about the 2/3 of the total workload.

Some technical points are given in the appendices.

CHAPTER II

NEARLY FERROMAGNETIC SUPERCONDUCTORS

2.1 Introduction

The work presented in this chapter has been previously published in Ref.[10] with coauthors D. Belitz and T. R. Kirkpatrick.

The coexistence of ferromagnetism and superconductivity was predicted[2, 13, 14] and observed,[15, 16] later it received renewed interest in the context of experimental observations in rare earth borocarbides.[17] More recently, interest in this subject has been revived by the observation of coexisting superconductivity and ferromagnetism in UGe_2 [18, 19] and $URhGe$,[20] where both types of order are believed to be due to electrons in the same band. Recent theoretical attention has centered on the structure of the phase diagram,[21] on the existence of spontaneous flux lattices,[17, 22, 23] and on the question of spin-triplet versus spin-singlet superconductivity.[24]

In contrast, less is known about the properties of superconductors on the paramagnetic side of, but close to, a ferromagnetic instability. We will refer to “paramagnetic superconductors” to describe systems in this regime, although the superconductivity of course leads to the usual strong diamagnetic effects. Such paramagnetic superconductors include systems below the superconducting transition temperature, but above the temperature below which coexistence of superconductivity and ferromagnetism occurs, as well as systems that never develop ferromagnetism, but are close to a ferromagnetic instability in some direction in parameter space other than temperature. An example of the latter is believed to be the non-oxide perovskite $MgCNi_3$, which superconducts below a critical temperature

$T_c \approx 8$ K.[25] There is no evidence for a ferromagnetic phase in this material, but it has been suggested that a ferromagnetic ground state can be reached upon a relatively small amount of hole doping.[26] This system may thus be close to a ferromagnetic instability everywhere in its superconducting phase.

A recent study of MgCNi₃ microfibers, with $T_c = 7.8$ K, has revealed an anomalous temperature dependence of the critical current density j_c .[27] The critical current density vanishes at T_c according to a power law $j_c \propto |T - T_c|^\alpha$, with $\alpha = 2$ between about 1% and 10% away from the critical point, and no crossover to the usual Ginzburg-Landau behavior, which predicts $\alpha = 3/2$. The authors of Ref. [27] have ruled out morphological effects as an explanation, which raises the question whether proximity to a ferromagnetic state may be responsible. Indeed, since ferromagnetic fluctuations are expected to weaken (singlet) superconductivity, this is a plausible suggestion for the origin of the weaker-than-expected temperature dependence of j_c .

The probable proximity to ferromagnetism has led to a debate about the nature and symmetry of the pairing in MgCNi₃.¹ This point has not been settled; some experimental evidence points to conventional s-wave pairing; other, to a superconducting order parameter with nodes. The nature of the pairing in the other materials mentioned above has not been unambiguously determined either. In this chapter we will focus on the behavior close to T_c , which is qualitatively independent of the symmetry of the order parameter and thus expected to be the same for all nearly ferromagnetic superconductors. We use a generalized Ginzburg-Landau theory to theoretically investigate the electrodynamic properties of a superconductor as a ferromagnetic instability is approached. We treat the superconductivity in the usual mean-field approximation, but the magnetic critical behavior exactly in a scaling sense. Somewhat counter-intuitively, strong magnetic fluctuations make, in a well-defined sense, the superconductivity more robust in certain respects. In particular, the penetration depth becomes anomalously short. The thermodynamic critical field, on

¹For a recent summary see, R. Prozorov and R. W. Gianetta, cond-mat/0605612

the other hand, becomes weaker, as one might intuitively expect. The temperature dependencies of the critical field H_c and the penetration depth λ depend on the magnetic critical exponents δ and γ , respectively. For the critical current $j_c \propto H_c/\lambda$, this results in an exponent α between 1.5 (the Ginzburg-Landau result) and 2.16 in various temperature regimes. We will discuss both the existing experimental observations, and predictions for new experiments, in the light of these results.

This chapter is organized as follows. In Sec. 2.2 we give elementary phenomenological arguments for the dependence of the thermodynamic critical field, the penetration depth, and the critical current density, on a constant normal-state magnetic permeability μ_n . We then generalize these results to the magnetically critical case, where one needs to distinguish between μ_n and the spin susceptibility μ_s in a superconducting state, and both μ_n and μ_s become nonanalytic functions of various control parameters. In Sec. 2.3 we derive these results from a generalized Ginzburg-Landau theory, and in Sec. 2.4 we give a discussion of our results.

2.2 Phenomenological Arguments

2.2.1 Paramagnetic Systems

We are interested in the electromagnetic properties of superconductors with ferromagnetic fluctuations. We denote the normal-state spin susceptibility, which describes the response of the spin degrees of freedom to an external magnetic field in the absence of superconductivity, by χ_n , and the corresponding spin permeability by $\mu_n = 1 + 4\pi\chi_n$. This is in contrast to the spin permeability $\mu_s = 1 + 4\pi\chi_s$, which includes the effects of the superconductivity on the spin response, and the magnetic permeability $\mu = 1 + 4\pi\chi$, which describes the response of the total magnetization, including the diamagnetic part. It is instructive to first recall the dependence of superconducting properties on a constant $\mu_n \neq 1$, neglecting the distinction between μ_n and μ_s . [28, 29] This can be done by means of elementary arguments.

2.2.1.1 Thermodynamic Critical Field

Consider the free energy density f of a system in a magnetic field. It obeys

$$df = df(H = 0) + \frac{1}{4\pi} H dB, \quad (2.1)$$

where H is the thermodynamic magnetic field, and B is the magnetic induction. For the sake of simplicity, we ignore the vector nature of various quantities in our free energy considerations. For fixed B , f is the appropriate thermodynamic potential whose minimum determines the equilibrium state. However, in an experiment H is fixed, since $(c/4\pi)\nabla \times \mathbf{H} = \mathbf{j}_{\text{ext}}$ is the external current density, and only the latter is experimentally controlled. One therefore must perform a Legendre transform to a thermodynamic potential $g = f - BH/4\pi$, [9, 30] which obeys

$$dg = df(H = 0) - \frac{1}{4\pi} B dH. \quad (2.2)$$

In a paramagnetic phase, including paramagnetic superconductors, the relation between B and H is

$$B = H + 4\pi M = (1 + 4\pi\chi)H = \mu H, \quad (2.3)$$

with M the magnetization, $\chi(T, H)$ the magnetic susceptibility, and $\mu = 1 + 4\pi\chi$ the magnetic permeability. Integration of Eq. (2.2) yields

$$g(T, H) = f(T, H = 0) - \frac{1}{4\pi} \int_0^H dh [1 + 4\pi\chi(T, h)] h. \quad (2.4)$$

This is generally valid. In a superconducting Meissner state, $B = 0$, and hence $\chi = -1/4\pi$ (ideal diamagnetism), and $f(T, H = 0) = f_0 + t|\psi|^2/2 + u|\psi|^4/4$, with f_0 the free energy density of the normal state, ψ the superconducting order parameter, $t \propto (T - T_c)/T_c$ the dimensionless distance from the superconducting critical point,

and u a parameter. In a normal metal far from a magnetic instability, and ignoring normal-state diamagnetic effects, $\chi(T, H) \approx \text{const.} \equiv \chi_n$, or $\mu_n = 1 + 4\pi\chi_n = \text{const.}$, and $f(T, H = 0) = f_0$. In a normal metal close to a ferromagnetic critical point, χ is a complicated function of T and H .

Now consider a superconductor with $\mu_n = \text{const.}$ According to Eq. (2.4), the magnetic energy density gained by the system allowing magnetic flux to penetrate, i.e., the free energy density difference between the Meissner state with $B = 0$ and the normal state with $B = \mu_n H$, is $E_m/V = \mu_n H^2/8\pi$. By contrast, the condensation energy density gained by the system becoming a superconductor is $E_{\text{cond}}/V = t^2/4u$. The thermodynamic critical field, which is defined by these two energies being equal, is thus

$$H_c = \sqrt{2\pi/u} |t|/\sqrt{\mu_n} = H_c^0/\sqrt{\mu_n}, \quad (2.5)$$

with $H_c^0 = \sqrt{2\pi/u} |t|$ the critical field for a system with $\mu_n = 1$. An increase in μ_n thus decreases the critical field, as one might expect since the externally applied field is amplified inside the material.

2.2.1.2 London Penetration Depth

The dependence of the London penetration depth λ on μ_n is intuitively less obvious. Consider a large superconducting sample, with linear dimension L , surrounded by vacuum and subject to a homogeneous external magnetic field $\mathbf{H} = (0, 0, H)$ in z -direction. Along the left edge of the sample, the magnetic induction will be of the form $\mathbf{B}(\mathbf{x}) = (0, 0, B(x))$ with $B(x) = B_0 e^{-x/\lambda}$ ($x > 0$). To determine B_0 , imagine a thin (thickness d) layer of normal conducting material around the superconductor. Except for the superconductivity, the normal layer should have the same properties as the superconductor, in particular, a magnetic permeability μ_n . Then we have $B = H$ in vacuum, and $B = \mu_n H$ inside the normal layer, see Fig. 2.1(a). Now let $d \rightarrow 0$. Then we have (Fig. 2.1(b))

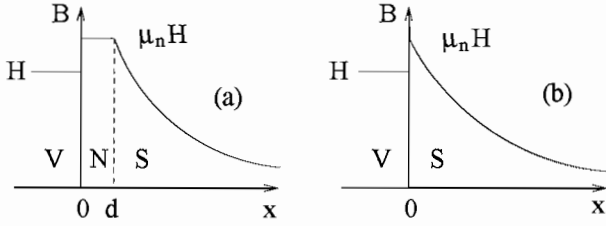


FIGURE 2.1: Magnetic induction schematically as a function of position at a vacuum (V) - normal metal (N) - superconductor interface (S) (a), and at a vacuum - superconductor interface (b).

$$B(x) = \begin{cases} H & \text{for } x < 0 \\ \mu_n H e^{-x/\lambda} & \text{for } x \geq 0 \end{cases}. \quad (2.6)$$

Now consider the current density associated with $B(x)$. From Ampere's law we have

$$\mathbf{j}(\mathbf{x}) = \frac{c}{4\pi} \nabla \times \mathbf{B}(\mathbf{x}) = (0, j(x), 0), \quad (2.7a)$$

with c the speed of light and

$$j(x) = \frac{c}{4\pi\lambda} B(x). \quad (2.7b)$$

This is the *total* current density. It has three contributions, namely, the supercurrent density \mathbf{j}_{sc} , the spin or magnetization current $\mathbf{j}_{\text{spin}} = c\nabla \times \mathbf{M}$, with \mathbf{M} the spin contribution to the total magnetization, and the external current density $\mathbf{j}_{\text{ext}} = c\nabla \times \mathbf{H}/4\pi$. The latter vanishes in the case we are considering. In a normal metal, the spin current is the only contribution if we ignore normal-state diamagnetic effects. The spin or normal-state susceptibility χ_n is defined as the response of \mathbf{M} to the total magnetic induction \mathbf{B} minus the contribution to \mathbf{B} of \mathbf{M} itself,

$$\mathbf{M} = \chi_n(\mathbf{B} - 4\pi\mathbf{M}) = (\chi_n/\mu_n) \mathbf{B}. \quad (2.8)$$

For the supercurrent density $\mathbf{j}_{\text{sc}} = \mathbf{j} - \mathbf{j}_{\text{spin}}$ this implies

$$\mathbf{j}_{\text{sc}} = \frac{c}{4\pi\mu_{\text{n}}} \nabla \times \mathbf{B}(\mathbf{x}) = (0, j_{\text{sc}}(x), 0), \quad (2.9a)$$

with

$$j_{\text{sc}}(x) = \frac{c}{4\pi\mu_{\text{n}}\lambda} B(x). \quad (2.9b)$$

Now consider one surface (area L^2) of the sample. Neglecting corner effects, and for $\lambda \ll L$, the total magnetic flux Φ through that surface is

$$\Phi = \int_0^L dy \int_0^L dx B(x) \approx L \int_0^\infty dx B(x) = L\lambda\mu_{\text{n}}H. \quad (2.10)$$

On the other hand, the total supercurrent flowing near that surface is, from Eq. (2.9b),

$$I_{\text{sc}} = \int d\mathbf{x} j_{\text{sc}} \approx L^2 \int_0^\infty dx j_{\text{sc}}(x) = \frac{c}{4\pi\mu_{\text{n}}} \frac{L}{\lambda} \Phi. \quad (2.11)$$

We thus can write the flux

$$\Phi = \frac{4\pi\mu_{\text{n}}}{c} \frac{\lambda}{L} I_{\text{sc}} = \frac{4\pi\mu_{\text{n}}}{c} \frac{\lambda}{L} Nqv, \quad (2.12)$$

where N is the number of supercurrent carrying particles, q is their charge, and v is their velocity. If m is their mass, then $E_{\text{kin}} = Nm v^2/2$ is the total kinetic energy of the supercurrent. The flux can thus be written

$$\Phi = \frac{4\pi\mu_{\text{n}}}{c} \frac{\lambda}{L} q \sqrt{2/m} \sqrt{N} \sqrt{E_{\text{kin}}}. \quad (2.13)$$

Now we make two observations. First, $N \approx L^2 \lambda n$, with $n = |\psi|^2$ the particle number density. Second, at the critical field strength the kinetic energy of the supercurrent must equal the condensation energy in the region where the current is flowing, which is (see Sec. 2.2.1.1) $E_{\text{cond}} = L^2 \lambda t^2/u$. With λ_0 the London penetration depth for

$$\mu_n = 1,$$

$$\lambda_0 = \sqrt{mc^2/4\pi q^2|\psi|^2} \propto 1/|t|^{1/2}, \quad (2.14)$$

this allows to write the flux at the critical field

$$\Phi_c = \lambda L H_c^0 \mu_n \lambda / \lambda_0 = L \lambda \mu_n H_c, \quad (2.15)$$

where the first equality follows from Eq. (2.13), and the second one from Eq. (2.10).

We thus obtain

$$H_c / \lambda = H_c^0 / \lambda_0, \quad (2.16a)$$

or [28, 29]

$$\lambda = \lambda_0 / \sqrt{\mu_n}. \quad (2.16b)$$

The penetration depth thus *decreases* with increasing μ_n , as does the critical field. This is somewhat counterintuitive, as it implies that the superconductivity becomes in some sense more robust. It also implies that a large normal-state magnetic permeability will make the superconductor necessarily of type I. [13] We will come back to this observation.

Notice that the above derivation relies only on very general energetic considerations and on Ampere's law. Also notice that it uses an identity at the critical field strength, where the superconductivity vanishes. This is fine for H_c , but the penetration depth is a property of the superconducting state, and hence the use of μ_n is not quite appropriate for this quantity, except in the limit $\lambda \rightarrow \infty$. More generally, λ depends on μ_s , which in turn depends on the superconducting properties. This makes no difference deep inside the paramagnetic superconducting phase, and Eq. (2.16b) is valid there. However, as we will see it makes a crucial difference close to a ferromagnetic instability.

2.2.1.3 Critical Current

In order to discuss the critical current, we assume a thin-wire geometry with wire radius R . [9, 30] The supercurrent density, which is the total current density minus the spin current density, can be written as a generalization of Eq. (2.9a),

$$\begin{aligned} j_{\text{sc}}(\mathbf{x}) &= \frac{c}{4\pi} [\nabla \times \mathbf{B}(\mathbf{x}) - 4\pi \nabla \times \mathbf{M}(\mathbf{x})] \\ &= \frac{c}{4\pi\mu(\mathbf{x})} \nabla \times \mathbf{B}(\mathbf{x}), \end{aligned} \quad (2.17)$$

where we have used Eq.(2.3) and $\mu(\mathbf{x})$ is the local magnetic susceptibility. Now integrate over the cross section of the wire. Assuming a homogeneous current density within a distance λ from the surface, and using Gauss's theorem on the right-hand side, we have

$$2\pi R\lambda j_{\text{sc}} = \frac{c}{4\pi\mu_n} \oint d\ell \cdot (\nabla \times \mathbf{B}(\mathbf{x})) = \frac{c}{2} RH$$

where we have used Eq. (2.6). The critical current density j_c is the one that produces the thermodynamic critical field H_c , which yields the familiar London theory result[9]

$$j_c = cH_c/4\pi\lambda. \quad (2.18)$$

This result is plausible: Dimensionally, j_c must be a magnetic field divided by a length. The relevant length scale is the thickness of the area that supports diamagnetic currents, which is λ . The relevant field scale should be the field that corresponds to the condensation energy, which is H_c . To the extent that $\mu_s \approx \mu_n = \text{const.}$, as we have assumed in Sec. 2.2.1.2, Eq. (2.16a) implies that j_c is independent of μ_n ,

$$j_c = j_c^0. \quad (2.19)$$

As we will see below, this result changes drastically in the vicinity of a ferromagnetic instability.

2.2.2 Systems at a Ferromagnetic Instability

In the vicinity of a ferromagnetic instability of the normal metal, the normal state magnetic susceptibility χ_n , and hence the permeability μ_n , become large and diverge as the phase transition is approached. At a ferromagnetic critical point, the region of linear response shrinks to zero, and χ_n and μ_n become strongly field dependent. This field dependence is characterized by the critical exponent δ , [7]

$$\mu_n \approx \chi_n \propto H^{1/\delta-1}. \quad (2.20)$$

The value of δ depends on the universality class the particular magnetic system belongs to. For all realistic universality classes, $\delta \approx 5$, whereas in Landau or mean-field theory, $\delta = 3$. [31] Substituting Eq. (2.20) into Eq. (2.5), we find for the thermodynamic critical field

$$H_c \propto |t|^{2\delta/(\delta+1)} \quad (2.21)$$

This result holds for a system where the distance t from the superconducting critical point can be changed while the system remains tuned to magnetic criticality (more precisely, to the parameter values where magnetic criticality would occur in the absence of superconductivity). Generically, the dimensionless distance r from magnetic criticality will change as well if t is changed, and we will discuss such more realistic situations in Sec. 2.4.

For the penetration depth, the situation is more complicated. In contrast to H_c , which compares the normal-state magnetic energy with the superconducting condensation energy that has nothing to do with spin magnetism, λ is entirely a property of the superconducting state, and the feedback of the superconductivity on the spin susceptibility, or the difference between μ_n and μ_s , cannot be neglected. As a result of this feedback, the magnetic transition in the presence of superconductivity does not occur at $r = 0$, but rather at a value $r \propto -\xi_m^0/\lambda_0$. [2] Here ξ_m^0 is the magnetic correlation length at zero temperature. This suggests that the spin susceptibility

at $r = 0$ will be effectively $\chi_s \propto \lambda_0/\xi_m^0 \gg 1$ in a mean-field approximation. More generally, one has $\mu_s \approx \chi_s \propto (\lambda_0/\xi_m^0)^\gamma$, with γ another critical exponent. Using this in Eq. (2.16b) with μ_n replaced by μ_s , we obtain

$$\lambda \propto \lambda_0^{1-\gamma/2} (\xi_m^0)^{\gamma/2} \propto |t|^{-1/2+\gamma/4}. \quad (2.22)$$

Since $\gamma \approx 1.4 > 0$ for ferromagnetic systems,[31] this implies that the penetration depth at magnetic criticality is anomalously short. Close to the superconducting transition, the superconductor will therefore also be of type I, in agreement with a conclusion drawn from studying the ferromagnetic phase.[13]

For the critical current density, Eqs. (2.18), (2.21), and (2.22) predict

$$j_c \propto |t|^\alpha \quad (2.23a)$$

with

$$\alpha = 2\delta/(\delta + 1) + 1/2 - \gamma/4 \quad , \quad (r = 0) \quad . \quad (2.23b)$$

With $\delta \approx 5$ and $\gamma \approx 1.4$ this yields $\alpha \approx 1.8$, in contrast to the Ginzburg-Landau result $\alpha = 3/2$.

These results hold at $r = 0$, and again we have assumed that t can be varied independently of r . Let us relax the former condition. From the above argument for the effective value of χ_s at $r = 0$ it also follows that Eq. (2.22) is valid only for $|r| < \xi_m^0/\lambda_0$. Since ξ_m^0 is typically on the order of a few \AA , while λ_0 is typically several hundred \AA or even larger even at zero temperature, and diverges as $|t|^{-1/2}$ for $t \rightarrow 0$, this is a very small range. By contrast, Eq. (2.20) can be valid for r as large as several percent, provided H is not too small. Not too close to T_c , where H_c goes to zero, Eq. (2.21) can thus be valid in a substantial r -range, while $\lambda = \lambda_0/\sqrt{\mu_n}$ except in an extremely small interval around $r = 0$. In that case,

$$\alpha = 2\delta/(\delta + 1) + 1/2 \quad , \quad (1 \gg r \gg \xi_m^0/\lambda_0) \quad , \quad (2.23c)$$

which yields $\alpha \approx 2.17$ if $\delta \approx 5$.

Finally, at larger values of r , or sufficiently close to T_c that H_c is small enough to invalidate Eq. (2.20), we are back to the paramagnetic case, Eq. (2.19) holds, and thus $\alpha = 3/2$.

One thus faces a rather complicated situation, where the exponent α can take on values between the Ginzburg-Landau value $3/2$ and a value larger than 2, Eq. (2.23c), depending on various parameters that are not easy to control or even determine experimentally. We will discuss this in more detail in Sec. 2.4. Before we do so, in the following section we will give a more technical and more detailed derivation of all of our results.

2.3 Generalized Ginzburg-Landau Theory

We now consider a coupled field theory that describes both superconducting and spin degrees of freedom in order to derive the above results from a more microscopic level and gain a deeper understanding of their origin. Specifically, we consider a generalization of the usual Ginzburg-Landau equations that includes the spin degrees of freedom. Far from magnetic criticality, the latter can be integrated out to yield ordinary Ginzburg-Landau theory with μ_n entering the magnetic energy density. At magnetic criticality, μ_n becomes field dependent, which changes the thermodynamic critical field. In addition, the leading term in the London equation vanishes, which leads to a generalized London equation that describes exponential decay on a length scale shorter than λ_0 , in agreement with the qualitative arguments in Sec. 2.2, and with implications for the critical current as discussed there. Unlike in the previous general discussion, in most of this section we will treat the magnetic critical behavior in a mean-field approximation.

2.3.1 LGW theory for Superconducting and Magnetic Fluctuations

Our starting point is an action for a complex scalar field ψ describing the superconducting degrees of freedom coupled to a vector potential \mathbf{A} , and a real vector field \mathbf{M} describing the spin degrees of freedom.[2, 22] We reiterate that the qualitative behavior near the superconducting T_c does not depend on the symmetry of the order parameter, so our restriction to a scalar order parameter does not imply a loss of generality. The action reads

$$\begin{aligned}
S = \int d\mathbf{x} & \left[\frac{1}{2m} |(\nabla - iq\mathbf{A}(\mathbf{x}))\psi(\mathbf{x})|^2 + \frac{t_1}{2} |\psi(\mathbf{x})|^2 + \frac{u_1}{4} |\psi(\mathbf{x})|^4 + \frac{1}{8\pi} \mathbf{B}^2(\mathbf{x}) \right. \\
& + \frac{a}{2} (\nabla\mathbf{M}(\mathbf{x}))^2 + \frac{t_2}{2} \mathbf{M}^2(\mathbf{x}) + \frac{u_2}{4} (\mathbf{M}^2(\mathbf{x}))^2 - \mathbf{M}(\mathbf{x}) \cdot \mathbf{B}(\mathbf{x}) \\
& \left. - \frac{1}{4\pi} \mathbf{H}(\mathbf{x}) \cdot \mathbf{B}(\mathbf{x}) \right]. \tag{2.24}
\end{aligned}$$

Here and in the remainder of this section we use units such that Planck's constant and the speed of light are unity, $\hbar = c = 1$. The first line is the standard Landau-Ginzburg-Wilson (LGW) functional for singlet superconductors. The first three terms in the second line are a standard vector- \mathbf{M}^4 theory, with $\mathbf{M}(\mathbf{x})$ the fluctuating magnetization. \mathbf{M} couples to the vector potential via the $\mathbf{M} \cdot \mathbf{B}$ term,² with $\mathbf{B} = \nabla \times \mathbf{A}$, and the last term is necessary to relate S to the appropriate Gibbs free energy, see Eq. (2.2). Notice that ψ and \mathbf{M} are coupled only indirectly via the vector potential \mathbf{A} . Spin-flip scattering of electrons by the magnetic moments does give rise to a direct coupling of the form $\mathbf{M}^2|\psi|^2$, [13] but these terms are not important for our purposes.

Minimizing this action with respect to ψ^* , \mathbf{A} , and \mathbf{M} yields the following saddle-

²One might consider it more physical to write $\mathbf{M} \cdot (\mathbf{B} - 4\pi\mathbf{M})$, which would make t_2 the inverse (normal) magnetic susceptibility. However, this just amounts to a shift of t_2 by 4π .

point equations,

$$t_1 \psi(\mathbf{x}) + u_1 |\psi(\mathbf{x})|^2 \psi(\mathbf{x}) - \frac{1}{m} (\nabla - iq\mathbf{A}(\mathbf{x}))^2 \psi(\mathbf{x}) = 0, \quad (2.25a)$$

$$-i \frac{q}{2m} [\psi^*(\mathbf{x}) \nabla \psi(\mathbf{x}) - \psi(\mathbf{x}) \nabla \psi^*(\mathbf{x})] - \frac{q^2}{m} |\psi(\mathbf{x})|^2 \mathbf{A}(\mathbf{x}) = \frac{1}{4\pi} \nabla \times [\mathbf{B}(\mathbf{x}) - \mathbf{H}(\mathbf{x}) - 4\pi \mathbf{M}(\mathbf{x})], \quad (2.25b)$$

$$t_2 \mathbf{M}(\mathbf{x}) - a \nabla^2 \mathbf{M}(\mathbf{x}) + u_2 \mathbf{M}^2(\mathbf{x}) \mathbf{M}(\mathbf{x}) = \nabla \times \mathbf{A}(\mathbf{x}) \quad (2.25c)$$

If we drop Eq. (2.25c) and put $\mathbf{M} = 0$ in Eq. (2.25b) (this corresponds to dropping \mathbf{M} from the action) we recover the usual Ginzburg-Landau equations.[9] A non-superconducting solution of the full equations is $\psi = 0$, $\mathbf{B} = \mathbf{H} + 4\pi \mathbf{M}$, and \mathbf{M} determined by the magnetic equation of state

$$(r - a \nabla^2) \mathbf{M}(\mathbf{x}) + u_2 \mathbf{M}^2(\mathbf{x}) \mathbf{M}(\mathbf{x}) = \mathbf{H}(\mathbf{x}), \quad (2.26)$$

where $r = t_2 - 4\pi$. For a small constant external field \mathbf{H} a solution of Eq. (2.26) is $\mathbf{M} = \chi_n \mathbf{H}$, with

$$\chi_n = 1/r \quad (2.27)$$

the normal-state magnetic susceptibility. At this point it is the bare susceptibility, but it is clear that by renormalizing the spin part of the action before constructing the saddle-point solution one can make it the physical susceptibility.

2.3.2 Effective Theory for Paramagnetic Superconductors

Now consider the full Eqs. (2.25). For a small and slowly varying $\mathbf{M}(\mathbf{x})$ we have from Eq. (2.25c)

$$\mathbf{M}(\mathbf{x}) = (\chi_n^{-1} + 4\pi)^{-1} \mathbf{B}(\mathbf{x}). \quad (2.28)$$

Substituting this into Eq. (2.25b) we obtain

$$\mathbf{j}_{\text{sc}}(\mathbf{x}) = \frac{1}{4\pi\mu_n} \nabla \times \mathbf{B}(\mathbf{x}) - \frac{1}{4\pi} \nabla \times \mathbf{H}(\mathbf{x}), \quad (2.29a)$$

where

$$\begin{aligned} \mathbf{j}_{\text{sc}}(\mathbf{x}) = & -i \frac{q}{2m} [\psi^*(\mathbf{x}) \nabla \psi(\mathbf{x}) - \psi(\mathbf{x}) \nabla \psi^*(\mathbf{x})] \\ & - \frac{q^2}{m} |\psi(\mathbf{x})|^2 \mathbf{A}(\mathbf{x}). \end{aligned} \quad (2.29b)$$

Together with Eq. (2.25a), these are the equations of motion for an effective action[29]

$$\begin{aligned} S_{\text{eff}} = & \int d\mathbf{x} \left[\frac{1}{2m} |(\nabla - iq\mathbf{A}(\mathbf{x})) \psi(\mathbf{x})|^2 + \frac{t}{2} |\psi(\mathbf{x})|^2 \right. \\ & \left. + \frac{u}{4} |\psi(\mathbf{x})|^4 + \frac{1}{8\pi\mu_n} \mathbf{B}^2(\mathbf{x}) - \frac{1}{4\pi} \mathbf{H}(\mathbf{x}) \cdot \mathbf{B}(\mathbf{x}) \right], \end{aligned} \quad (2.30)$$

where we have dropped the now-superfluous subscript on the Landau parameters t and u . The same result is of course obtained by starting with Eq. (2.24) and integrating out \mathbf{M} in a Gaussian approximation.

The quantity \mathbf{j}_{sc} in Eqs. (2.29) is indeed the supercurrent, as can be seen by comparing Eq. (2.29a) with Eq. (2.9a). It does not explicitly depend on μ_n , see Eq. (2.29b), and this is important for the flux quantum to be independent of μ_n . The magnetic energy $\mathbf{B}^2/8\pi\mu_n$, which does explicitly depend on μ_n , does not appreciably contribute to the free energy of a thin film or wire sample, and the standard determination of the critical current, Ref. [9], thus leads to the usual Ginzburg-Landau result with no correction due to $\mu_n \neq 1$. This corroborates the educated guess in Sec. 2.2.1.3.

For all other quantities, the usual analysis of Ginzburg-Landau theory now applies.[9] One characteristic length scale is given by the square root of the ratio

of the coefficients of the gradient-squared term and the ψ^2 term in Eq. (2.30). This is the superconducting coherence length $\xi = \sqrt{1/m|t|}$. Another one is given by the square root of the ratio of the coefficients of the terms quadratic in \mathbf{A} . For a constant ψ , this is the London penetration depth

$$\lambda = \sqrt{m/4\pi q^2 \psi^2 \mu_n} \equiv \lambda_0 / \sqrt{\mu_n}. \quad (2.31)$$

This is identical with Eq. (2.16b), which had been deduced on elementary phenomenological grounds.

For the Ginzburg-Landau parameter $\kappa = \lambda/\xi$ we now have $\kappa = \kappa_0/\sqrt{\mu_n}$, with κ_0 the value of the parameter for $\mu_n = 1$. This implies that the superconductor is of type I or type II, respectively, for $\kappa_0 < \sqrt{\mu_n/2}$ or $\kappa_0 > \sqrt{\mu_n/2}$. While one can show this by an explicit analysis of the effective action, a fast way to relate the theory for arbitrary values of μ_n to the one for $\mu_n = 1$ is to rewrite the action in terms of dimensionless quantities.[32] In conventional Ginzburg-Landau theory, this is done by introducing

$$\mathbf{x} = \lambda_0 \hat{\mathbf{x}}, \quad \psi(\mathbf{x}) = \psi_0 \hat{\psi}(\hat{\mathbf{x}}), \quad \mathbf{A}(\mathbf{x}) = \sqrt{2}H_c^0 \lambda_0 \hat{\mathbf{A}}(\hat{\mathbf{x}}), \quad (2.32)$$

Here $\psi_0 = \sqrt{-t/u}$ is the superconducting order parameter scale. In terms of these quantities, the effective action reads[32]

$$\begin{aligned} S_{\text{eff}} = & \frac{(H_c^0)^2 \lambda_0^3}{4\pi} \int d\hat{\mathbf{x}} \left[\left| \left(\frac{1}{\kappa_0} \hat{\nabla} - i \hat{\mathbf{A}}(\hat{\mathbf{x}}) \right) \hat{\psi}(\hat{\mathbf{x}}) \right|^2 \right. \\ & - |\hat{\psi}(\hat{\mathbf{x}})|^2 + \frac{1}{2} |\hat{\psi}(\hat{\mathbf{x}})|^4 + \frac{1}{\mu_n} \left(\hat{\nabla} \times \hat{\mathbf{A}}(\hat{\mathbf{x}}) \right)^2 \\ & \left. - 2 \hat{H}(\hat{\mathbf{x}}) \cdot \left(\hat{\nabla} \times \hat{\mathbf{A}}(\hat{\mathbf{x}}) \right) \right], \end{aligned} \quad (2.33)$$

A simple further rescaling procedure shows that S_{eff} depends only on a single

dimensionless parameter, rather than the two parameters κ_0 and μ_n . Define

$$\hat{\mathbf{x}} = \tilde{\mathbf{x}}/\kappa_0, \quad \hat{\mathbf{A}}(\tilde{\mathbf{x}}/\kappa_0) = \tilde{\mathbf{A}}(\tilde{\mathbf{x}}), \quad \hat{\psi}(\tilde{\mathbf{x}}/\kappa_0) = \tilde{\psi}(\tilde{\mathbf{x}}). \quad (2.34)$$

Then

$$\begin{aligned} S_{\text{eff}} &= \frac{(H_c^0)^2 \xi^3}{4\pi} \int d\tilde{\mathbf{x}} \left[\left| \left(\tilde{\nabla} - i\tilde{\mathbf{A}}(\tilde{\mathbf{x}}) \right) \tilde{\psi}(\tilde{\mathbf{x}}) \right|^2 \right. \\ &\quad - |\tilde{\psi}(\tilde{\mathbf{x}})|^2 + \frac{1}{2} |\tilde{\psi}(\tilde{\mathbf{x}})|^4 + \frac{\kappa_0^2}{\mu_n} \left(\tilde{\nabla} \times \tilde{\mathbf{A}}(\tilde{\mathbf{x}}) \right)^2 \\ &\quad \left. - 2 \frac{\kappa_0}{\sqrt{\mu_n}} \left(\sqrt{\mu_n} \tilde{\mathbf{H}}(\tilde{\mathbf{x}}) \right) \cdot \left(\tilde{\nabla} \times \tilde{\mathbf{A}}(\tilde{\mathbf{x}}) \right) \right]. \end{aligned} \quad (2.35)$$

This shows that the theory with an arbitrary μ_n maps onto ordinary Ginzburg-Landau theory with the replacements

$$\kappa_0 \rightarrow \kappa_0/\sqrt{\mu_n} \equiv \kappa, \quad \mathbf{H} \rightarrow \sqrt{\mu_n} \mathbf{H}. \quad (2.36)$$

$\kappa_0 = \sqrt{\mu_n/2}$ thus indeed marks the demarcation between type I and type II superconductors, and the critical fields can be immediately obtained from the usual results at $\mu_n = 1$. [9] For the thermodynamic critical field H_c , the upper critical field H_{c2} , the lower critical field H_{c1} , and the surface critical field H_{c3} we obtain

$$H_c = H_c^0/\sqrt{\mu_n}, \quad (2.37a)$$

$$H_{c2} = H_{c2}^0/\mu_n = \sqrt{2}\kappa_0 H_c^0/\mu_n, \quad (2.37b)$$

$$H_{c1} = H_{c1}^0 \frac{g(\kappa_0/\sqrt{\mu_n})}{g(\kappa_0)} = \frac{H_c^0}{\sqrt{2}\kappa_0} g(\kappa_0/\sqrt{\mu_n}). \quad (2.37c)$$

$$H_{c3} = 1.695 H_{c2}. \quad (2.37d)$$

where the universal function g has the limiting behavior

$$g(x) = \begin{cases} \ln x + 0.08 + O(1/x) & \text{for } x \gg 1/\sqrt{2}, \\ 1 & \text{for } x = 1/\sqrt{2}. \end{cases} \quad (2.37e)$$

If one neglects the weak dependence of g on its argument, H_{c1} is approximately independent of μ_n .

2.3.3 Superconductors at Magnetic Criticality

As one approaches a ferromagnetic instability, μ_n keeps increasing and can no longer be treated as a constant. There are two effects that become important for our purposes. First, in a normal metal μ_n becomes strongly field or induction dependent. At $r = 0$ this dependence is nonanalytic and described by the critical exponent δ . Second, as r becomes on the order of ξ_m^0/λ (see Sec. 2.2.2) in a superconducting phase, the difference between μ_n and μ_s can no longer be neglected. Related to this, the gradient squared term in Eq. (2.25c) must be taken into account. We now consider these effects, starting with the nonanalytic field dependence in the normal state.

2.3.3.1 Thermodynamic Critical Field

At magnetic criticality in the normal state, $r = 0$, one has[7]

$$\chi_n(r = 0, H) = \chi_0 \left(H/\tilde{H}_0 \right)^{1/\delta-1}. \quad (2.38)$$

Here χ_0 is a microscopic susceptibility, and \tilde{H}_0 is a microscopic field scale. M and, for small values of H , B are therefore proportional to $H^{1/\delta}$, or $H \propto B^\delta$. For small B , the number μ_n should thus be replaced by a function of B with the following leading B -dependence,

$$\mu_n \rightarrow (H_0/B)^{\delta-1}, \quad (2.39)$$

with $H_0 = (4\pi\chi_0)^{\delta/(\delta-1)}\tilde{H}_0$. The magnetic energy cost of the flux expulsion that results from the formation of a Meissner phase (which equals minus the normal-state magnetic energy) is now obtained by using Eq. (2.39) in Eq. (2.30). It is $E_m/V = HB/4\pi - B^{\delta+1}/8\pi H_0^{\delta-1} = H_0^{1-1/\delta}H^{1+1/\delta}/8\pi$. The condensation energy is still given by $E_{\text{cond}}/V = t^2/4u$, which yields

$$H_c = \left(\frac{2\pi}{u}\right)^{\delta/(\delta+1)} \frac{1}{H_0^{(\delta-1)/(\delta+1)}} |t|^{2\delta/(\delta+1)}. \quad (2.40)$$

The thermodynamical critical field is thus weaker than in the paramagnetic case, and the t -dependence is consistent with Eq. (2.21). By comparing with Eq. (2.5), we see that with respect to the thermodynamical critical field, μ_n effectively scales like $\mu_n \sim 1/|t|^{2(\delta-1)/(\delta+1)}$ at magnetic criticality.

Equations (2.38) through (2.40) hold also for small but nonzero values of r as long as one is in the field scaling regime, i.e., as long as H in appropriate units is large compared to r to an appropriate power. We will discuss this in more detail in Sec. 2.4. At this point we only mention that, since H_c vanishes as $|t| \rightarrow 0$, sufficiently close to T_c one will lose the field scaling for any nonzero value of r , and H_c will be given by Eq. (2.37a).

2.3.3.2 Generalized London Equation

The ordinary London equation is obtained from Eq. (2.25b) by dropping $\mathbf{M}(\mathbf{x})$ and treating $\psi(\mathbf{x}) \equiv \psi$ as a constant (London approximation). With $\nabla \times \mathbf{H}(\mathbf{x}) = 0$ this leads to

$$-\lambda_0^{-2} \mathbf{B}(\mathbf{x}) = \nabla \times \nabla \times \mathbf{B}(\mathbf{x}). \quad (2.41)$$

Now take \mathbf{M} into account. Using Eq. (2.25c) in Eq. (2.25b), we can eliminate \mathbf{B} and derive an equation for \mathbf{M} . Once \mathbf{M} is known, \mathbf{B} follows from Eq. (2.25c). Within

the London approximation one finds

$$\begin{aligned} \mathbf{M}(\mathbf{x}) = & -(\lambda_0^2/\mu_n)\nabla \times \nabla \times \mathbf{M}(\mathbf{x}) + \left(\tilde{\xi}_m^0\right)^2 \nabla^2 \mathbf{M}(\mathbf{x}) + \left(\tilde{\xi}_m^0\right)^2 \lambda_0^2 \nabla \times \nabla \times \nabla^2 \mathbf{M}(\mathbf{x}) \\ & -\tilde{u} \mathbf{M}^2(\mathbf{x})\mathbf{M}(\mathbf{x}) - \tilde{u}\lambda_0^2 \nabla \times \nabla \times \mathbf{M}^2(\mathbf{x})\mathbf{M}(\mathbf{x}). \end{aligned} \quad (2.42)$$

Here $\mu_n = (4\pi + r)/r$ as in Sec. 2.3.2, $\tilde{\xi}_m^0 = \xi_m^0/\sqrt{4\pi + r} \equiv \sqrt{a/(4\pi + r)}$, and $\tilde{u} = u/(4\pi + r)$.

As long as $\mu_n \approx 1$, the first term on the right-hand side of Eq. (2.42) leads to a variation of \mathbf{M} on a length scale $\lambda = \lambda_0/\sqrt{\mu_n}$. The second term is a small correction to the first one since $\xi_m^0 \ll \lambda_0$. So is the third term, which is of order $\left(\tilde{\xi}_m^0\right)^2 \nabla^2 \sim \left(\tilde{\xi}_m^0\right)^2 / \lambda_0^2 \ll 1$ relative to the first one. The linearized version of Eq. (2.42) thus reduces to the ordinary London equation, Eq. (2.41), with $\lambda_0 \rightarrow \lambda$. However, for $r = 0$ the first term vanishes. This makes the second term the leading one, and the third term, which is of order $\lambda_0^2 \nabla^2$ compared to the second one, cannot be neglected either. The linearized equation thus reads

$$\mathbf{M}(\mathbf{x}) = \left(\tilde{\xi}_m^0\right)^2 \nabla^2 [1 + \lambda_0^2 \nabla \times \nabla \times] \mathbf{M}(\mathbf{x}). \quad (2.43)$$

With the same interface geometry as in Sec. 2.2.1.2 this takes the form

$$M(x) = \left(\tilde{\xi}_m^0\right)^2 M''(x) - \left(\tilde{\xi}_m^0\right)^2 \lambda_0^2 M^{(iv)}(x). \quad (2.44)$$

This linear quartic ODE is solved by an exponential ansatz, $M(x) = M_0 e^{-\rho x}$. The real solution that falls off for $x \rightarrow \infty$ shows damped oscillatory behavior. From Eq. (2.25c) we see that $B(x)$ shows the same behavior as $M(x)$, up to corrections of $O(\tilde{\xi}_m^0/\lambda_0)$. With the boundary condition $B(x=0) = \mu_n H$ we finally obtain

$$B(x) = \mu_n H e^{-x/\sqrt{2\tilde{\xi}_m^0 \lambda_0}} \cos\left(x/\sqrt{2\tilde{\xi}_m^0 \lambda_0}\right). \quad (2.45)$$

This is the solution of the linearized version of Eq. (2.42) at $r = 0$. In addition to leaving out the terms of $O(M^3)$, we have also ignored the fact that the permeability, whether μ_n or μ_s , does depend on B or M at magnetic criticality. In a mean-field approximation, $\mu_n \propto 1/B^2$ at $r = 0$, see Eq. (2.39), which also leads to terms of $O(M^3)$ in the nonlinear equation. Depending on the ratio of the external field to H_0 , these terms may or may not be important for the initial decay of M or B near the normal metal-to-superconductor boundary. However, once M or B has decayed sufficiently, these terms become subleading compared to the linear ones in Eq. (2.44), and the asymptotic behavior as $B \rightarrow 0$ is always given by Eq. (2.45).

In order to make contact with the discussion in Sec. 2.2.2 for small but nonzero values of r , let us consider the linearized Eq. (2.42) while keeping the first term. Instead of Eq. (2.44) we then have

$$M(x) = \left(\lambda_0^2/\mu_n + \left(\tilde{\xi}_m^0 \right)^2 \right) M''(x) - \left(\tilde{\xi}_m^0 \right)^2 \lambda_0^2 M^{(iv)}(x). \quad (2.46)$$

This is solved by

$$M(x) = M_0 e^{\rho x}, \quad (2.47a)$$

with

$$\rho^2 = \frac{1}{2\lambda_0^2 \left(\tilde{\xi}_m^0 \right)^2} \left[\lambda_0^2/\mu_n + \left(\tilde{\xi}_m^0 \right)^2 - \sqrt{\left(\lambda_0^2/\mu_n + \left(\tilde{\xi}_m^0 \right)^2 \right)^2 - 4\lambda_0^2 \left(\tilde{\xi}_m^0 \right)^2} \right]. \quad (2.47b)$$

Here we have chosen the solution for ρ^2 that yields $\rho^2 \rightarrow 1/\lambda_0^2$ for $r \rightarrow \infty$. Equation (2.47b) still provides two solutions for ρ , and the physical solution for M is determined by the requirement that M be real.

A discussion of Eq. (2.47b) shows that ρ^2 becomes purely real and negative at $r = r_s = -4\sqrt{\pi}\tilde{\xi}_m^0/\lambda_0 + O\left(\left(\tilde{\xi}_m^0\right)^2/\lambda_0^2\right)$. This is in agreement with the results of

Blount and Varma,[2] who showed that spiral magnetic order coexisting with the superconductivity occurs at this point. For $|r| \ll \tilde{\xi}_m^0/\lambda_0$ one has $\rho^2 \approx -i/\tilde{\xi}_m^0\lambda_0$, which leads to Eq. (2.45). For $r \gg \tilde{\xi}_m^0/\lambda_0$ one finds $\rho^2 \approx \mu_n/\lambda_0^2$, which leads to

$$B(x) = \mu_n H e^{-x\sqrt{\mu_n}/\lambda_0}, \quad (2.48)$$

in agreement with Eq. (2.31).

2.3.3.3 Penetration Depth, and Critical Current

Equation (2.45) shows that the effective penetration depth at magnetic criticality is

$$\lambda = \sqrt{2\tilde{\xi}_m^0\lambda_0} \quad , \quad (|r| \ll \tilde{\xi}_m^0/\lambda_0), \quad (2.49)$$

in agreement with the conclusions of Ref. [13] drawn from studying the ferromagnetic phase, and with Eq. (2.22) with $\gamma = 1$. The latter approximation results from the fact that our saddle-point equations of motion describe the magnetic equation of state in a mean-field approximation. The discussion of Eq. (2.47b) shows that this result is valid for $|r| \ll \tilde{\xi}_m^0/\lambda_0$. By comparing with Eq. (2.16b) or (2.31), we see that with respect to the penetration depth, μ_n at magnetic criticality scales like $\mu_n \sim 1/\sqrt{|t|}$ in mean-field approximation, or $\mu_n \sim 1/|t|^{\gamma/2}$ in general. The fact that $1/\sqrt{\mu_n}$ in Eqs. (2.5) and (2.16b), respectively, must be interpreted differently for $\mu_n \rightarrow \infty$ is a consequence of the influence of the superconductivity on the spin response.

For $r \gg \tilde{\xi}_m^0/\lambda_0$ we have, from Eq. (2.48)

$$\lambda = \lambda_0/\sqrt{\mu_n}, \quad (2.50)$$

in agreement with Eq. (2.31).

The expression for the critical current given by Eq. (2.18) is general within the London approximation. We have now given a derivation of the behavior of the

thermodynamical critical field and the penetration depth given on phenomenological grounds in Eqs. (2.21) and (2.22), respectively. The behavior of the critical current at or near magnetic criticality is thus given by Eqs. (2.23).

2.3.3.4 Critical Field H_{c2}

The critical exponent γ is positive ($\gamma \approx 1.4$ for typical ferromagnetic universality classes in three dimensions[31]). The result for λ , Eq. (2.22) or (2.46) in mean-field approximation, of the previous subsection therefore means that λ diverges more slowly for $|t| \rightarrow 0$ than the superconducting coherence length $\xi \propto 1/\sqrt{|t|}$. Consequently, superconductors at magnetic criticality ($|r| \ll \tilde{\xi}_m^0/\lambda_0$) are necessarily of type I.[13]

This observation notwithstanding, the critical field H_{c2} , which in a type-II superconductor signals the boundary of the vortex phase, still has a physical meaning: It is the minimum field to which the normal metal can be ‘supercooled’ before it discontinuously develops a nonzero superconducting order parameter.[9] It is thus still of interest to determine H_{c2} . Furthermore, the behavior will be necessarily of type I only for $|r|$ in an extremely narrow region. Outside of this region, Eq. (2.50) holds, and for a sufficiently large value of $\kappa_0 = \lambda_0/\xi$ the superconductor will still be of type II. The determination of H_{c2} is done by linearizing the Ginzburg-Landau equation, Eq. (2.25a), in ψ . It then turns into a Schrödinger equation for a particle in a vector potential \mathbf{A} , with $-t_1/2 \equiv -t/2$ playing the role of the energy eigenvalue. By means of standard arguments[9] this leads to a critical value of the magnetic induction $\mathbf{B} = \nabla \times \mathbf{H}$ given by $B_{c2} \equiv H_{c2}^0 = -tm/q$. In a paramagnetic superconductor, this leads to

$$H_{c2} = H_{c2}^0/\mu_n \quad (\mu_n = \text{const.}), \quad (2.51)$$

which is the same as Eq. (2.37b). At magnetic criticality, we have, cf. Eq. (2.39),

$$H_{c2} = B_{c2}^\delta/H_0^{(\delta-1)} \propto |t|^\delta. \quad (2.52)$$

Notice that, in this context, μ_n scales as $\mu_n \sim 1/|t|^{\delta-1}$, whereas it scales as $\mu_n \sim 1/|t|$ if the relevant field scale is H_c . Since H_{c2} vanishes much faster than H_c , Eq. (2.40), the field scaling region will be restricted to larger values of $|t|$, and H_{c2} will be given by Eq. (2.51) in a substantial range of t -values. Will come back to this in Sec. 2.4.

2.4 Discussion and Conclusion

To summarize, we have determined the electrodynamic properties of superconductors close to a ferromagnetic instability, i.e., materials that, in the absence of superconductivity, would be paramagnetic with large ferromagnetic fluctuations. This work complements previous studies of the coexistence of superconductivity with ferromagnetic order.[2, 13] We have treated the superconductivity in mean-field (Ginzburg-Landau) approximation. In addition, we have employed the London approximation, treating the superconducting order parameter as a constant. The ferromagnetic critical point we have treated explicitly in a mean-field approximation, and we have used scaling arguments to consider the consequences of the exact magnetic critical behavior for the superconductivity. We have found that the thermodynamical critical field H_c decreases due to the ferromagnetic fluctuations, as one would expect, and depends on the magnetic critical exponent δ , see Eqs. (2.40) and (2.21). However, the London penetration depth also decreases, which is intuitively less obvious. At magnetic criticality the behavior of the magnetic induction at a vacuum-to-superconductor (or normal metal-to-superconductor) interface is still characterized by exponential decay, but the characteristic length scale λ is different from the usual London penetration depth λ_0 . Within a mean-field description of the magnetic criticality it is the geometric mean of the zero-temperature magnetic correlation length and λ_0 , see Eqs. (2.45) and (2.49); more generally, it depends on the magnetic critical exponent γ , see Eq. (2.22). However, this behavior of the penetration depth is valid only within an extremely small region of width $\tilde{\xi}_m^0/\lambda_0$ around magnetic criticality. Outside of this region, but still within the ferromagnetic critical region, the temperature dependence

of the penetration depth is the same as in Ginzburg-Landau theory, see Eq. (2.50). For the critical current $j_c \propto H_c/\lambda$ this implies a dependence on the reduced temperature given by $|t|^\alpha$, where the exponent α depends on both δ and γ , or on δ only, depending on the value of r , see Eqs. (2.23). With exponent values appropriate for the usual ferromagnetic universality classes, $\alpha \approx 1.8$ extremely close to magnetic criticality, and $\alpha \approx 2.15$ somewhat farther away.

Let us now discuss these results in some more detail, and relate them to the experimental observations reported in Ref. [27].

For the temperature dependencies of various observables at magnetic criticality we have assumed that the system stays tuned to magnetic criticality while the temperature is varied. Let us discuss to what extent this assumption is realistic. Consider a phase diagram in a plane spanned by the temperature and some non-thermal control parameter x , e.g., the hole doping concentration in the case of MgCNi_3 , [26] and consider the following two qualitatively different possibilities. Figure 2.2 shows a situation where the magnetic phase separation line does not cross the line $x = 0$. The stoichiometric compound thus does not enter a magnetic phase upon cooling, although the system is close to a magnetic transition for all temperatures below the superconducting T_c . This scenario is believed to apply to MgCNi_3 . Figure 2.3 shows a situation where the magnetic phase separation line does cross the line $x = 0$, so that the stoichiometric compound enters a phase where superconductivity and magnetism coexist at some temperature below T_c . This is the situation that was discussed in Refs. [2] and [13] and observed in ErRh_4B_4 and HoMo_6S_8 . [15, 16] The magnetic transition is to a phase with spiral magnetic order at a temperature T_s slightly below the temperature T_m^0 where ferromagnetism would occur in the absence of superconductivity. [2]

We now can see what is required to keep r constant while varying t , namely, a situation as shown in Fig. 2.2 with the dashed line essentially parallel to the T -axis. r is then given by the dimensionless distance between the two lines. In order for

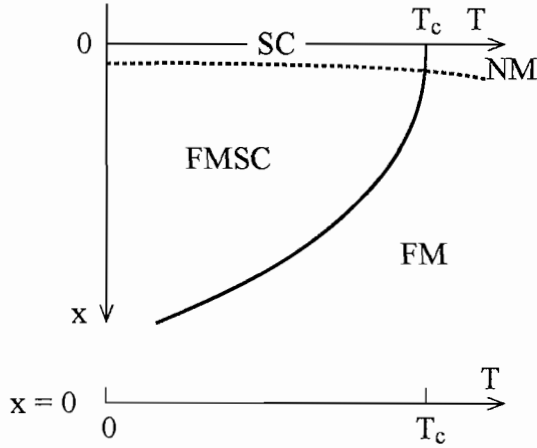


FIGURE 2.2: Schematic phase diagram showing a normal metal (NM), a ferromagnet (FM), a superconductor (SC), and a ferromagnetic superconductor (FMSC) in a temperature (T) - control parameter (x) plane. The solid line denotes the superconducting transition, the dashed line, the magnetic one. Along $x = 0$ there is only one phase transition at the superconducting T_c . See the text for additional explanation.

the penetration depth to display the non-Ginzburg-Landau behavior described by Eq. (2.49) or, more generally, Eq. (2.22), the two lines would have to be extremely close, in order to keep r smaller than $\tilde{\xi}_{\text{sm}}^0/\lambda_0$, see Eq. (2.49). This would result in a temperature dependence of the critical current given by Eqs. (2.23a, 2.23b). While this is possible, it is a very non-generic situation, and it would result in a very large magnetic susceptibility of the normal metal just above the superconducting transition temperature.

A situation that is still very non-generic, but requires somewhat less fine-tuning, is one where the dashed line is still essentially parallel to the T -axis, but in a somewhat larger r -range, say, with r on the order of a few percent. In this case the penetration depth will show the usual $1/|t|^{1/2}$ temperature dependence, see Eq. (2.50). The temperature dependence of the thermodynamic critical field will be more complicated

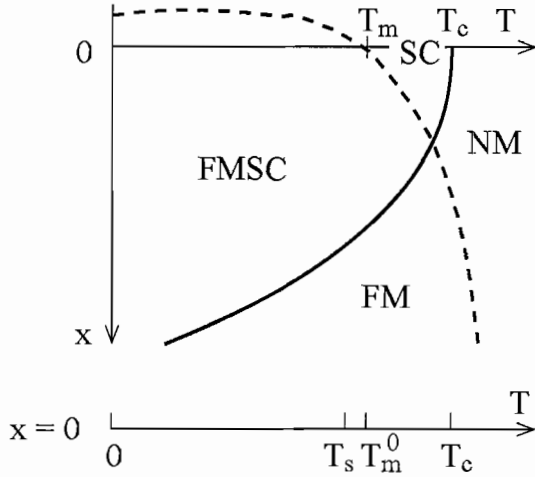


FIGURE 2.3: Same as Fig. 2.2, but with a magnetic transition for $x = 0$ at a temperature $T_m < T_c$. On the $x = 0$ axis it is shown that T_m splits into the bare magnetic transition temperature T_m^0 and the physical transition temperature T_s to a state with spiral magnetic order, Ref.[2]. See the text for additional explanation.

in this case. The generalization of Eq. (2.20) to nonzero values of r is

$$\chi_n = r^{-\gamma} f_x(H/r^{\beta\delta}), \quad (2.53)$$

with $\gamma = \beta(\delta - 1)$, β , and δ the usual critical exponents for the magnetic transition. In order for Eq. (2.20) to hold, the H must be large compared to $r^{\beta\delta}$ in suitable units. The latter are not determined by any universal arguments, but an analysis of the critical equation of state for both the high-temperature ferromagnet Ni ($T_m \approx 630$ K)[33] and the low-temperature ferromagnet CrBr₃ ($T_m \approx 33$ K)[34] shows that in either case the relevant energy or field scale (we use units such that $k_B = \mu_B = 1$) is given by T_m , which is plausible. The crossover between the field scaling that leads to Eq. (2.21) and the static scaling that leads to Eq. (2.5) thus occurs at a crossover field

$$H_x \approx T_m^0 r^{\beta\delta}. \quad (2.54)$$

$\beta\delta \approx 5/3$ for ferromagnetic phase transitions, and with $T_m \approx 10$ K and $r \approx 0.1$, one

finds $H_x \approx 0.02T_m^0$. For MgCNi_3 in the vicinity of T_c , this leads to $H_x \approx 0.2\text{ T}$. With H_{c2} at *zero temperature* on the order of 14 T and $\kappa \approx 40$, [35] one expects $H_c(T=0) = H_{c2}/\sqrt{2\kappa} \approx 0.25\text{ T}$. Since H_c vanishes at T_c , this means that H_c will be given by Eq. (2.21) sufficiently far away from T_c , but cross over to $H_c \propto |t|$ near T_c . Consequently, the critical current exponent α will be given by Eq. (2.23c) at some distance from T_c , and cross over to the Ginzburg-Landau result $\alpha = 3/2$ as $|t| \rightarrow 0$. In the experiment of Ref. [27], no such crossover was observed down to $|t| \approx 0.01$.

At least within the London approximation, our results confirm the conclusion of Ref. [13] that superconductors near a ferromagnetic instability are necessarily of type I. However, we have also shown that this conclusion is inevitable only within an extremely small region around the (bare) magnetic critical point. The fact that MgCNi_3 is observed to be of type II [35] is therefore not necessarily in contradiction to the notion that this material is almost ferromagnetic. However, Eq. (2.52) predicts a strong deviation from Ginzburg-Landau behavior for the upper critical field H_{c2} . Since H_{c2} goes to zero rapidly as $|t| \rightarrow 0$, this behavior will show only at substantial values of $|t|$ even if r is very small. No anomalous behavior was observed for $|t|$ up to 0.5. [35] This is reconcilable with close proximity to a magnetic instability only if r is very small close to T_c , and grows with decreasing temperature, in which case H_{c2} might never show the magnetic critical behavior. A signature of this situation would be a large magnetic susceptibility in the normal state just above T_c .

The conclusion from this discussion with respect to the experimental observations in Ref. [27] is as follows. While it is possible that proximity to a ferromagnetic instability is the cause of the observed anomalous behavior of the critical current, such an explanation requires fine tuning of the phase diagram, and would have to be accompanied by a very large enhancement of the spin susceptibility in the normal phase just above T_c . Explaining the lack of an anomaly in the temperature dependence of H_{c2} probably requires that the material is closer to the magnetic instability near T_c than at $T = 0$ (i.e., the dashed line in Fig. 2.2 comes closer to the T -axis with

increasing T). A direct measurement of the spin susceptibility in the normal phase would be of great interest in this context.

Finally, we discuss our predictions for the case of a superconductor that does undergo a transition to a magnetic state below T_c , i.e., the situation represented by Fig. 2.3. In the (very small) temperature interval of width $2|T_m^0 - T_s|$ around T_m^0 , both the thermodynamic critical field H_c and the penetration depth λ will show an anomalous temperature dependence, and the critical current exponent will be given by Eq. (2.23b). Outside of this region, but not too close to T_c , H_c will be anomalous, but λ will be conventional, and the critical current exponent will be given by Eq. (2.23c). Upon approaching T_c , H_c will fall below the crossover field given by Eq. (2.54), and its temperature dependence will cross over to the usual linear Ginzburg-Landau behavior. The critical current exponent close to T_c will thus be the conventional $\alpha = 3/2$. The location of this crossover depends on the critical field scale, and will thus be material dependent. Critical current measurements in the materials like ErRh_4B_4 , or HoMo_6S_8 , which are believed to fall into this class, would be very interesting.

CHAPTER III

NATURE OF PHASE TRANSITION IN P-WAVE SUPERCONDUCTORS

3.1 Introduction

BCS theory predicts that the phase transition from the normal state to the superconducting state in *s*-wave superconductors is continuous or second order. However, in 1974 Halperin, Lubensky, and Ma [36] showed that the coupling between the superconducting order parameter and the electromagnetic vector potential tends to render the transition first order. This conclusion is inevitable for extreme type-I superconductors where fluctuations of the order parameter are negligible and the vector potential can be integrated out exactly, and the mechanism is analogous to the spontaneous mass generation known in particle physics as the Coleman-Weinberg mechanism.[37] When order parameter fluctuations cannot be neglected, and especially for type-II superconductors, the problem cannot be solved exactly. The authors of Ref. [36] generalized the problem by considering an $n/2$ -dimensional complex order parameter and conducting a renormalization-group (RG) analysis in $d = 4 - \epsilon$ dimensions. The physical case of interest is $n = 2$ and $d = 3$. To first order in ϵ they found that a RG fixed point corresponding to a continuous phase transition exists only for $n > 365.9$, which suggests that for physical parameter values the transition is first order even in the type-II case. They corroborated this conclusion by performing a large- n expansion for fixed $d = 3$. To first order in $1/n$, the critical exponent ν is positive only for $n > 9.72$, which again strongly suggests that the transition in the physical case $n = 2$ is first order. For superconductors, the size

of the effect is too small to be observable, whereas for the analogous smectic-A to nematic transition in liquid crystals it was predicted to be much larger. Experiments that showed a clear second order transition in liquid crystals later prompted a re-examination of the theory by Dasgupta and Halperin.[38] Using Monte Carlo data and duality arguments, these authors argued that a type-II superconductor in $d = 3$ should show a second order transition after all. The discrepancy between these theoretical results has never been clarified.

Recently there has been substantial interest in unconventional superconductivity. In particular, Sr_2RuO_4 has emerged as a convincing case of p -wave superconductivity,[39, 40] and UGe_2 is another candidate.[41] This raises the question whether for such systems the fluctuation-induced first order mechanism also is applicable, or whether the additional order parameter fluctuations allow for a second order transition in situations that lead to a first order transition in the s -wave case. Here we investigate this problem. By conducting an analysis for p -wave superconductors analogous to the one of Ref. [36] we predict a first order transition as in the s -wave case, although the restrictions are somewhat less stringent.

This chapter is organized as follows. In Sec. 3.2 we define our model and derive the mean-field phase diagram. In Sec. 3.3 we determine the nature of the phase transition. We do so first in a renormalized mean-field approximation that neglects fluctuations of the superconducting order parameter. We then take such fluctuations into account, first by means of a renormalization-group analysis in $d = 4 - \epsilon$ dimensions, and then by means of a $1/n$ -expansion. In Sec. 3.4 we discuss our results.

3.2 Model

Let us consider a Landau-Ginzburg-Wilson (LGW) functional appropriate for describing spin-triplet superconducting order. The superconducting order parameter is conveniently written as a matrix in spin space, [42] $\Delta_{\sigma_1\sigma_2} = \sum_{\mu=1}^3 d_{\mu}(\mathbf{k}) (\sigma_{\mu}i\sigma_2)_{\sigma_1\sigma_2}$. Here $\sigma_{1,2,3}$ are Pauli matrices, \mathbf{k} is a wave vector, and the d_{μ} are the components of a

complex 3-vector $\mathbf{d}(\mathbf{k})$. p -wave symmetry implies $d_\mu(\mathbf{k}) = \sum_{j=1}^3 d_{\mu j} \hat{k}_j$, with $\hat{\mathbf{k}}$ a unit wave vector. The tensor field $d_{\mu j}(\mathbf{x})$ is the general order parameter for a spin-triplet p -wave superconductor and it allows for a very rich phenomenology. For definiteness we will constrain our discussion to a simplified order parameter describing the so-called β -state,[42] which has been proposed to be an appropriate description of UGe₂. [41] It is given by a tensor product $d = \boldsymbol{\psi} \otimes \boldsymbol{\phi}$ of a complex vector $\boldsymbol{\psi}$ in spin space and a real unit vector $\boldsymbol{\phi}$ in orbital space. The ground state is given by $\boldsymbol{\psi} = \Delta_0(1, i, 0)$, $\boldsymbol{\phi} = (0, 0, 1)$. In a weak-coupling approximation that neglects terms of higher than bilinear order in $\boldsymbol{\psi}^2$, $\boldsymbol{\phi}^2$, and ∇^2 the action depends only on $\boldsymbol{\psi}$,

$$S = \int d\mathbf{x} \left[t|\boldsymbol{\psi}|^2 + c|\mathbf{D}\boldsymbol{\psi}|^2 + u_0|\boldsymbol{\psi}|^4 + v_0|\boldsymbol{\psi} \times \boldsymbol{\psi}^*|^2 + \frac{1}{8\pi\mu}(\nabla \times \mathbf{A})^2 \right]. \quad (3.1)$$

Here \mathbf{A} is the vector potential, $\mathbf{D} = \nabla - ie\mathbf{A}$ is the gauge invariant gradient with e the Cooper pair charge, and $|\mathbf{D}\boldsymbol{\psi}|^2 = (D_i\psi_\sigma)(D_i^*\psi_\sigma^*)$ with summations over i and σ implied. μ is the normal-state magnetic permeability, and t , c , u_0 , and v_0 are the parameters of the LGW functional. The fields $\boldsymbol{\psi}$ and \mathbf{A} are understood to be functions of the position \mathbf{x} .

For later reference we now generalize the vector $\boldsymbol{\psi}$ from a complex 3-vector to a complex m -vector with components ψ_α , so that the total number of order parameter degrees of freedom is $n = 2m$. In order to generalize the term with coupling constant v we use of the following identity for 3-vectors,

$$|\boldsymbol{\psi} \times \boldsymbol{\psi}^*|^2 = \psi_\alpha \psi_\alpha^* \psi_\beta \psi_\beta^* - \psi_\alpha \psi_\alpha \psi_\beta^* \psi_\beta^* \quad (3.2)$$

and notice that the right-hand side is well defined for a complex m -vector. Our

generalized action now reads

$$\begin{aligned}
S = \int d\mathbf{x} & \left[t \psi_\alpha \psi_\alpha^* + c (D_i \psi_\alpha) (D_i \psi_\alpha^*) + u \psi_\alpha \psi_\alpha^* \psi_\beta \psi_\beta^* \right. \\
& \left. + v \psi_\alpha \psi_\alpha \psi_\beta^* \psi_\beta^* + \frac{1}{8\pi\mu} \epsilon_{ijk} (\partial_j A_k) \epsilon_{ilm} (\partial_l A_m) \right],
\end{aligned} \tag{3.3}$$

with $\alpha, \beta = 1, \dots, m$, $i, j, \dots = 1, 2, 3$, and summation over repeated indices implied. Here we have defined new coupling constants $u = u_0 + v_0$ and $v = -v_0$. In addition to the generalization of the order parameter to an m -vector we will also consider the system in a spatial dimension d close to $d = 4$. The physical case of interest is $m = d = 3$.

3.3 Nature of The Phase Transition

3.3.1 Mean Field Approximation

The simplest possible approximation ignores both the fluctuations of the order parameter field $\boldsymbol{\psi}$ and the electromagnetic fluctuations described by the vector potential \mathbf{A} . The order parameter is then a constant, $\boldsymbol{\psi}(\mathbf{x}) \equiv \boldsymbol{\psi}$, and the free energy density f reduces to

$$f = t |\boldsymbol{\psi}|^2 + u_0 |\boldsymbol{\psi}|^4 + v_0 |\boldsymbol{\psi} \times \boldsymbol{\psi}^*|^2. \tag{3.4}$$

In order to determine the phase diagram we parameterize the order parameter as follows,[3]

$$\boldsymbol{\psi} = \psi_0 (\hat{n} \cos \phi + i \hat{m} \sin \phi). \tag{3.5}$$

Here ψ_0 is real-valued amplitude, \hat{n} and \hat{m} are independent real unit vectors, and ϕ

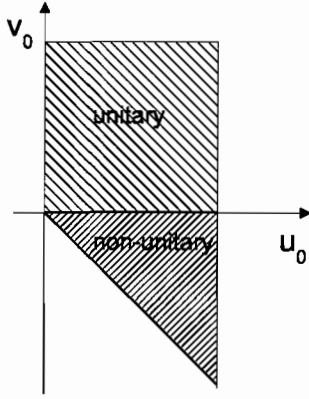


FIGURE 3.1: Mean-field phase diagram of a p -wave superconductor as described by Eq. (3.1). See the text for additional information.

is a phase angle. The free energy density can then be written

$$f = t\psi_0^2 + u_0\psi_0^4 + v_0\psi_0^4(1 - (\hat{n} \cdot \hat{m})^2) \sin^2 2\phi. \quad (3.6)$$

We now need to distinguish between two cases.

case 1: $v_0 > 0$. The free energy is minimized by $\hat{n} = \hat{m}$, and $\psi_0^2 = -t/2u_0$. The condition $u_0 > 0$ must be fulfilled for the system to be stable.

case 2: $v_0 < 0$. The free energy is minimized by $\hat{n} \perp \hat{m}$ and $\phi = \pi/4$, and $\psi_0^2 = -t/2(u_0 + v_0)$. The condition $u_0 + v_0 > 0$ must be satisfied for the system to be stable.

The first case implies $\boldsymbol{\psi} \times \boldsymbol{\psi}^* = 0$. This is referred to as the unitary phase. In the second case, $\boldsymbol{\psi} \times \boldsymbol{\psi}^* \neq 0$, which is referred to as the non-unitary phase. In either case, mean-field theory predicts a continuous phase transition from the disordered phase to an ordered phase at $t = 0$. The mean-field phase diagram in the u_0 - v_0 plane is shown in Fig. 3.1.

3.3.2 Renormalized Mean-field Theory

A better approximation is to still treat the order parameter as a constant, $\boldsymbol{\psi}(\mathbf{x}) \equiv \boldsymbol{\psi}$, but to keep the electromagnetic fluctuations. The part of the action that depends on the vector potential then takes the form

$$S_A = \frac{1}{8\pi\mu} \int d\mathbf{x} [k_\lambda^2 \mathbf{A}^2(\mathbf{x}) + (\nabla \times \mathbf{A}(\mathbf{x}))^2], \quad (3.7a)$$

where

$$k_\lambda = (1/8\pi\mu c e^2 \boldsymbol{\psi}^2)^{-1/2} \quad (3.7b)$$

is the inverse London penetration depth. Since \mathbf{A} enters S_A only quadratically, it can be integrated out exactly, and the technical development is identical to the s -wave case.[36]The result for the leading terms in powers of $|\boldsymbol{\psi}|^2$ in $d = 3$ is

$$f = t |\boldsymbol{\psi}|^2 + u_0 |\boldsymbol{\psi}|^4 - w (|\boldsymbol{\psi}|^2)^{3/2} + v_0 |\boldsymbol{\psi} \times \boldsymbol{\psi}^*|^2. \quad (3.8)$$

Here $w \propto \sqrt{\mu e^2}$ is a positive coupling constant whose presence drives the phase transition first order.

There are several interesting aspects of this result. First, the additional term in the mean-field free energy, with coupling constant w , is not analytic in $|\boldsymbol{\psi}|^2$. This is a result of integrating out the vector potential, which is a soft or massless fluctuation. Second, the resulting first-order transition is an example of what is known as the Coleman-Weinberg mechanism in particle physics,[37] or a fluctuation-induced first-order transition in statistical mechanics.[36]

Let us discuss the validity of the renormalized mean-field theory. The length scale given by the London penetration depth $\lambda = k_\lambda^{-1}$ needs to be compared with the second length scale that characterizes the action, Eq. (3.1), which is the superconducting coherence length $\xi = \sqrt{c/|t|}$. The ratio $\kappa = \lambda/\xi$ is the Landau-Ginzburg parameter. For $\kappa \rightarrow 0$, order parameter fluctuations are negligible (this is the limit of an extreme

type-I superconductor), and the renormalized mean-field theory becomes exact. For nonzero values of κ the fluctuations of the order parameter cannot be neglected, and the question arises whether or not they change the first-order nature of the transition. We will investigate this question next by means of two different technical approaches.

3.3.3 ϵ -expansion about $d = 4$

Here, we will follow notations of reference [43, 36] and apply the momentum shell renormalization group to the action Eq. (3.3). By this method, we can treat both the magnetic and superconducting fluctuations at about dimension 4. $\epsilon = 4 - d$ is presumed to be a small and positive parameter which will justify the asymptotic expansion of free energy functional. Eventually ϵ can be loosely treated to be 1, so the critical behavior of the system at spatial dimension 3 could be extrapolated.

First, the bare propagator for the complex OP field in the Fourier space can be identified from the quadratic terms from Eq. (3.3)

$$\langle \psi_\alpha(q) \psi_\beta^*(q) \rangle = \frac{\delta_{\alpha\beta}}{t + cq^2} \quad (3.9)$$

Coulomb gauge $\nabla \cdot A = 0$ will be used through this chapter. We denote photon propagator as,

$$\langle A_i(q) A_j(-q) \rangle = \frac{4\pi\mu p_{ij}(q)}{q^2}, \quad (3.10)$$

where $p_{ij}(q)$ is the transverse projection operator $p_{ij}(q) = \delta_{ij} - \frac{q_i q_j}{q^2}$. The vertices which can be read from Eq. (3.3) are listed in the Fig. 3.2. Recursion relations for the coupling constants can be obtained from doing the momentum shell integrals for the diagrams in Fig. 3.3 and Fig. 3.4. Now the RG flow equations for the coupling parameters read,

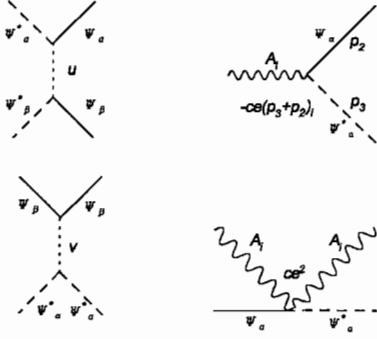


FIGURE 3.2: Vertices from Eq. (3.3). Solid lines denote the ψ field and dashed lines its complex conjugate. Wavy lines denote the vector potential. Dotted lines separate the localized interaction between paired electrons.

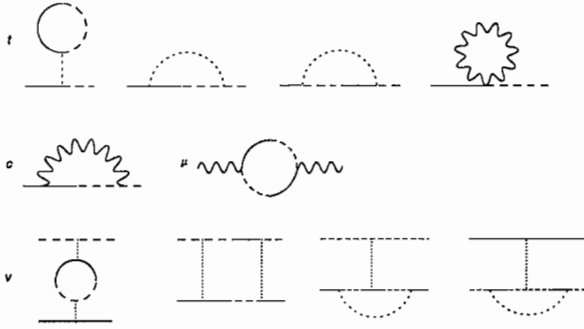


FIGURE 3.3: Diagrams renormalize the coupling parameters

$$\frac{dt}{dl} = (d + 2\chi)t + \frac{3ce^2}{\mu}k_d + \frac{4v + (n + 2)u}{t + c}k_d \quad (3.11)$$

$$\frac{du}{dl} = (d + 4\chi)u - \frac{(n + 8)u^2 + 8v^2 + 8uv}{(t + c)^2}k_d - 48\pi^2\mu^2c^2e^4k_d \quad (3.12)$$

$$\frac{dv}{dl} = (d + 4\chi)v - \frac{nv^2 + 12uv}{(t + c)^2}k_d \quad (3.13)$$

$$\frac{d\mu^{-1}}{dl} = (d - 2 + 2\chi_A)\mu^{-1} + \frac{2\pi nc^3e^2}{3(t + c)^4}(3t + c)k_d \quad (3.14)$$

$$\frac{dc}{dl} = (d - 2 + 2\chi - \frac{12\pi\mu ce^2}{(t + c)}k_d)c \quad (3.15)$$

$$\frac{de}{dl} = (1 + \chi_A)e \quad (3.16)$$

Here χ and χ_A are the rescaling parameters of fields ψ and A respectively k_d is the surface area of the d -dimensional ($d = 4$ in this case) unit sphere.

When the parameter $v = 0$, the above flow equations recover the recursion relation of H.L.M [36] as should be the case.

The case $e = 0$ case which corresponds to a p -wave superfluid, will not be discussed here. We are looking for physical fixed points for $e \neq 0$ case.

We choose χ to keep the parameter c fixed and $\chi_A = -1$ to keep the charge e fixed and assume that the parameter t has a fixed point of order ϵ . We find the value of $\mu^{*-1} = \frac{2\pi n k_d}{3\epsilon} e^2$ from the recursion relationship Eq.(3.14). By setting the right hand side of Eqs. (3.12,3.13) equal to zero, we get coupled quadratic algebraic equations which describe the fixed point values of parameters u and v . Let $u = \frac{\epsilon c^2}{k_d} x$ and $v = \frac{\epsilon c^2}{k_d} y$. From Eqs. (3.12,3.13) we get

$$x\left(1 + \frac{36}{n}\right) - ((n+8)x^2 + 8xy + 8y^2) - \frac{108}{n^2} = 0 \quad (3.17a)$$

$$y\left(1 + \frac{36}{n}\right) - ny^2 - 12xy = 0 \quad (3.17b)$$

If $y = 0$, Eq.(3.17a) naturally recovers s-wave case discussed by H.L.M [36] who found a real valued fixed point for $n > 365.9$, there exist real valued fixed points. For

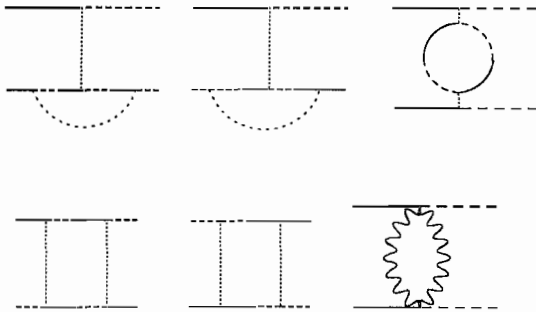


FIGURE 3.4: Diagrams renormalize the coupling parameter u

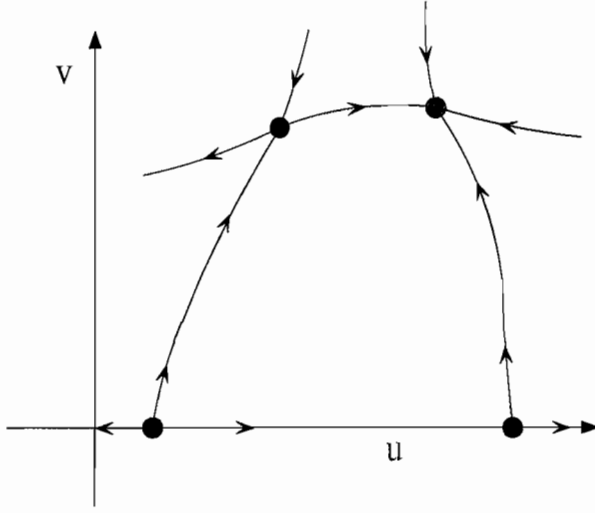


FIGURE 3.5: Renormalization group flows for $n=500$. The top right fixed point is stable in the u - v plane, so it is the critical fixed point

$y \neq 0$, the coupled quadratic equations can be reduced to one quadratic equation of y only, whose discriminant is

$$\Delta = -248832 - 6912n - 5424n^2 - 408n^3 + n^4 \quad (3.18)$$

To have Δ positive, n must be larger than $n_c = 420.928$. For any $n > n_c$, there exist new fixed points besides the s -wave ones. It can be easily verified that these newly appearing fixed points are falling in the non-unitary region in Fig. 3.1. We will refer to them as p -wave fixed points. The stability of a fixed point can be analyzed by linearizing the recursion relationship at that point to get the eigenfunctions and eigenvalues. A typical flow in the $u - v$ plane is plotted in Fig. 3.5.

Although the s -wave fixed point appears first when $n > 365.9$, it never controls the phase transition. Only when $n > n_c$, one of the p -wave fixed points takes the role of the critical fixed point. The critical fixed point in the large n limit takes the form

$$u^* \sim \frac{\varepsilon}{n}, v^* \sim \frac{\varepsilon}{n}, \mu^* \sim \frac{ne^2}{\varepsilon} \quad (3.19)$$

The non-vanishing value of v^* implies as least close to dimension 4, p-wave superconductors would belong to a different universality class from their s-wave cousins. From Fig. 3.5, the left bottom corner and top corner show a typical "run-away" flow. This "run-away" flow goes to the $u < 0$ and $v > 0$ region which falls off from the continuous phase transition region in the mean field graph Fig.3.1. It is a strong signature of first order phase transition which is also consistent with the extreme type I case discussion in section 3.3.2.

At first sight, the fact that a p-wave critical fixed point requires a larger number of components than the s-wave case may lead to the conclusion that it is more unlikely for p-wave superconductors to have a second order phase transition. However, we need to keep in mind that the ϵ -expansion is valid only for small ϵ , so this fixed point theory may only apply to dimensions very close to 4. To get n_c for $d = 3$, one would have to take the ϵ -expansion to higher loop order, which is a formidable job. Another issue is the limitation of the ϵ -expansion method which assumes perturbatively accessible fixed points, so it may apply only to a small parameter region. Outside of this region, other methods may have to be applied to study the nature of the phase transition, for instance dual theory.[38]

Another way to partly answer this question was pointed out[36] in the s-wave case: a lower bound $n_{cl} = 9.7$ for the critical value of n in the s-wave case was obtained by a large n expansion in $d = 3$. We will now apply this techniques to the p-wave case.

3.3.4 $1/n$ -expansion in $d = 3$

We refer to the literature,[36, 44] for the general large n technique. The basic idea is very similar to the ϵ -expansion we have shown. In the ϵ -expansion case, the expansion is performed at the Gaussian fixed point. Large n limit $O(n)$ model is usually referred to as spherical model and is solvable. So perturbation expansion around its saddle point is doable. Through the expansion, the most infrared divergent

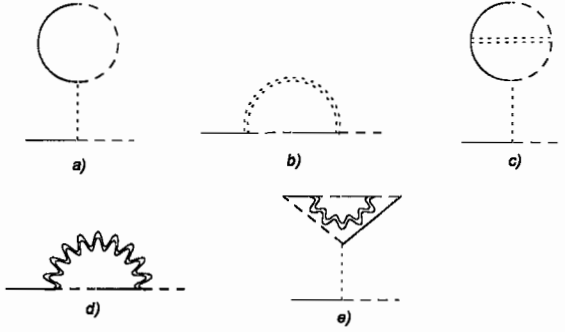


FIGURE 3.6: All the self energy graphs contribute to the critical exponent. The first row is from the ungauged part and the second row is from gauged part.

terms will be summed and we will show they contribute to the critical exponents in terms of $1/n$.

We make the assumption for the following perturbed parameters,

$$u \sim \frac{1}{n}, \quad v \sim \frac{1}{n}, \quad \text{and} \quad e^2 \sim \frac{1}{n} \quad (3.20)$$

This is reasonable by setting $\epsilon = 1$ in Eq. (3.19). In this section we set $c = 1$ and $\mu = 1$ for simplicity. To get critical exponents η and γ in terms of $1/n$, we will calculate a two point electron correlation function perturbatively. In Fourier space for small momentum k at critical temperature it reads

$$G(k) \equiv \langle \psi_\alpha(k) \psi_\alpha^*(k) \rangle_c \sim k^{-2+\eta} \quad (3.21)$$

Eq.(3.21) is the usual definition of critical exponent η . Here, c denotes the cumulant expansion of the full action Eq. (3.3). Now we show that, given Eq. (3.20), all the diagrammatic contributions to $G(k)$ can be controlled by an expansion in powers of $1/n$. Therefore, η can be expressed in terms of $1/n$. Eq.(3.21) for small η can be rewritten as

$$k^2 G(k) \sim k^\eta \sim (1 + \eta \log k + O(\eta^2)) \quad (3.22)$$

So the ultimate purpose is to do the perturbation for the renormalized Green's function, and extract the logarithmic dependence of momentum terms. Following the notation in [44], we define the renormalized mass t and self energy Σ by

$$t = G^{-1}(t, k = 0) \quad (3.23)$$

$$G^{-1}(t, k) = t_0 + k^2 + \Sigma(t, k) \quad (3.24)$$

Where t_0 is the bare parameter of free energy Eq.(3.3). In the following calculation, we will use $(t + k^2)^{-1}$ as the electron propagator, which leads to the renormalization rule: whenever we get a quantity of self energy insertions $\Sigma(t, k)$, we have to subtract the bare self energy $\Sigma(t, k = 0)$. For instance, applying this rule directly to Eq(3.24), we get

$$G^{-1}(t, k) = t + k^2 + \Sigma(t, k) - \Sigma(t, k = 0) \quad (3.25)$$

A less obvious example will be given when calculating the critical exponent γ .

Now compare Eq.(3.21,3.22) and Eq.(3.25), in order to get the critical exponent η , we need to extract the $-k^2 \log k$ term from $\Sigma(t = 0, k) - \Sigma(t = 0, k = 0)$. The self energy graphs of order $1/n$ are listed in Fig. 3.6. We only show order $1/n$ graphs that contribute to this critical exponent.

In the following calculations, we will apply dimensional regularization and Feynman integral tricks which are given in the appendix.

The self energy graphs a) and c) in Fig. 3.6 have no dependence k at all, so their contribution to η is zero. Before really calculate graph b), we refer to Fig. 3.7 for the definition of the double dashed line. The figure shows that every bubble has double contractions of the spin indices α, β , which amounts to order n , so graph b) actually is a sum of a series of graphs which are of order $1/n$. The single bubble repeats itself in the sum which will be defined as polarization bubble.

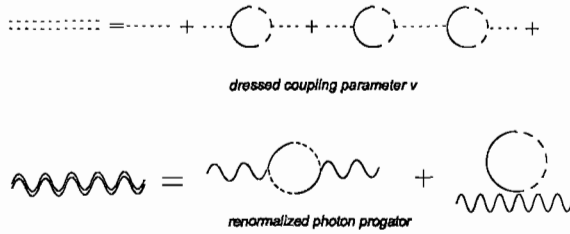


FIGURE 3.7: Dressed coupling parameter and renormalized photon propagator.

The polarization bubble in the Fig. 3.7 is

$$\Pi(t, k) = \int \frac{d^d p}{(2\pi)^d} \frac{1}{(p^2 + t)((p - k)^2 + t)} \quad (3.26)$$

Using the methods explained in the appendix, this integral can be easily done in dimension 3. with the result

$$\Pi(t, k) = \frac{1}{(4\pi)^{3/2}} \frac{2\sqrt{\pi}}{k} \arctan\left(\frac{1}{2\sqrt{t/k^2}}\right) \quad (3.27)$$

at criticality $t = 0$, so $\Pi(0, k) = \frac{1}{8k}$.

A ladder resummation of the bubble graphs gives us the double dashed line. In Fig. 3.7, we show how the double dashed line can be constructed from v vertices. The double dashed line constructed by the u vertices can be obtained in the same manner. By working out the combinatorial factor before every graph, we know this sum is actually a geometric series, for example, if we take consideration of the graph from v vertex as a piece for self energy of graph b). The contribution from this kind of vertex is

$$\Sigma_b(0, k) = \int \frac{d^d q}{(2\pi)^d} \frac{4v}{1 + 2vm\Pi(0, q)} \frac{1}{(q + k)^2} \quad (3.28)$$

As mentioned before, the first factor in the integrand is just the geometric

summation of the polarization bubbles. In the small q limit, it is

$$\frac{2}{m\Pi(0, q)} \quad (3.29)$$

. The parameter v drops out from the integrand which makes sense for the expected universal property of the critical exponent.

In $d = 3$, the integral in Eq. 3.28 is elementary: by extracting the $-k^2 \log k$ from $\Sigma_b(0, k) - \Sigma_b(0, 0)$, the contribution to η is $\frac{16}{3n\pi^2}$. The contribution from the u vertex is straightforward to get, the result is $\frac{8}{3n\pi^2}$. So the overall contribution to η so far is

$$\eta_b = \frac{16}{3n\pi^2} + \frac{8}{3n\pi^2} = \frac{8}{n\pi^2}$$

We now check the limit $v = 0$, which corresponds to s-wave case. From the above analysis, it does give the correct $\frac{8}{3n\pi^2}$ contribution to η as obtained by Ma [44].

The gauge field also contributes to the critical exponent η , via the self energy graph d). The double wavy line is the renormalized photon propagator as shown in Fig. 3.7. We choose Coulomb gauge as before, so the bare photon propagator is $\frac{p_{ij}(q)}{q^2}$. The self energy graph of the gauged field propagator is listed in Fig. 3.7. and reads

$$\Pi^{ij}(k) = \frac{ne^2}{2} \int \frac{d^d q}{(2\pi)^d} \frac{(2q+k)_i(2q+k)_j}{(t+q^2)(t+(k+q)^2)} + \int \frac{d^d q}{(2\pi)^d} \frac{\delta_{ij}}{(t+q^2)} \quad (3.30)$$

After some algebra, we get

$$\begin{aligned} \Pi^{ij}(k) &= \frac{ne^2}{32\pi} \left(4\sqrt{t} - 2\frac{k^2+4t}{k} \arcsin\left(\frac{k}{\sqrt{k^2+4t}}\right) \right) p_{ij}(k) \\ &\equiv \Pi_e(k) p_{ij}(k) \end{aligned} \quad (3.31)$$

The photon self energy has the same structure as the gauge propagator. So the renormalized photon propagator is

$$\frac{p_{ij}(k)}{k^2 - \Pi_e(k)}$$

Now we can calculate graph d) which reads

$$\Sigma_d(0, k) = -e^2 \int \frac{d^d p}{(2\pi)^d} \frac{(2k-p)_i (2k-p)_j}{(k-p)^2} \frac{p_{ij}(p)}{p^2 + \frac{ne^2}{32} p}$$

Again, we extract the $-k^2 \log k$ term from above integral, and obtain $\eta_d = \frac{-128}{3n\pi^2}$. This is a contribution from the gauge field only and has an opposite sign to the ungauged part. This contribution to the critical exponent η is the dominant part, so the overall critical exponent η is

$$\eta = \frac{-104}{3n\pi^2} \quad (3.32)$$

which has a negative value just as in the s-wave case though its absolute value is somewhat smaller.

Now we calculate the critical exponent γ . By a technique similar to the one we used for η , here we need to extract $\sqrt{t} \log(t)$ from the self energy graph. In this calculation, all the external momenta k are set to zero. We just show some typical contribution from self energy graphs to show how it works.

From graph a), we get

$$\Sigma_a(t, 0) = \frac{mu}{2} \int \frac{d^d p}{(2\pi)^d} \frac{1}{(p^2 + t)^2} \int \frac{-u}{1 + \frac{u}{2} m \Pi(0, q)}$$

This integral can be easily done and the mass dependence is proportional to \sqrt{t} , so $\gamma = 2$ which is the result for the spherical model.[7]

Graph c) is an example of the Feynman rule mentioned right below Eq. (3.24). Here, $\Sigma_b(t, 0)$ is inserted into graph a), so the expression reads

$$\Sigma_c(t, 0) = \frac{mu}{2} \int \frac{d^d p}{(2\pi)^d} \frac{1}{(p^2 + t)^2} (-\Sigma_b(t, 0) + \Sigma_b(t, 0)) \quad (3.33)$$

Summing all the graphs of this kind constructed from all possible vertices, we get a contribution to γ for anisotropic ungauged part is

$$\gamma = 2\left(1 - \frac{36}{n\pi^2}\right) \quad (3.34)$$

The gauge field also contributes to γ in a very similar way from graph e)

$$\gamma_e = -\frac{128}{n\pi^2} \quad (3.35)$$

So the overall critical exponent is

$$\gamma = 2\left(1 - \frac{100}{n\pi^2}\right)$$

For the physical value of $n = 6$, this is negative. This suggests a 1st order phase transition, and the smallest number of components to yield a positive γ is 10.1. Compared to the s-wave case, $\gamma = 2\left(1 - \frac{76}{n\pi^2}\right)$, which require $n > 7.7$ with a physical $n = 2$, we conclude it is a little more likely for the p-wave superconductors to have a second order phase transition.

The critical exponent $\nu = 1 - \frac{352}{3n\pi^2}$ can be easily obtained from the relation $\gamma = \nu(2 - \eta)$ which requires $n > 11.89$ for a continuous phase transition to be realized.

3.4 Discussion and Conclusion

The critical behavior of the p-wave superconductors with m complex components order parameter has been studied both in an ϵ -expansion and a large n expansion technique at dimension 3 to the first order of the control parameter. In the physical parameter region, a fluctuation induced first order phase transition is found. However, from one-loop ϵ -expansion, a new kind of critical fixed point is found for parameter $n > 420.9$. This corresponds to a continuous phase transition into the non-unitary

phase. The large n result is consistent with the RG result: to have a continuous phase transition, a number of components n larger than some n_c is required. However, the critical lower bound of $n_c = 11.9$ in the p-wave case is closer to the physical value $n = 6$ than in the s-wave case, which suggests that p-wave critical behavior is more likely to occur. This is the result of a leading expansion only, higher order expansions are necessary to consolidate these results.

CHAPTER IV

SKYRMION IN P-WAVE SUPERCONDUCTORS

4.1 Introduction

The shorter version of this chapter has been published in Ref.[11] with John Toner and Dietrich Belitz.

One of the most fascinating phenomena exhibited by conventional, *s*-wave, type-II superconductors is the appearance of an Abrikosov flux lattice of vortices in the presence of an external magnetic field \mathbf{H} in a range $H_{c1} < |\mathbf{H}| < H_{c2}$ between a lower critical field H_{c1} and an upper critical field H_{c2} . [9] It has been known for quite some time both theoretically [45, 46, 47, 48] and experimentally [49, 50] that these flux lattices can melt. The melting curve separates an Abrikosov vortex lattice phase from a vortex liquid phase, and the vortex lattice is found to melt in the vicinity of both H_{c1} and H_{c2} , as shown in Fig. 4.1. The melting occurs because the elastic constants of the flux lattice (i.e., the shear, bulk, and tilt moduli) vanish exponentially near these field values. As a result, in clean superconductors, root-mean-square positional thermal fluctuations $\sqrt{\langle |\mathbf{u}(\mathbf{x})|^2 \rangle}$ grow exponentially as these fields are approached. According to the Lindemann criterion, when these fluctuations become comparable to the lattice constant a , the translational order of the flux lattice is destroyed; i.e., the lattice melts.

Vortices are topological defects in the texture of the superconducting order parameter, and in *s*-wave superconductors, where the order parameter is a complex scalar, only one type of defect is possible. In *p*-wave superconductors, the more complicated structure of the order parameter allows for an additional type of

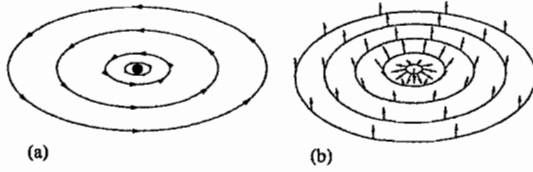


FIGURE 4.2: Order parameter configurations showing a vortex (a), and a skyrmion (b). The local order parameters are represented by arrows on loci of equal distance from the center of the defect. If the order parameter space is two-dimensional, only vortices are possible, and there is a singularity at the center of each vortex, (a). If the order-parameter space is three-dimensional, a skyrmion can form instead, where the spin direction changes smoothly from “down” at the center to “up” at infinity, (b).

Recent evidence of p -wave superconductivity in Sr_2RuO_4 [39, 40]² provides a motivation for further exploring the properties of skyrmion flux lattices in such systems. It was shown numerically by Knigavko et al.[3] that the interaction between skyrmions falls off only as $1/R$ with distance R , as opposed to the exponentially decaying interaction between vortices. As result, skyrmion lattices have a very different dependence of the magnetic induction on the external magnetic field near H_{c1} than do vortex lattices. In this chapter we confirm and expand on these results. We show analytically that the skyrmion-skyrmion interaction, in addition to a leading $1/R$ -dependence, has a correction proportional to $\ln R/R^2$ that explains a small discrepancy between the numerical results in Ref. [3] and a strict $1/R$ fit, and we calculate the interaction energy up to $O(1/R^2)$. We further show that the melting curve of a skyrmion lattice is qualitatively different from that of a vortex lattice. Namely, skyrmion lattices melt *nowhere* in the vicinity of H_{c1} , so there is a direct transition from the Meissner phase to the skyrmion lattice, see Fig. 4.8 below. Finally, we predict and discuss the magnetic induction distribution $n(B)$ of a skyrmion lattice state as observed in a muon spin resonance (μSR) experiment. For a vortex lattice,

²The precise nature of the order parameter in Sr_2RuO_4 is still being debated, see Ref. [58].

the exponential decay of the magnetic induction B at large distances from a vortex core implies $n(B) \propto \ln B/B$. For a skyrmion lattice, we find that B decays only algebraically, which leads to $n(B) \propto B^{-3/2}$. Some of these results have been reported before in Ref. [11].

The chapter is organized as follows. In Sec. 4.2 we review the formulation in Ref. [3] of the skyrmion problem. In particular, we start from the Ginzburg-Landau (GL) model for p -wave superconductors and consider the free energy in a London approximation. We parameterize the skyrmion solution of the saddle-point equations, and express the energy in terms of the solution of the saddle-point equations. In Sec. 4.3 we analytically solve these saddle-point equations perturbatively for large skyrmion radius R , and we calculate the energy of a single skyrmion as a power series in $1/R$ to order $1/R^2$. In Sec. 4.4 we determine the elastic properties of the skyrmion lattice, and we predict the magnetic induction distribution $n(B)$ as observed in a μ SR experiment.

4.2 Formulation of the Skyrmion Problem

In this section we review the formulation of the skyrmion problem presented in Ref. [3], who derived an effective action that allows for skyrmions as saddle-point solutions. The resulting ordinary differential equations (ODEs) describing skyrmions [3] are the starting point for our analytic treatment.

4.2.1 The Action in The London Approximation

We start from a Landau-Ginzburg-Wilson (LGW) functional appropriate for describing spin-triplet superconducting order,

$$S = \int d\mathbf{x} \mathcal{L}(\boldsymbol{\psi}(\mathbf{x}), \mathbf{A}(\mathbf{x})), \quad (4.1a)$$

with an action density

$$\begin{aligned} \mathcal{L}(\boldsymbol{\psi}, \mathbf{A}) = & t|\boldsymbol{\psi}|^2 + u|\boldsymbol{\psi}|^4 + v|\boldsymbol{\psi} \times \boldsymbol{\psi}^*|^2 + \frac{1}{2m}|\mathbf{D}\boldsymbol{\psi}|^2 \\ & + \frac{1}{8\pi}(\boldsymbol{\nabla} \times \mathbf{A})^2. \end{aligned} \quad (4.1b)$$

Here $\boldsymbol{\psi}(\mathbf{x})$ is a 3-component complex order parameter field,

$\mathbf{A}(\mathbf{x})$ is the electromagnetic vector potential, and $\mathbf{D} = \boldsymbol{\nabla} - iq\mathbf{A}$ denotes the gauge invariant gradient operator. m and q are the mass and the charge, respectively, of a Cooper pair, and we use units such that $\hbar = c = 1$. t , u , and v are the parameters of the LGW theory.

Let us look for saddle-point solutions to this action. In a large part of parameter space, namely, for $v < 0$ and $u > -v$, the stable saddle-point solution has the form $\boldsymbol{\psi}(\mathbf{x}) \equiv \boldsymbol{\psi} = f_0(1, i, 0)/\sqrt{2}$, where the amplitude f_0 is determined by minimization of the free energy.[42] This is known as the β -phase, and it is considered the most likely case to be realized in any of the candidates for p -wave superconductivity.³ Fluctuations about this saddle point are conveniently parameterized by writing the order parameter field as

$$\boldsymbol{\psi}(\mathbf{x}) = \frac{1}{\sqrt{2}} f(\mathbf{x}) (\hat{\mathbf{n}}(\mathbf{x}) + i\hat{\mathbf{m}}(\mathbf{x})), \quad (4.2)$$

where $\hat{\mathbf{n}}(\mathbf{x})$ and $\hat{\mathbf{m}}(\mathbf{x})$ are unit real orthogonal vectors in order-parameter space and $f(\mathbf{x})$ is the modulus of order parameter. With this parameterization, the action density can be written

$$\begin{aligned} \mathcal{L} = & t f^2 + (u + v) f^4 \\ & + \frac{1}{2m} \left[(\boldsymbol{\nabla} f)^2 + f^2 \left[\frac{1}{2} (\partial_i \hat{\mathbf{l}})^2 + (\hat{\mathbf{n}} \cdot \partial_i \hat{\mathbf{m}} - q A_i)^2 \right] \right] \\ & + \frac{1}{8\pi} (\boldsymbol{\nabla} \times \mathbf{A})^2, \end{aligned} \quad (4.3)$$

³See the discussion in Ref. [3], and references therein.

where $\hat{\boldsymbol{l}} = \hat{\boldsymbol{n}} \times \hat{\boldsymbol{m}}$, summation over repeated indices is implied, and we have made use of the identities listed in Appendix B.1.

There are two length scales associated with the action density, Eq. (4.3). The coherence length ξ is determined by comparing the f^2 term with the $(\nabla f)^2$ term,

$$\xi = 1/\sqrt{2m|t|}. \quad (4.4a)$$

It is the length scale over which the amplitude of the order parameter will typically vary. The London penetration depth λ is determined by comparing the \mathbf{A}^2 term with the $(\nabla \times \mathbf{A})^2$ term,

$$\lambda = \sqrt{m/4\pi q^2 \langle f \rangle^2}. \quad (4.4b)$$

The ratio of these two length scales, $\kappa \equiv \lambda/\xi$, is the Ginzburg-Landau parameter. Now we write $f(\mathbf{x}) = f_0 + \delta f(\mathbf{x})$, with $f_0 = \sqrt{-t/2(u+v)}$. Deep inside the superconducting phase, where $-t > 0$ is large, the amplitude fluctuations δf are massive, and to study low-energy excitations one can integrate out f in a tree approximation. This approximation becomes exact in the limit of large κ and is known in this context as the London approximation. We introduce dimensionless quantities by measuring distances in units of λ and the action in units of $\Phi_0^2/32\pi^3\lambda$, and we introduce a dimensionless vector potential $\mathbf{a} = 2\pi\lambda\mathbf{A}/\Phi_0$, with $\Phi_0 = 2\pi/q$ the magnetic flux quantum. Ignoring constant contributions to the action we can then write the action density in London approximation as follows,[3]

$$\mathcal{L}_L = \frac{1}{2} (\partial_i \hat{\boldsymbol{l}})^2 + (\hat{\boldsymbol{n}} \partial_i \hat{\boldsymbol{m}} - a_i)^2 + \mathbf{b}^2, \quad (4.5)$$

with $\mathbf{b} = \nabla \times \mathbf{a}$. The above derivation makes it clear that this effective action is a generalization of the $O(3)$ nonlinear sigma model (represented by the first term on

the right-hand side of Eq. (4.5)) that one obtains for a real 3-vector order parameter by integrating out the amplitude fluctuations in tree approximation.[31]

It should be noticed the parametrization of p-wave order parameter Eq. (4.3) is valid only in the parameter region discussed above. The stable saddle point solution has the property $\boldsymbol{\psi} \times \boldsymbol{\psi}^* \neq 0$ which corresponds to the non-unitary phase. However, there is another possibility which is referred as unitary phase and has been discussed in Chapter III. Namely, $\hat{\mathbf{n}} = \hat{\mathbf{m}}$. In this case, the parameterization of order parameter can be written as,

$$\boldsymbol{\psi}(\mathbf{x}) = f(\mathbf{x})\hat{\mathbf{n}}(\mathbf{x}) \times e^{i\phi(\mathbf{x})}, \quad (4.6)$$

This equation is nothing more than a straight forward analogy from a scalar order parameter of s-wave to a vector one. It can be expected if some p-wave superconductors happen to be described by Eq. (4.6), all the s-wave discussion can be directly applied to such case. A discussion of this analogy can be found in the reference [3], here we will focus on the non-unitary phase only.

4.2.2 Saddle-point Solutions of the Effective Action

We now are looking for saddle-point solutions to the effective field theory, Eq. (4.5). Considering $\hat{\mathbf{l}}$ and $\hat{\mathbf{n}}$ independent variables, and minimizing with respect to $\hat{\mathbf{l}}$ subject to the constraints $\hat{\mathbf{l}}^2 = \hat{\mathbf{n}}^2 = 1$ and $\hat{\mathbf{l}} \cdot \hat{\mathbf{n}} = 0$ yields

$$\nabla^2 \hat{\mathbf{l}} - \hat{\mathbf{l}}(\hat{\mathbf{l}} \cdot \nabla^2 \hat{\mathbf{l}}) + 2J_i(\hat{\mathbf{l}} \times \partial_i \hat{\mathbf{l}}) = 0, \quad (4.7a)$$

with

$$\mathbf{J} = \nabla \times \mathbf{b} \quad (4.7b)$$

the supercurrent. The variation with respect to \mathbf{a} is straightforward and yields a

generalized London equation,

$$a_i + J_i = \hat{\mathbf{n}} \partial_i \hat{\mathbf{m}}. \quad (4.7c)$$

It is convenient to take the curl of Eq. (4.7c) and use Eq. (B.3) to express the right-hand side of the resulting equation in terms of $\hat{\mathbf{l}}$. We then obtain the saddle-point equations as a set of coupled partial differential equations (PDEs) in terms of \mathbf{b} and $\hat{\mathbf{l}}$ only:

$$b_i - \nabla^2 b_i = \frac{1}{2} \epsilon_{ijk} \hat{\mathbf{l}} \cdot (\partial_j \hat{\mathbf{l}} \times \partial_k \hat{\mathbf{l}}), \quad (4.8a)$$

$$\nabla^2 \hat{\mathbf{l}} - \hat{\mathbf{l}} (\hat{\mathbf{l}} \cdot \nabla^2 \hat{\mathbf{l}}) + 2 \epsilon_{ijk} \partial_j b_k (\hat{\mathbf{l}} \times \partial_i \hat{\mathbf{l}}) = 0. \quad (4.8b)$$

Notice that the right-hand side of Eq. (4.8a) is valid in this form only at points where $\hat{\mathbf{l}}(\mathbf{x})$ is differentiable, see Eq. (B.3). Field configurations that obey these PDEs have an energy

$$E = \int d\mathbf{x} \left[\frac{1}{2} (\partial_i \hat{\mathbf{l}})^2 + (\hat{\mathbf{n}} \cdot \partial_i \hat{\mathbf{m}} - \mathbf{a})^2 + \mathbf{b}^2 - 2\mathbf{h} \cdot \mathbf{b} \right]. \quad (4.9)$$

where we have added a uniform external magnetic field \mathbf{h} measured in units of $\Phi_0/2\pi\lambda^2$. Notice that the energy depends on $\hat{\mathbf{n}}$ and $\hat{\mathbf{m}}$, whereas Eqs. (4.8) depend only on $\hat{\mathbf{l}}$, and that different choices of $\hat{\mathbf{n}}$ and $\hat{\mathbf{m}}$ can lead to the same $\hat{\mathbf{l}}$. Therefore, a field configuration satisfying Eqs. (4.8) is only necessary for making the energy stationary, but not sufficient.

4.2.2.1 Meissner Solution

A very simple order parameter configuration consists of constant $\hat{\mathbf{n}}(\mathbf{x})$ and $\hat{\mathbf{m}}(\mathbf{x})$ everywhere, see Fig. 4.3.

This leads to an $\hat{\mathbf{l}}(\mathbf{x}) \equiv \hat{\mathbf{l}}$ that is constant everywhere. Equation (4.8b) is then

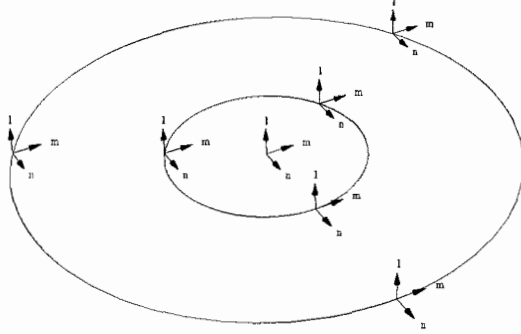


FIGURE 4.3: Configurations of the vectors $\hat{\ell}$, \hat{m} , and \hat{n} in a Meissner phase. All three vectors point in the same direction everywhere.

trivially satisfied. The right-hand side of Eq. (4.8a) vanishes, and hence the PDE for \mathbf{b} reduces to the usual London equation with a solution $\mathbf{b}(\mathbf{x}) \equiv 0$ in the bulk. This solution describes a Meissner phase with energy $E_M = 0$.

4.2.2.2 Vortex Solution

Now consider a field configuration where $\hat{\mathbf{n}}(\mathbf{x})$ and $\hat{\mathbf{m}}(\mathbf{x})$ are confined to a plane (say, the x - y plane), but rotate about an arbitrarily chosen point of origin:

$$\begin{aligned}\hat{\mathbf{n}}(\mathbf{x}) &= (\cos \phi, \sin \phi, 0), \\ \hat{\mathbf{m}}(\mathbf{x}) &= (-\sin \phi, \cos \phi, 0),\end{aligned}\tag{4.10}$$

where ϕ denotes the azimuthal angle in the x - y plane with respect to the x -axis. This field configuration, known as a vortex and shown in Fig. 4.4, corresponds to a constant $\hat{\mathbf{l}}$ everywhere except at the origin, where there is a singularity. Therefore, the right-hand side of Eq. (4.8a) is not applicable, and we return to Eq. (4.7c), which

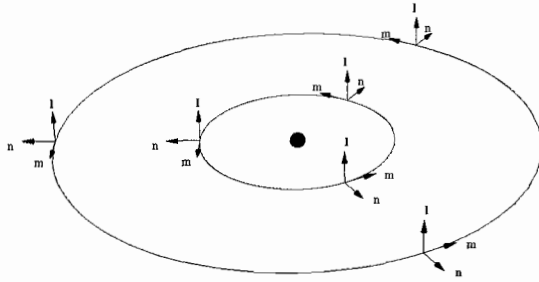


FIGURE 4.4: Configurations of the vectors $\hat{\ell}$, \hat{m} , and \hat{n} for a vortex. $\hat{\ell}$ is constant, whereas \hat{m} and \hat{n} rotate about the vortex core. Notice that the vector shown in Fig. 4.2(a) is \hat{n} .

takes the form

$$a_i + \epsilon_{ijk} \partial_j a_k = \partial_i \phi. \quad (4.11)$$

For any closed path \mathcal{C} in the x - y plane that surrounds the origin one has

$$\oint_{\mathcal{C}} d\ell \cdot \nabla \phi(\mathbf{x}) = 2\pi, \quad (4.12a)$$

or, by Stokes' theorem,

$$\int_{\mathcal{A}} d\mathbf{s} \cdot (\nabla \times \nabla \phi(\mathbf{x})) = 2\pi, \quad (4.12b)$$

where \mathcal{A} is the surface whose boundary is \mathcal{C} .⁴ This quantization condition shows that, instead of Eq. (4.8a), we have

$$\mathbf{b}(\mathbf{x}) - \nabla^2 \mathbf{b}(\mathbf{x}) = 2\pi \hat{z} \delta(x) \delta(y). \quad (4.13)$$

⁴More generally, ϕ is an element of the circle or one-sphere S_1 , and hence $\oint_{\mathcal{C}} d\ell \cdot \nabla \phi(\mathbf{x}) = 2\pi n$ with n an integer. n is a topological invariant that characterizes the singularity (known as a vortex), and the number of flux quanta that penetrate the vortex is $N = |n|$. The vortex with $n = 1$ has the lowest energy within this family of solutions (apart from the trivial “non-vortex” with $n = 0$).

This is solved by a \mathbf{b} that is equal to the boundary condition value everywhere along the z -axis and that falls off exponentially away from the z -axis. This solution is known as a vortex, and the amount of magnetic flux contained in one vortex is one flux quantum Φ_0 .

It is the precise analog of, and, indeed, essentially identical to, the familiar vortex in conventional s-wave superconductors.

The energy of a vortex given by Eq. (4.13), as calculated from Eq. (4.9), is logarithmically infinite. This is due to the point-like nature of the vortex core where the amplitude of the order parameter goes discontinuously to zero. In reality, the amplitude cannot vary on length scales shorter than the coherence length ξ , which provides an ultraviolet cutoff. The energy is then proportional to $\ln \kappa$. [9] In an external magnetic field this energy cost is offset by the magnetic energy gain due to letting some flux penetrate the sample. For κ larger than a critical value $\kappa_c = 1/\sqrt{2}$, and for external fields larger than the lower critical field H_{c1} , a hexagonal lattice of vortices has a lower energy than the Meissner phase. This state is known as an Abrikosov flux lattice, and is precisely the same as that in conventional s-wave superconductors. [9]

4.2.2.3 Skyrmion Solution

Due to the three-component nature of the order parameter, more complicated solutions of the saddle-point equations can be constructed for which the vector $\hat{\mathbf{l}}$ is not fixed. Let θ be the angle between $\hat{\mathbf{l}}$ and the z -axis, and consider a cylindrically symmetric field configuration parameterized as

$$\begin{aligned}\hat{\mathbf{l}} &= \hat{\mathbf{e}}_z \cos \theta(r) + \hat{\mathbf{e}}_r \sin \theta(r), \\ \hat{\mathbf{n}} &= (\hat{\mathbf{e}}_z \sin \theta(r) - \hat{\mathbf{e}}_r \cos \theta(r)) \sin \varphi + \hat{\mathbf{e}}_\varphi \cos \varphi \\ \hat{\mathbf{m}} &= (\hat{\mathbf{e}}_z \sin \theta(r) - \hat{\mathbf{e}}_r \cos \theta(r)) \cos \varphi - \hat{\mathbf{e}}_\varphi \sin \varphi.\end{aligned}$$

(4.14)

For this to minimize the energy, $\hat{\mathbf{l}}$ at large distances from the origin must be constant because of the first term in the energy, Eq. (4.9), and for a skyrmion centered in a cylinder of radius R we take $\hat{\mathbf{l}}$ to point in the $+z$ -direction for $r = R$, $\theta(r = R) = 0$. The quantization condition analogous to Eq. (4.12b) for the vortex is

$$\int dx dy \epsilon_{ij} \hat{\mathbf{l}} \cdot (\partial_i \hat{\mathbf{l}} \times \partial_j \hat{\mathbf{l}}) = 8\pi \quad (4.15)$$

To be consistent with this, $\hat{\mathbf{l}}$ must point in the $-z$ -direction at the origin, $\theta(r = 0) = \pi$.

Equation (4.14) parameterizes the order parameter in terms of a function $\theta(r)$. In addition, the energy depends on the vector potential which we take to be purely azimuthal, in accordance with our cylindrically symmetric *ansatz*,

$$\mathbf{a}(\mathbf{x}) = a(r) \hat{\mathbf{e}}_\varphi. \quad (4.16)$$

With this parameterization, we obtain from Eq. (4.9) the energy per unit length, along the cylinder axis, of a cylindrically symmetric skyrmion in a region of radius R ,

$$\begin{aligned} E/E_0 &= \frac{1}{2} \int_0^R dr r \left[(\theta'(r))^2 + \frac{1}{r^2} \sin^2 \theta(r) \right] \\ &+ \int_0^R dr r \left[\frac{1}{r} (1 + \cos \theta(r)) + a(r) \right]^2 \\ &+ \int_0^R dr r \left[\frac{a(r)}{r} + a'(r) \right]^2, \end{aligned} \quad (4.17)$$

where $E_0 = (\Phi_0/4\pi\lambda)^2$. This expression was first obtained in Ref. [3]. The three terms correspond to the three terms in the London action, Eq. (4.5). They represent the energy of the nonlinear sigma model, the kinetic energy of the supercurrent, and the magnetic energy, respectively. Minimization of E with respect to $\theta(r)$ and $a(r)$

yields Euler-Lagrange equations

$$\theta''(r) + \frac{1}{r} \theta'(r) = \frac{-\sin \theta(r)}{r} \left[\frac{2 + \cos \theta(r)}{r} + 2a(r) \right], \quad (4.18a)$$

$$a''(r) + \frac{1}{r} a'(r) - \frac{1}{r^2} a(r) = a(r) + \frac{1}{r} [1 + \cos \theta(r)]. \quad (4.18b)$$

This set of coupled, nonlinear ODEs must be solved subject to the boundary conditions $\theta(r = 0) = \pi$ and $\theta(r = R) = 0$, as explained above. The solution is known as a skyrmion, and each skyrmion contains two flux quanta.⁵ Since Eqs. (4.8) are necessary for making the energy stationary, the solution of Eqs. (4.18), inserted in Eqs. (4.14, 4.16), is guaranteed to be a solution of Eqs. (4.8) as well.

The energy of a single skyrmion is finite even in London approximation, see Sec. 4.3 below. For large values of the Ginzburg-Landau parameter κ a skyrmion therefore has a lower energy than a vortex, and the value of the lower critical field H_{c1} , at which the Meissner phase becomes unstable, is correspondingly lower for skyrmions than for vortices. This is the basis for the expectation that, in strongly type-II (i.e., large- κ) p -wave superconductors, a skyrmion flux lattice will be realized rather than a vortex flux lattice.

4.3 Analytic Solution of the Single-skyrmion Problem

We now need to solve the coupled ODEs (4.18). Due to their nonlinear nature, this is a difficult task, and in Ref. [3] it was done numerically. It turns out, however, that one can construct a perturbative analytical solution in the limit of large skyrmion radius, $R \gg \lambda$, with λ/R as a small parameter. This provides information about the

⁵More generally, $\int dx dy \epsilon_{ij} \hat{\mathbf{l}} \cdot (\partial_i \hat{\mathbf{l}} \times \partial_j \hat{\mathbf{l}}) = 8\pi Q$, with Q an integer. Q is a topological invariant that characterizes the defect (known as a skyrmion), and the number of flux quanta that penetrate the skyrmion is $N = 2Q$. [3] The skyrmion with $Q = 1$ has the lowest energy within this family of solutions.

superconducting state near H_{c1} , where the system is always in that limit. We will construct the perturbative solution, and calculate the energy, to second order in the small parameter. Our general strategy is as follows. We use Eq. (4.18b) to iteratively express a in terms of θ and its derivatives. Substitution in Eq. (4.18a) then yields a closed ODE for $\theta(r)$ that has to be solved.

4.3.1 Zeroth Order Solution

Let us first consider $R = \infty$. For $r \rightarrow \infty$, the left-hand side of Eq. (4.18b) falls off as $1/r^2$, and hence the vector potential, to zeroth order for large r , is given by

$$a_\infty(r) = -\frac{1}{r} [1 + \cos \theta(r)]. \quad (4.19)$$

Note that we use the *exact* $\theta(r)$ in this expression, *not* the zeroth order approximation to it. Since we can only compute $\theta(r)$ perturbatively, this expression for the zeroth order vector potential will itself have to be expanded perturbatively later. Substitution in Eq. (4.18a) yields

$$r^2 \theta''(r) + r \theta'(r) = \frac{1}{2} \sin(2\theta(r)). \quad (4.20)$$

The solution obeying the appropriate boundary condition is[3]

$$\theta_\infty(r) = f(r/\ell), \quad (4.21a)$$

with

$$f(x) = 2 \arctan(1/x). \quad (4.21b)$$

The length scale ℓ is arbitrary at this point and will be determined later from the

requirement $\theta(r = R < \infty) = 0$. For $R \gg 1$ it will turn out that $\ell \propto \sqrt{R}$. The skyrmion solution is schematically shown in Fig. 4.5.

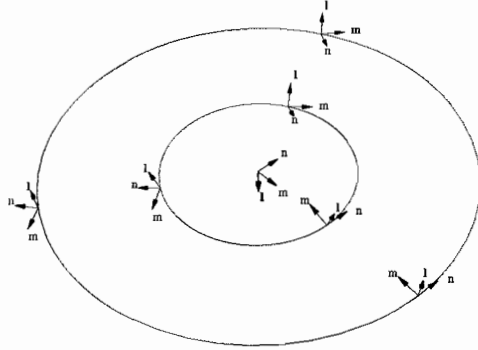


FIGURE 4.5: Configurations of the vectors $\hat{\ell}$, \hat{m} , and \hat{n} for a skyrmion. Notice that the vector shown in Fig. 4.2(b) is $\hat{\ell}$.

4.3.2 Perturbation Theory for $R \gg 1$

We now determine the corrections to the zeroth order solution. Let us write $\theta(r) = \theta_\infty(r) + \delta\theta(r)$ and $a(r) = a_\infty(r) + \delta a(r)$ and require $|\delta a(r)| \ll |a_\infty(r)|$ and $|\delta\theta(r)| \ll 1$.⁶ An inspection of the ODEs (4.18) shows that for $r \gg \ell$, the corrections can be expanded in a series in powers of $1/\ell$,

$$\delta\theta(r) = \frac{1}{\ell^2} g(r/\ell) + \frac{1}{\ell^4} h(r/\ell) + O(1/\ell^6), \quad (4.22a)$$

$$\delta a(r) = \frac{1}{\ell^3} \alpha(r/\ell) + \frac{1}{\ell^5} \beta(r/\ell) + O(1/\ell^7). \quad (4.22b)$$

The functions α and β can be determined by substituting Eq. (4.22b) in Eq. (4.18b) and equating coefficients of powers of $1/\ell$. The resulting equations for α and β are

⁶We emphasize that we do *not* require $|\delta\theta(r)| \ll |\theta_\infty(r)|$, as this requirement is neither necessary nor desirable. Rather, we expand, for instance, $\sin(\theta_\infty + \delta\theta) = \sin\theta_\infty \cos\delta\theta + \cos\theta_\infty \sin\delta\theta = \cos\theta_\infty \delta\theta + O(\delta\theta^2)$, which is valid for *all* $\delta\theta \ll 1$, *not* just for those that satisfy $|\delta\theta(r)| \ll |\theta_\infty(r)|$.

linear *algebraic* equations, not ODE's, because terms involving derivatives of α and β only enter at higher order in $1/\ell$, as one can verify by direct calculation. Hence, the solutions for α and β can be read off at once, and are:

$$\alpha(x) = \frac{16x}{(1+x^2)^3}, \quad (4.23a)$$

$$\begin{aligned} \beta(x) = & 2 \frac{(3x^4 - 6x^2 - 1)}{x^2(1+x^2)^3} g(x) - 2 \frac{(3x^2 - 1)}{x(1+x^2)^2} g'(x) \\ & + \frac{2}{1+x^2} g''(x) + A(x), \end{aligned} \quad (4.23b)$$

where

$$\begin{aligned} A(x) &= \alpha''(x) + \frac{1}{x} \alpha'(x) - \frac{1}{x^2} \alpha(x) \\ &= \frac{384x(x^2 - 1)}{(1+x^2)^5}. \end{aligned} \quad (4.23c)$$

Similarly, by comparing coefficients in Eq. (4.18a) we find ODEs for the functions g and h ,

$$g''(x) + \frac{1}{x} g'(x) - \frac{1}{x^2} \cos(2f(x)) g(x) = -\frac{2}{x} \sin(f(x)) \alpha(x), \quad (4.24a)$$

$$\begin{aligned} h''(x) + \frac{1}{x} h'(x) - \frac{1}{x^2} \cos(2f(x)) h(x) &= -\frac{2}{x} \sin(f(x)) \beta(x) \\ -\frac{1}{x^2} \sin(2f(x)) g^2(x) - \frac{2}{x} \cos(f(x)) \alpha(x) g(x), & \quad (4.24b) \end{aligned}$$

with $f(x)$ from Eq. (4.24b).

The ODE (4.24a) for g can be solved by standard methods, see Appendix B.2. The physical solution is the one that vanishes for $x \rightarrow 0$; it is proportional to x for

$x \gg 1$. We find

$$g(x) = -\frac{4}{3} \frac{x[x^2(4+x^2) + 2(1+x^2)\ln(1+x^2)]}{(1+x^2)^2}, \quad (4.25a)$$

the large- x asymptotic behavior of which is

$$g(x \gg 1) = -\frac{4}{3}x - \frac{16}{3} \frac{\ln x}{x} - \frac{8}{3x} + O\left(\frac{\ln x}{x^2}\right). \quad (4.25b)$$

This determines both the function $\beta(x)$, Eq. (4.23b), and the inhomogeneity of the ODE (4.24b) for $h(x)$. The latter can again be solved in terms of tabulated functions, see Appendix B.2, but we will need only the two leading terms for $x \rightarrow \infty$. The physical solution is again the one that vanishes for $x \rightarrow 0$, and its large- x asymptotic behavior is

$$h(x \gg 1) = -\frac{32}{9}x \ln x + \frac{536}{135}x + O(1/x). \quad (4.26)$$

Finally, we need to fix the length scale ℓ . It is determined by the requirement $\theta(r = R) = 0$. We find

$$\ell^2 = \sqrt{\frac{c}{2}}R \left[1 + \frac{\sqrt{2c}}{R} \ln R + \frac{\delta}{R} + O\left(\frac{\ln R}{R^{3/2}}\right) \right], \quad (4.27a)$$

where

$$\delta = \sqrt{2c} \left[\frac{1}{12}(7 - 6d/c^2) - \frac{1}{2} \ln(c/2) \right], \quad (4.27b)$$

and

$$c = 4/3, \quad (4.27c)$$

$$d = 536/135, \quad (4.27d)$$

are the absolute values of the coefficients of the terms proportional to x in the large- x expansions of $g(x)$ and $h(x)$, respectively. We see that, for $R \gg 1$, ℓ is indeed proportional to \sqrt{R} , as we had anticipated above. That is, the characteristic skyrmion length scale ℓ is the geometric mean of the London penetration depth λ (recall that we measure all lengths in units of λ) and the skyrmion size R . We now can also check our requirement $\delta\theta \ll 1$: from Eq. (4.22a) we see that for $r \ll \ell$, $\delta\theta(r) \propto 1/R$, while for $r \gg \ell$, $\delta\theta(r)$ is bounded by a term proportional to $1/R^{1/2}$. For R large compared to the penetration depth the condition is thus fulfilled for all r . Similarly, δa is found to be small compared to a_∞ for all r .

4.3.3 Energy of a Single Skyrmion

By using our perturbative solution in Eq. (4.17), we are now in a position to calculate the energy of a single skyrmion to $O(1/R^2)$. It is convenient to first expand the energy in powers of $1/\ell^2$, and then determine the R -dependence by using Eqs. (4.27).

Let us first consider the supercurrent energy E_c , i.e., the second term in Eq. (4.17). It can be written

$$E_c/E_0 = \int_0^R dr r (\delta a(r))^2 = \frac{1}{\ell^6} \int_0^R dr r (\alpha(r/\ell))^2 + O(1/\ell^6). \quad (4.28)$$

Using Eqs. (4.23a) we find

$$E_c/E_0 = \frac{32}{5} \frac{1}{\ell^4} + O(1/\ell^6). \quad (4.29)$$

Now consider the magnetic energy E_m , which is the third term in Eq. (4.17). It can be written

$$E_m/E_0 = \int_0^R dr r b^2(r), \quad (4.30)$$

with

$$b(r) = \frac{1}{r} a_\infty(r) + a'_\infty(r) + \frac{1}{r} \delta a(r) + \delta a'(r), \quad (4.31a)$$

the magnetic induction in our reduced units. Notice that in calculating $a_\infty(r)$, $\theta(r)$ in Eq. (4.19) needs to be expanded to first order in $\delta\theta$, as noted earlier. The two leading contributions to b^2 are then

$$b^2(r) = \frac{16}{\ell^4} \frac{1}{(1+x^2)^4} - \frac{8}{\ell^6} \frac{1}{(1+x^2)^2} \left[2 \frac{1-x^2}{x(1+x^2)^2} g(x) + \frac{2g'(x)}{1+x^2} + \frac{1}{x} \alpha(x) + \alpha'(x) \right] + O(1/\ell^8), \quad (4.31b)$$

where $x = r/\ell$. Performing the integral yields

$$E_m/E_0 = \frac{8}{3} \frac{1}{\ell^2} - \frac{112}{135} \frac{1}{\ell^4} + O(1/\ell^6). \quad (4.32)$$

Finally, we need to calculate the energy E_s coming from the gradient terms in the first term in Eq. (4.17). The expansion of the two terms in the integrand yields seven integrals that contribute to the desired order, they are listed in Appendix B.3. The

result is

$$\begin{aligned}
 E_s/E_0 &= 2 + \frac{8}{3} \frac{1}{\ell^2} + \frac{64}{9} \frac{\ln \ell}{\ell^4} \\
 &+ \left(-\frac{1,832}{135} - 2c\sqrt{2c}\delta + 4c^2 \ln(2/c) \right) \frac{1}{\ell^4} \\
 &+ O(1/\ell^6).
 \end{aligned}
 \tag{4.33}$$

Adding the three contributions, and using Eqs. (4.27), we find our final result for the energy of a skyrmion of radius $R \gg 1$,

$$\begin{aligned}
 E/E_0 &= 2 + \frac{8\sqrt{6}}{3} \frac{1}{R} - \frac{16}{3} \frac{\ln R}{R^2} \\
 &- \frac{4}{45} [7 + 30 \ln(3/2)] \frac{1}{R^2} + O(\ln^2 R/R^3).
 \end{aligned}
 \tag{4.34}$$

Knigavko et al.[3] solved the Eqs. (4.18) numerically, and thereby numerically determined the energy, which they fit to a $1/R$ -dependence. Their results are shown in Fig. 4.6 together with the analytical result given in Eq. (4.34). The perturbative solution up to $O(\ln R/R^2)$ was first given in Ref. [11]. We have also solved the equations numerically, using spectral methods to convert the boundary value problem to a set of algebraic equations for the unknown coefficients in an expansion in Chebyshev polynomials[59]. For the R -range shown, and on the scale of the figure, the result is indistinguishable from the perturbative one.

4.3.4 Spectral Methods

In this section, we will briefly review some of the most important concepts in the spectral method and apply the method to solve Eqs. (4.18).

Spectral methods have been utilized to solve both the differential and integral

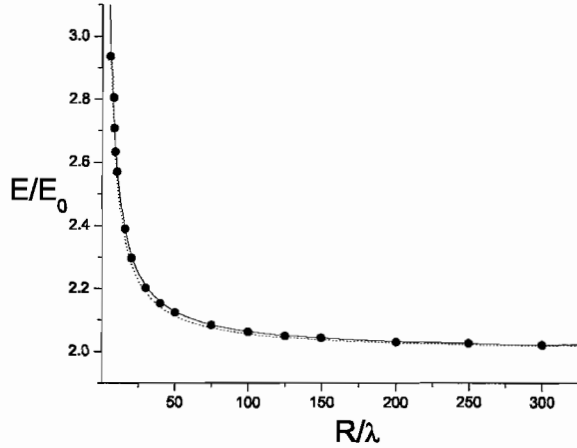


FIGURE 4.6: Numerical data for the energy per skyrmion per unit length (circles) together with the best fit to a pure $1/R$ behavior (dashed line) from Ref. [3], and the perturbative analytic solution given by Eq. (4.34) (solid line). A numerical solution using spectral methods is indistinguishable from the perturbative one.

equations. The basic idea is to assume that the unknown variables in the equations interested can be expanded by $N+1$ basis functions $\phi_n(x)$.

$$u(x) \approx u_N(x) \equiv \sum_{n=0}^N a_n \phi_n(x) \quad (4.35)$$

A candidate for the basis functions could be the *sin* functions, the Hermit polynomials, or the Chebyshev functions, etc. In our case, since we know the perturbation solutions are smooth rational functions without any periodic nodes, we will choose the Chebyshev series. The Chebyshev functions are defined as,

$$T_n(\cos \theta) \equiv \cos(n \theta) \quad (4.36)$$

So $T_n(x)$ is a polynomial functions in x . It can be seen easily that the Chebyshev polynomial are defined in the range $[-1, 1]$. This means that in order to use the

Chebyshev basis, the boundary value problems have to be transformed to this range by using a linear variable transformation.

The Chebyshev basis has many nice properties, for instance, it has a larger convergence basin than the Taylor power series with faster convergence. These properties can guarantee that for not very large N , the approximated sum of series in Eq. (4.35) will acquire a high enough accuracy.

In general, a differential equation can be written as

$$Lu(x) = f(x) \quad (4.37)$$

Here, L is a differential operator which has a linear or nonlinear property. If the variable $u(x)$ is replaced by the approximation $u_N(x)$ with fixed order N , in general, Eq. (4.37) will not be satisfied and let it be denoted as a residual function $R(x)$,

$$R(x) \equiv Lu_N(x) - f(x) \quad (4.38)$$

We want to minimize $R(x)$ by determining $N+1$ unknown coefficients a_n . So a differential equation is transformed to a set of algebraic equations. A $N+1$ conditions have to be artificially input to let these algebraic equation for a_n have a closed form. One way is to choose at most $N+1$ collocation (interpolation) points in the range $[-1, 1]$. It should be noted that boundary conditions will also reduce the number of chosen collocation points.

In our case, the appropriate boundary condition is $a(0) = 0$, $a(R) = 1/\pi R$, $\theta(0) = \pi$, and $\theta(R) = 0$. These boundary conditions naturally reduce $N + 1$ to $N - 1$ interpolation points. The simplest choice of interpolation points is an evenly distributed $N - 1$ points between $[-1, 1]$. Though this choice leads to a qualitatively accurate result, it is not the best choice. This is because that the true solution $\theta(r)$ as we have already known is sharp at the left bound and decays extremely slowly at the right bound. So it is natural to think a better choice could be larger

point density at the left bound and diluter point density at the right end. It turns out a Chebyshev grid choice is a better choice,

$$x_i \equiv -\cos\left[\frac{2i-1}{2(N+1)}\pi\right], \quad i = 1, 2, \dots, N-1 \quad (4.39)$$

After the collocation points are chosen, we are facing to solve $2N+2$ coupled non-linear algebraic equations (NLAEs). An reasonable guess of the roots of these NLAEs is taken to be the coefficients of the Chebyshev transformation of the zeroth order solutions, Eq.(4.21b) and Eq.(4.19). Then sophisticated computational packages, for instance, command FindRoot in Mathematica, can be applied to find the roots of those NLAEs. It turns out the computed Chebyshev series solution fit extremely well to our analytic solution for a reasonably large value of R . For small R , our analytic solution breaks down and this numerical solution will provide a complementary method to give the correct solution.

4.4 Observable Consequences of the Skyrmion Energy

Our calculation of the skyrmion energy in Sec. 4.3 has been for a cylindrically symmetric skyrmion. The result shows that each skyrmion will try to maximize its radius in order to minimize the energy, which leads to a repulsive interaction between skyrmions whose potential is proportional to $1/R$. Skyrmions are thus expected to form a lattice structure, as do vortices, and they will thus *not* be cylindrically symmetric, since the lattice is not. One expects a hexagonal lattice, as in the case of the vortex lattice, and our treatment involves the same approximation as in the numerical work of Ref. [3]; namely, approximating the hexagonal unit cell by a circle of the same area. We expect this approximation to recover the correct scaling of the energy, and to reproduce the coefficients of that scaling to the same accuracy as radius of the circle of the same area reproduces the distance from the center of a hexagon to the nearest point on its edge; i.e., $\sqrt{2\sqrt{3}/\pi} - 1 \approx 0.05$. We will now proceed to

calculate observable consequences of the dependence of the energy on the radius of the unit cell. These include the relation $B(H)$ between the magnetic induction B and the external magnetic field H , the elastic properties of the skyrmion lattice and the resulting phase diagram in the H - T -plane, and the μ SR signature of the skyrmion lattice.

4.4.1 $B(H)$ for a Skyrmion Lattice

We start by calculating the dependence of the equilibrium lattice constant R on an external magnetic field H . This is done by minimizing the energy per unit volume, which is the energy per unit length per skyrmion, Eq. (4.34), divided by the area per skyrmion, πR^2 , plus a reduction in the energy of $-2\Phi_0 H/4\pi$ due to the external field. The latter is obtained from the last term in Eq. (4.9) by noting that the magnetic flux $\int dx dy (\hat{z} \cdot \mathbf{b}) = 2\Phi_0$ for each skyrmion in the lattice. This negative external field contribution must also be divided by πR^2 to give the energy per unit volume. Returning to ordinary units, we thus find a Gibbs free energy per unit volume

$$g(R) = \frac{K}{4\pi^2} \left[-\frac{\Delta}{R^2} + \frac{4\sqrt{6}\lambda}{3R^3} + O\left(\frac{\lambda^2 \ln(R/\lambda)}{R^4}\right) \right], \quad (4.40)$$

where $K = \Phi_0^2/2\pi\lambda^2$, and

$$\Delta \equiv 1 - H/H_{c1}, \quad (4.41)$$

with $H_{c1} \equiv K/2\Phi_0$. For $H < H_{c1}$, we have $\Delta > 0$, and the free energy is minimized by $R = \infty$; i.e., the skyrmion density is zero. This is the Meissner phase. For $H > H_{c1}$ the free energy is minimized by

$$R = R_0 = 2\sqrt{6}\lambda/\Delta, \quad (4.42)$$

and there is a nonzero skyrmion density. We see that H_{c1} is indeed the lower critical field. Note that the equilibrium flux lattice constant R_0 diverges as $1/\Delta$, whereas in the case of a vortex lattice it diverges only logarithmically as $\ln(1/\Delta)$. [9] For the averaged magnetic induction $B = 2\Phi_0/\pi R_0^2$ this implies

$$B(H) = \frac{1}{3} H_{c1} \Delta^2. \quad (4.43)$$

For $H \rightarrow H_{c1}$ from above, $B(H)$ in the case of a skyrmion lattice thus vanishes with zero slope, whereas in the case of a vortex lattice it vanishes with an infinite slope. [9] This result, with a slightly different prefactor, was first obtained from the aforementioned numerical determination of $E(R)$ in Ref. [3]. Note that the only material parameter that appears in this expression for B is H_{c1} .

4.4.2 Elastic Properties of the Skyrmion Lattice

Now we turn to the elastic properties of skyrmion lattice. Let the equilibrium position of the i^{th} skyrmion line be described by a two-dimensional lattice vector $\mathbf{R}_i = (X_i, Y_i)$, and the actual position by

$$\mathbf{r}_i(z) = (X_i + u_x(\mathbf{R}_i, z), Y_i + u_y(\mathbf{R}_i, z), z), \quad (4.44)$$

where $\mathbf{u} = (u_x, u_y)$ is the two-dimensional displacement vector, and we use z as the parameter of the skyrmion line. The strain tensor $u_{\alpha\beta}$ is defined as

$$u_{\alpha\beta}(\mathbf{x}) = \frac{1}{2} \left(\frac{\partial u_\alpha}{\partial x_\beta} + \frac{\partial u_\beta}{\partial x_\alpha} \right). \quad (4.45)$$

For a hexagonal lattice of lines parallel to the z -axis, the elastic Hamiltonian is [60]

$$H_{\text{el}} = \frac{1}{2} \int d\mathbf{x} \left[2\mu (u_{\alpha\beta}(\mathbf{x})u_{\alpha\beta}(\mathbf{x})) + \lambda_L (u_{\alpha\alpha}(\mathbf{x}))^2 + K_{\text{tilt}} |\partial_z \mathbf{u}(\mathbf{x})|^2 \right]. \quad (4.46)$$

Here summation over repeated indices is implied. μ , λ_L , and K_{tilt} are the shear, bulk, and tilt moduli, respectively, of the lattice, and we now need to determine these elastic constants.

The combination $\mu + \lambda_L$ can be obtained by considering the energy change of the system upon a dilation of the lattice. Let R change from R_0 to $R_0(1 + \epsilon)$, with a dilation factor $\epsilon \ll 1$. Such a dilation corresponds to a displacement field $\mathbf{u}(\mathbf{x}) = \epsilon \mathbf{x}_\perp$, where \mathbf{x}_\perp is the projection of \mathbf{x} perpendicular to the z -axis.[60] The strain tensor is thus $u_{\alpha\beta} = \epsilon \delta_{\alpha\beta}$. Inserting this in the elastic Hamiltonian, Eq. (4.46), yields the energy per unit volume for the dilation,

$$E_{\text{dil}}/V = 2(\mu + \lambda_L) \epsilon^2. \quad (4.47a)$$

This should be compared with the energy as given by Eq. (4.40),

$$\begin{aligned} E_{\text{dil}}/V &= g(R_0(1 + \epsilon)) - g(R_0) = \frac{1}{2} \left(\frac{\partial^2 g}{\partial R^2} \right)_{R_0} (\epsilon R_0)^2 \\ &= \frac{K \Delta^3}{96\pi^2 \lambda^2} \epsilon^2. \end{aligned} \quad (4.47b)$$

Comparing Eqs. (4.47a) and (4.47b) yields

$$\mu + \lambda_L = K \Delta^3 / 192\pi^2 \lambda^2. \quad (4.48)$$

To obtain μ (or λ_L) separately, we should consider shear deformations, which change the shape, but not the area, of the unit cell. Since we have already approximated the hexagonal unit cell by a circle, this is difficult to do, and we resort to the following heuristic method, which will give the correct scaling of μ with Δ (but not the correct prefactors). To this end we observe that our result for the Gibbs free energy, Eq. (4.40), is of the same form we would have obtained if the skyrmions interacted via a pair potential $U(r)$ that for distances $r \lesssim R_0$ is of order $K\lambda/r$, and for larger distances falls off sufficiently rapidly that only nearest-

neighbor interactions need to be considered. Treating the skyrmion lattice as if such an “equivalent potential” were the origin of the skyrmion energy allows us to calculate the shear modulus as follows:

If the lattice is subjected to a uniform $x - y$ shear - i.e., a displacement field $\mathbf{u}(\mathbf{x}) = 2\epsilon y \hat{\mathbf{x}}$ - for which $u_{xy} = u_{yx} = \epsilon$, and all other components of $u_{\alpha\beta} = 0$, the elastic energy, Eq. (4.46) predicts an elastic energy per unit volume of

$$E/V = 2\mu\epsilon^2. \quad (4.49)$$

Such a shear skews each fundamental triangle of the skyrmion lattice by displacing the top (or bottom, for the downward-pointing triangles) to the right (or the left, for downward-pointing triangles) by an amount of order ϵR_0 , where R_0 is the skyrmion lattice spacing found earlier, Eq. (4.42) (see Fig. 4.7). This shortens the length of

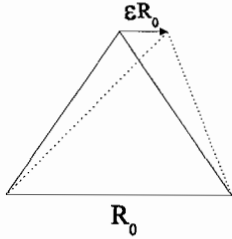


FIGURE 4.7: Shearing of the skyrmion lattice results in a change in the distance between skyrmion centers, and hence in their effective interaction. See the text for additional information.

one bond of the triangle by an amount of order ϵR_0 , and increases the opposite bond’s length by the same amount. Hence, the linear in ϵ change in the “equivalent potentials” of these two bonds cancels, and the total change ($\Delta E/\text{triangle}$) in the energy per unit length of fundamental triangle, per triangle, is given by:

$$\frac{\Delta E}{\text{triangle}} = U''(R_0)(\epsilon R_0)^2 \times O(1) \quad (4.50)$$

where the $O(1)$ factor includes both geometrical factors (e.g., sines and cosines), and counting factors (e.g., to avoid multiple counting of each triangle). If we take $U(r) = K\lambda/r$ as suggested above, we have

$$U''(R_0) = \frac{K\lambda}{R_0^3} \times O(1). \quad (4.51)$$

Inserting this into Eq. (4.50) gives

$$\frac{\Delta E}{\text{triangle}} = \frac{K\lambda}{R_0} \epsilon^2 \times O(1). \quad (4.52)$$

This is the change in energy per unit cell. To get the energy per unit volume, we must divide by the unit cell area, which is πR_0^2 . Doing so gives

$$\frac{\Delta E}{V} = \frac{K\lambda}{R_0^3} \epsilon^2 \times O(1). \quad (4.53)$$

Comparing this with Eq. (4.49) then determines μ :

$$\mu = \frac{K\lambda}{R_0^3} \times O(1). \quad (4.54)$$

Using Eq. (4.42) for R_0 then leads to our final result for μ :

$$\mu = \frac{K\Delta^3}{\lambda^2} \times O(1). \quad (4.55a)$$

From Eq. (4.48) we see that the bulk modulus or Lamè coefficient is given given by the same expression,

$$\lambda_L = \frac{K\Delta^3}{\lambda^2} \times O(1). \quad (4.55b)$$

We now turn to the tilt modulus K_{tilt} . This can be obtained by considering a uniform tilt of the axes of the skyrmions away from the z -axis, i.e., away from

the direction of the external magnetic field H , by an angle $\vartheta \ll 1$. For small ϑ , $\vartheta = |\partial \mathbf{u} / \partial z|$. Therefore, the tilt energy in Eq. (4.46) is identical with the change of the $\mathbf{B} \cdot \mathbf{H}$ term in Eq. (4.9). This contribution to the energy is, per unit length and in ordinary units, given by $-\Phi_0 H \cos \theta / 2\pi$, and its change due to tilting is $\Phi_0 H (1 - \cos \vartheta) / 2\pi \approx \Phi_0 H \vartheta^2 / 4\pi = \Phi_0 H |\partial_z \mathbf{u}|^2 / 4\pi$. Dividing this result by the unit cell area πR_0^2 , using Eq. (4.42) for R_0 , and identifying the result with the tilt term in the elastic Hamiltonian, Eq. (4.46), yields K_{tilt} in the vicinity of H_{c1} ,

$$K_{\text{tilt}} = \frac{1}{12\pi} H_{c1}^2 \Delta^2. \quad (4.56)$$

We now are in a position to calculate the mean-square positional fluctuations $\langle |\mathbf{u}(\mathbf{x})|^2 \rangle$. Taking the Fourier transform of Eq. (4.46), and using the equipartition theorem, yields

$$\langle |\mathbf{u}(\mathbf{x})|^2 \rangle_{\text{T}} = \frac{k_{\text{B}} T}{V} \sum_{\mathbf{q} \in \text{BZ}} \frac{1}{\mu q_{\perp}^2 + K_{\text{tilt}} q_z^2} \quad (4.57\text{a})$$

for the transverse fluctuations, and

$$\langle |\mathbf{u}(\mathbf{x})|^2 \rangle_{\text{L}} = \frac{k_{\text{B}} T}{V} \sum_{\mathbf{q} \in \text{BZ}} \frac{1}{(2\mu + \lambda_{\text{L}}) q_{\perp}^2 + K_{\text{tilt}} q_z^2} \quad (4.57\text{b})$$

for the longitudinal ones. Here \mathbf{q}_{\perp} and q_z are the projections of the wave vector \mathbf{q} orthogonal to and along the z -direction, respectively. The Brillouin zone BZ of the skyrmion lattice is a hexagon (which we have approximated by a circle) of edge length $O(1)/R_0$ in the plane perpendicular to the z -axis, and extends infinitely in the z -direction.

Since μ and λ_{L} are the same apart from a prefactor of $O(1)$ which we have not determined, see Eqs. (4.55), the same is true for the transverse and longitudinal contributions to the fluctuations, and it suffices to consider the former. Performing

the integral over q_z yields

$$\begin{aligned} \langle |\mathbf{u}(\mathbf{x})|^2 \rangle &= \langle |\mathbf{u}(\mathbf{x})|^2 \rangle_L + \langle |\mathbf{u}(\mathbf{x})|^2 \rangle_T \\ &\propto \langle |\mathbf{u}(\mathbf{x})|^2 \rangle_T = \frac{k_B T}{\sqrt{\mu K_{\text{tilt}}}} \int_{\text{BZ}} \frac{d^2 q_{\perp}}{8\pi^2} \frac{1}{q_{\perp}}. \end{aligned} \quad (4.58)$$

The remaining integral over the perpendicular part of the Brillouin zone is proportional to $1/R_0$, and using Eqs. (4.55) and (4.42) we obtain

$$\langle |\mathbf{u}(\mathbf{x})|^2 \rangle = \frac{k_B T}{\lambda H_{c1}^2} \frac{1}{\Delta^{3/2}} \times O(1). \quad (4.59)$$

Using Eq. (4.42) again we see that, near H_{c1} , $\langle |\mathbf{u}(\mathbf{x})|^2 \rangle \propto R_0^{3/2} \ll R_0^2$. That is, in this regime the positional fluctuations are small compared to the lattice constant, which tells us that the lattice will be stable against melting. To elaborate on this, let us consider the Lindemann criterion for melting, which states that the lattice will melt when the ratio $\Gamma_L = \langle |\mathbf{u}(\mathbf{x})|^2 \rangle / R_0^2$ exceeds a critical value $\Gamma_c = O(1)$. In our case,

$$\Gamma_L = \frac{k_B T}{H_{c1}^2 \lambda^{5/2}} \Delta^{1/2} \times O(1). \quad (4.60)$$

As $H \rightarrow H_{c1}$, $\Delta \rightarrow 0$, and the Lindemann ratio vanishes. Hence, the skyrmion lattice does not melt at any temperature for H close to H_{c1} .

We finally determine the shape of the melting curve $H_m(T)$ near the superconducting transition temperature T_c . Since, in mean field theory, $H_{c1} \propto (T_c - T)$, and $\lambda \propto 1/\sqrt{T_c - T}$, [9] we find from Eq. (4.60) by putting $\Gamma_L = \text{const.} = O(1)$,

$$H_m - H_{c1} \propto (T_c - T)^{5/2}. \quad (4.61)$$

The resulting phase diagram is shown schematically in Fig. 4.8. Comparing with Fig. 4.1 we see the qualitative difference between the vortex and skyrmion flux

lattices: whereas the vortex lattice always melts near H_{c1} , the skyrmion lattice melts nowhere near H_{c1} . This is a direct consequence of the long-ranged interaction between skyrmions, as opposed to the screened Coulomb interaction between vortices.

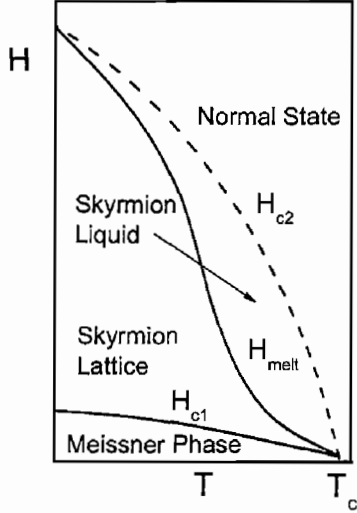


FIGURE 4.8: External field (H) vs. temperature (T) phase diagram for skyrmion flux lattices. In contrast to the vortex case, see Fig. 4.1, there is a direct transition from the skyrmion flux lattice to the Meissner phase. The theory predicts the shape of the melting curve only close to T_c , see Eq. (4.61); the rest of the curve is an educated guess.

4.4.3 μ SR Signature of a Skyrmion Flux Lattice

Muon spin rotation (μ SR) is a powerful tool which has been extensively applied to study the vortex state in type-II superconductors. [61, 62] A crucial quantity in this type of experiment is the μ SR line shape $n(B)$, which is the probability density that a muon experiences a local magnetic induction B and precesses at the Larmor frequency that corresponds to B . It is defined as

$$n(B) \equiv \langle \delta(B(\mathbf{x}) - B) \rangle, \quad (4.62)$$

where $B(\mathbf{x})$ is the magnitude of the local magnetic induction, and $\langle \dots \rangle$ denotes the spatial average over a flux lattice unit cell.

To predict the μ SR line shape for a skyrmion flux lattice near H_{c1} it is sufficient, for large R_0 , to use only the lowest solution for the magnetic induction obtained in Sec. 4.3.1. Inserting Eqs. (4.21) into Eq. (4.19), we find for the magnetic induction in reduced units

$$b(r) = -\frac{4\ell^2}{(r^2 + \ell^2)^2}. \quad (4.63)$$

Restoring physical units then gives

$$B(r) = \frac{H_{c1}\lambda^2}{2} \frac{\ell^2}{(r^2 + \ell^2)^2}, \quad (4.64)$$

where we've dropped the minus sign since only the magnitude of B can be detected in μ SR measurements.

From Eq. (4.62) we then find, for H near H_{c1} , where our theory is valid,

$$n(B) = \frac{1}{24\sqrt{2}} \left(\frac{H_{c1}\Delta}{B} \right)^{\frac{3}{2}} \frac{1}{H_{c1}} \quad (\text{skyrmions}). \quad (4.65)$$

Of course, $n(B)$ is only non-zero for those values of B that actually occur inside the unit cell of the skyrmion lattice. From Eq. (4.64), we see that the maximum value of B will occur at the center of the unit cell ($r = 0$), which gives

$$|B|_{\max} = |B(r = 0)| = \frac{H_{c1}\lambda^2}{2\ell^2} = \frac{H_{c1}\Delta}{8}, \quad (4.66a)$$

The minimum value of B occurs at the edge of the unit cell (i.e., $r = R$), where Eq. (4.64) gives

$$|B|_{\min} = |B(r = R)| = \frac{H_{c1}\lambda^2\ell^2}{2R^4} = \frac{H_{c1}\Delta^3}{288}. \quad (4.66b)$$

In the second equalities in Eqs. (4.66) we have used Eqs. (4.27) and (4.42) to express ℓ in terms of R and R in terms of Δ , respectively.

To summarize: the prediction of our cylindrical approximation for $n(B)$ is that the simple power law Eq. (4.65) holds for $B_{\min} < B < B_{\max}$. For $B < B_{\min}$ or $B > B_{\max}$, $n(B) = 0$.

Since the above results were derived in the cylindrical approximation, we expect the numerical coefficients in Eqs. (4.66) to be off by the approximately 5% mentioned in the opening paragraph of Sec. 4.4 throughout most of the range $B_{\min} < B < B_{\max}$. When B gets close to B_{\min} , however, we expect more radical departures from the cylindrical approximation. This is because contours of constant B near the edge of the hexagonal unit cell will, for B within 5% or so of B_{\min} or so, start intersecting the unit cell boundary, leading to van Hove-like singularities in $n(B)$. Such subtleties cannot be captured within the cylindrical approximation. Note, however, that they only occur over a very small range of B ; for the remainder of the large window $B_{\min} < B < B_{\max}$ (which spans three decades even for Δ as big as 0.2), Eq. (4.65) holds, up to the aforementioned 5% numerical error in its overall coefficient.

To compare this result with the corresponding one for a vortex flux lattice, we recall that in that case $B(r)$ is given by a modified Bessel function which for distances $r \gg \lambda$ takes the form

$$B(r) \propto \frac{1}{\sqrt{r/\lambda}} e^{-r/\lambda}. \quad (4.67)$$

For small B , we then find from Eq. (4.62)

$$n(B) \propto \frac{\ln(1/B)}{B} \quad (\text{vortices}). \quad (4.68)$$

We see that the μ SR line shape is qualitatively different in the two cases, due to the long-range nature of $B(r)$ in the skyrmion case versus the exponential decay in the vortex case.

4.5 Conclusion

In summary, we have considered properties of a flux lattice formed by the topological excitations commonly referred to as skyrmions, rather than by ordinary vortices. For strongly type-II materials in the β -phase, skyrmions are more stable than vortices.[3] We have presented an analytical calculation of the energy of a cylindrically symmetric skyrmion of radius R up to $O(1/R^2)$ in an expansion in powers of $1/R$. This provides excellent agreement with numerical solutions of the skyrmion equations. The interaction between skyrmions is long-ranged, falling off only as the inverse distance, in contrast to the exponentially decaying interaction between vortices. As a result, the elastic properties of a skyrmion flux lattice are very different from those of a vortex flux lattice, which leads to qualitatively different melting curves for the two systems. The phase diagram thus provides a smoking gun for the presence of skyrmions. In addition, the μ SR line width for skyrmions is qualitatively different from the vortex case.

We finally mention two limitations of our discussion. First, we have restricted ourselves to a discussion of a particular p -wave ground state, namely, the non-unitary state sometimes referred to as the β -phase. This state breaks time-reversal symmetry and the recently reported absence of experimental evidence for the latter in Sr_2RuO_4 [58] suggests to also consider other possible p -wave states and their topological excitations, in analogy to the rich phenomenology in Helium 3.[53] Second, in a real crystalline material, crystal-field effects will invalidate our isotropic model at very long distances, and cause the skyrmion interaction to fall off exponentially. This is the same effect that makes, for instance, the isotropic Heisenberg model of ferromagnetism inapplicable at very long distances and gives the ferromagnetic magnons a small mass. It should be emphasized that this is usually an extremely weak effect that is also material dependent. Once p -wave superconductivity has been firmly established in a particular material, this point needs to be revisited in order to determine the energy scales on which the above analysis is valid.

APPENDIX A

INTEGRAL FORMULAS USED IN CHAPTER III

Feynman integral tricks are useful to transform the anisotropic denominator into isotropic one.

$$\frac{1}{A^a B^b} = \frac{\Gamma(a+b)}{\Gamma(a)\Gamma(b)} \int_0^1 \frac{x^{a-1}(1-x)^{b-1}}{[Ax + B(1-x)]^{a+b}}$$

Dimensional regularization integral formula which is extensively used in this paper.

$$\int \frac{d^d p}{(2\pi)^d} \frac{1}{(p^2 + \Delta^2)^n} = \frac{1}{(4\pi)^{d/2}} \frac{\Gamma(n-d/2)}{\Gamma(n)} \left(\frac{1}{\Delta^2}\right)^{n-d/2}$$

$$\int \frac{d^d p}{(2\pi)^d} \frac{p^2}{(p^2 + \Delta^2)^n} = \frac{1}{(4\pi)^{d/2}} \frac{d}{2} \frac{\Gamma(n-d/2-1)}{\Gamma(n)} \left(\frac{1}{\Delta^2}\right)^{n-d/2-1}$$

Let $R = a + bx + cx^2$.

$$\int \frac{dx}{\sqrt{R}} = \frac{-1}{\sqrt{-c}} \arcsin\left(\frac{2cx + b}{\sqrt{-\Delta}}\right) \tag{A.1}$$

where $\Delta = 4ac - b^2$. The above integral is true if $c < 0$ and $\Delta < 0$.

APPENDIX B

MISCELLANEOUS TECHNIQUES IN CHAPTER IV

B.1 Properties of Orthogonal Unit Vectors

Let $\hat{\mathbf{n}}$ and $\hat{\mathbf{m}}$ be orthogonal real unit vectors, and $\hat{\mathbf{l}} = \hat{\mathbf{n}} \times \hat{\mathbf{m}}$. Then the normalization condition $\hat{n}_i \hat{n}_i = \hat{m}_i \hat{m}_i = 1$ and the orthogonality condition $\hat{n}_i \hat{m}_i = 0$ imply

$$\hat{n}_j \partial_i \hat{n}_j = \hat{m}_j \partial_i \hat{m}_j = 0, \quad (\text{B.1a})$$

$$\hat{n}_j \partial_i \hat{m}_j = -\hat{m}_j \partial_i \hat{n}_j. \quad (\text{B.1b})$$

With these relations it is straightforward to show that

$$\partial_i \hat{n}_j \partial_i \hat{n}_j + \partial_i \hat{m}_j \partial_i \hat{m}_j = 2(\hat{n}_j \partial_i \hat{m}_j)(\hat{n}_k \partial_i \hat{m}_k) + \partial_i \hat{l}_j \partial_i \hat{l}_j. \quad (\text{B.2})$$

Finally, in regions where $\hat{\mathbf{l}}(\mathbf{x})$ is differentiable the Mermin-Ho relation[63] holds,

$$\hat{\mathbf{l}} \cdot (\partial_i \hat{\mathbf{l}} \times \partial_j \hat{\mathbf{l}}) = \partial_i \hat{\mathbf{n}} \cdot \partial_j \hat{\mathbf{m}} - \partial_i \hat{\mathbf{m}} \cdot \partial_j \hat{\mathbf{n}}. \quad (\text{B.3})$$

B.2 Solutions of the ODEs for g and h

The functions g and h in Sec. 4.3.2 both satisfy an ODE of the form (see Eqs.

(4.24))

$$F''(x) + \frac{1}{x} F'(x) - \frac{(x^4 - 6x^2 + 1)}{x^2(1 + x^2)^2} F(x) = q(x), \quad (\text{B.4})$$

with an inhomogeneity q given by the right-hand side of Eq. (4.24a) or (4.24b), respectively. It is easy to check that the corresponding homogeneous equation, obtained from Eq. (B.4) by putting $q(x) \equiv 0$, is solved by

$$F_h(x) = x/(1 + x^2). \quad (\text{B.5})$$

(This is the solution that vanishes as $x \rightarrow 0$. The second solution diverges in this limit.) Now write $F(x) = F_h(x) G(x)$, and let $y(x) = G'(x)$. Then y is found to obey the elementary first-order ODE

$$y'(x) + p(x)y(x) = q(x)/F_h(x), \quad (\text{B.6a})$$

with

$$p(x) = [2F_h'(x) + F_h(x)/x]/F_h(x). \quad (\text{B.6b})$$

The solution is

$$y(x) = e^{-\int dx p} \left[C_1 + \int dx q e^{\int dx p} \right], \quad (\text{B.7})$$

with C_1 an integration constant. A second integration yields $G(x)$, and hence $F(x)$ in terms of two integration constants. The latter can be determined by requiring that for small x the solution coincides with the asymptotic solution that vanishes as $x \rightarrow 0$. By using a power-law ansatz for g and h in Eqs. (4.24) we find $g(x \rightarrow 0) = -8x^3 + O(x^4)$, and $h(x \rightarrow 0) = 256x^3 + O(x^4)$, which suffices to fix the integration constants. For

$g(x)$ we find the expression given in Eq. (4.25a). For $h(x)$ we obtain

$$\begin{aligned}
h(x) = & \frac{1}{(270x(1+x^2)^4)} \left(592 + 2x^2 \left(8(-1, 119 + 90x^2 + 286x^4 + 240x^6 + 30x^8) + \right. \right. \\
& 10, 320(1+x^2)^3 \left. \right) + 2, 296(-1+x^2)(1+x^2)^4 + 4x^2(1+x^2)^3 + 1, 704 \ln x \\
& + 32 \ln(1+x^2) \left(-30 + 142x^2 + 276x^4 + 171x^6 + 52x^8 - 15x^{10} - 15(3+x^2) \right. \\
& \left. \left. (x+x^3)^2 \ln(1+x^2) \right) - 1, 920x^2(1+x^2)^3 \text{Li}_2(-x^2) \right), \tag{B.8}
\end{aligned}$$

with Li the polylogarithm function. The asymptotic behavior for large x is given by Eq. (4.26).

B.3 Contributions to E_s

By expanding the integrand of the first term in Eq. (4.17), we can express the energy E_s to $O(1/R^2)$ in terms of seven integrals,

$$E_s/E_0 = \sum_{i=1}^7 I_i + O(1/\ell^6), \tag{B.9}$$

with

$$I_1 = 4 \int_0^{R/\ell} dx \frac{x}{(1+x^2)^2}, \tag{B.10a}$$

$$I_2 = \frac{2}{\ell^2} \int_0^{R/\ell} dx \frac{1}{1+x^2} \left(\frac{(x^2-1)}{x^2+1} g(x) - xg'(x) \right), \tag{B.10b}$$

$$I_3 = \frac{1}{2\ell^4} \int_0^{R/\ell} dx \left[x (g'(x))^2 + \frac{(x^4 - 6x^2 + 1)}{x(1+x^2)^2} g^2(x) \right], \tag{B.10c}$$

$$I_4 = \frac{2}{\ell^4} \int_0^{R/\ell} dx \frac{1}{1+x^2} \left(\frac{(x^2-1)}{x^2+1} h(x) - xh'(x) \right), \quad (\text{B.10d})$$

$$I_5 = \frac{1}{\ell^6} \int_0^{R/\ell} dx \left(xg'(x)h'(x) + \frac{(x^4-6x^2+1)}{x(1+x^2)^2} g(x)h(x) \right), \quad (\text{B.10e})$$

$$I_6 = -\frac{4}{3\ell^6} \int_0^{R/\ell} dx \frac{(x^2-1)}{(1+x^2)^2} g^3(x), \quad (\text{B.10f})$$

$$I_7 = -\frac{1}{6\ell^8} \int_0^{R/\ell} dx \frac{(x^2-1)^2}{x(1+x^2)^2} g^4(x). \quad (\text{B.10g})$$

Evaluating the integrals to $O(1/\ell^4)$ yields Eq. (4.33).

BIBLIOGRAPHY

- [1] P. Chaikin and T. C. Lubensky, *Principles of Condensed Matter Physics* (Cambridge University, Cambridge, 1995).
- [2] E. I. Blount and C. M. Varma, Phys. Rev. Lett. **42**, 1079 (1979).
- [3] A. Knigavko, B. Rosenstein, and Y. F. Chen, Phys. Rev. B **60**, 550 (1999).
- [4] S. K. Sinha, G. W. Crabtree, D. G. Hinks, and H. Mook, Phys. Rev. Lett. **48**, 950 (1982).
- [5] V.L.Ginzburg, Sov. Phys. Solid State **2**, 1824 (1961).
- [6] E. Stanley, *Introduction to Phase Transitions and Critical Phenomena* (Oxford University Press, Oxford, 1971).
- [7] S.-K. Ma, *Modern Theory of Critical Phenomena* (Benjamin, Reading, MA, 1976).
- [8] J. M. Kosterlitz and D. Thouless, J. Phys. C. **6**, 1181 (1973).
- [9] M. Tinkham, *Introduction to Superconductivity* (McGraw-Hill, New York, 1975).
- [10] Q. Li, D. Belitz, and T. R. Kirkpatrick, Phys. Rev. B. **74**, 134 505 (2006).
- [11] Q. Li, J. Toner, and D. Belitz, Phys. Rev. Lett. **98**, 187002 (2007).
- [12] Q. Li, J. Toner, and D. Belitz .
- [13] H. S. Greenside, E. I. Blount, and C. M. Varma, Phys. Rev. Lett. **46**, 49 (1981).
- [14] C. G. Kuper, M. Revzen, and A. Ron, Phys. Rev. Lett. **44**, 1545 (1980).
- [15] D. E. Moncton, D. B. McWhan, P. H. Schmidt, G. Shirane, W. Thomlinson, M. B. Maple, H. B. MacKay, L. D. Woolf, Z. Fisk, and D. C. Johnston, Phys. Rev. Lett. **45**, 2060 (1980).
- [16] J. W. Lynn, G. Shirane, W. Thomlinson, and R. N. Shelton, Phys. Rev. Lett. **46**, 368 (1981).
- [17] T. K. Ng and C. M. Varma, Phys. Rev. Lett. **78**, 330 (1997).

- [18] A. Huxley, I. Sheikin, E. Ressouche, N. Kernavanois, D. Braithwaite, R. Calemczuk, and J. Flouquet, *Phys. Rev. B* **63**, 144 519 (2001).
- [19] S. S. Saxena, P. Agarwal, K. Ahilan, F. M. Grosche, R. K. W. Haselwimmer, M. J. Steiner, E. Pugh, I. R. Walker, S. R. Julian, P. Monthoux, G. G. Lonzarich, A. Huxley, L. Sheikin, D. Braithwaite, and J. Flouquet, *Nature* **406**, 587 (2000).
- [20] D. Aoki, A. Huxley, E. Ressouche, D. Braithwaite, J. Floquet, J. P. Brison, E. Lhotel, and C. Paulsen, *Nature* **413**, 613 (2001).
- [21] T. R. Kirkpatrick and D. Belitz, *Phys. Rev. B* **67**, 024 515 (2003).
- [22] L. Radzihovsky, E. M. Ettouhami, K. Saunders, and J. Toner, *Phys. Rev. Lett.* **87**, 027 001 (2001).
- [23] S. Tewari, D. Belitz, T. R. Kirkpatrick, and J. Toner, *Phys. Rev. Lett.* **93**, 177 002 (2004).
- [24] D. Belitz and T. R. Kirkpatrick, *Phys. Rev. B* **69**, 184 502 (2004).
- [25] T. He, Q. Huang, A. P. Ramirez, Y. Wang, K. A. Regan, N. Rogado, M. A. Hayward, M. K. Haas, J. S. Slusky, K. Inumara, H. Zandbergen, N. P. Ong, and R. J. Cava, *Nature* **411**, 54 (2001).
- [26] H. Rosner, R. Weht, M. D. Johannes, W. E. Pickett, and E. Tosatti, *Phys. Rev. Lett.* **88**, 027 001 (2002).
- [27] A. P. Young, M. Moldovan, and P. W. Adams, *Phys. Rev. B* **70**, 064 508 (2004).
- [28] V. L. Ginzburg, *Zh. Eksp. Teor. Fiz.* **31**, 202 (1956). [*Sov. Phys. JETP* **4**, 153 (1957)].
- [29] J. H. Chen, T. C. Lubensky, and D. R. Nelson, *Phys. Rev. B* **17**, 4274 (1978).
- [30] P. G. DeGennes, *Superconductivity of Metals and Alloys* (Addison-Wesley, Redwood City, CA, 1989).
- [31] J. Zinn-Justin, *Quantum Field Theory and Critical Phenomena* (Oxford University Press, Oxford, 1996).
- [32] D. Saint-James, G. Sarma, and E. J. Thomas, *Type II Superconductivity* (Pergamon, Oxford, 1969).
- [33] J. S. Kouvel and J. B. Comly, *Phys. Rev. Lett.* **20**, 1237 (1968).
- [34] J. T. Ho and J. D. Litster, *Phys. Rev. Lett.* **22**, 603 (1969).

- [35] A. P. Young, M. Moldovan, D. D. Craig, P. W. Adams, and J. Y. Chan, *Phys. Rev. B* **68**, 020 501 (2003).
- [36] B. I. Halperin, T. C. Lubensky, and S. K. Ma, *Phys. Rev. Lett.* **32**, 292 (1974).
- [37] S. Coleman and E. Weinberg, *Phys. Rev. D* **7**, 1888 (1973).
- [38] C. Dasgupta and B. I. Halperin, *Phys. Rev. Lett.* **47**, 1556 (1981).
- [39] K. D. Nelson, Z. Q. Mao, Y. M. Maeno, and Y. Liu, *Science* **306**, 1151 (2004).
- [40] M. Rice, *Science* **306**, 1142 (2004).
- [41] K. Machida and T. Ohmi, *Phys. Rev. Lett.* **86**, 850 (2001).
- [42] D. Vollhardt and P. Wölfle, *The Superfluid Phases of Helium 3* (Taylor & Francis, 1990).
- [43] K. G. Wilson and J. Kogut, *Phys. Rep.* **12**, 75 (1974).
- [44] S. Ma, *Phys. Rev. A* **10**, 1818 (1974).
- [45] B. A. Huberman and S. Doniach, *Phys. Rev. Lett.* **43**, 950 (1979).
- [46] D. S. Fisher, *Phys. Rev. B* **22**, 1190 (1980).
- [47] D. R. Nelson and H. S. Seung, *Phys. Rev. B* **39**, 9153 (1989).
- [48] E. H. Brandt, *Phys. Rev. Lett.* **63**, 1106 (1989).
- [49] P. L. Gammel, L. F. Schneemeyer, J. V. Wasczak, and D. J. Bishop, *Phys. Rev. Lett.* **61**, 1666 (1988).
- [50] H. Safar, P. L. Gammel, D. H. Huse, D. J. Bishop, J. P. Rice, and D. M. Ginsberg, *Phys. Rev. Lett.* **69**, 824 (1992).
- [51] T. Skyrme, *Proc. Roy. Soc. A* **260**, 127 (1961).
- [52] P. W. Anderson and G. Toulouse, *Phys. Rev. Lett.* **38**, 508 (1977).
- [53] M. M. Salomaa and G. E. Volovik, *Rev. Mod. Phys.* **59**, 533 (1987).
- [54] D. C. Wright and N. D. Mermin, *Rev. Mod. Phys.* **61**, 385 (1989).
- [55] S. L. Sondhi, A. Karlhede, S. A. Kivelson, and E. H. Rezayi, *Phys. Rev. B* **47**, 16 419 (1993).
- [56] C. Timm, S. M. Girvin, and H. A. Fertig, *Phys. Rev. B* **58**, 10 634 (1998). And references therein.

- [57] U. Roessler, A. Bogdanov, and C. Pfeiderer, *Nature* **442**, 797 (2006).
- [58] P. G. Björnsson, Y. Maeno, M. E. Huber, and K. A. Moler, *Phys. Rev. B* **72**, 012 504 (2005).
- [59] J. P. Boyd, *Chebyshev & Fourier Spectral Methods* (Springer, Berlin, 1989).
- [60] L. D. Landau and E. M. Lifshitz, *Theory of Elasticity* (Pergamon, Oxford, 1986).
- [61] J. E. Sonier, J. H. Brewer, and R. F. Kiefl, *Rev. Mod. Phys.* **72**, 769 (2000).
- [62] A. Schenck, *Muon Spin Rotation: Principles and Applications in Solid State Physics* (Adam Hilger, Bristol, 1986).
- [63] N. D. Mermin and T.-L. Ho, *Phys. Rev. Lett.* **36**, 594 (1976).